DISSERTATION

CLINICAL IMPLEMENTATION OF

INTENSITY MODULATED RADIOTHERAPY

BASED ON SEGMENTAL MULTILEAF COLLIMATION

ausgeführt zum Zwecke der Erlangung des akademischen Grades

eines Doktors der technischen Wissenschaften unter der Leitung von

Univ.-Prof. Dipl.-Ing. Dr. techn. Hannes Aiginger

E141, Atominstitut der Österreichischen Universitäten

und

Univ.-Doz. Dipl.-Ing. Dr. techn. Dietmar Georg

Univ.-Klinik für Strahlentherapie und Strahlenbiologie, Medizinische Universität Wien

eingereicht an der Technischen Universität Wien

Fakultät für Physik

von

Dipl.-Ing. Bernhard KROUPA

Matr.-Nr. 9225949

Hauptstraße 3a/1/17

3013 Tullnerbach

Wien, am 15. Mai 2005

KURZFASSUNG

Die Intensitätsmodulierte Strahlentherapie (IMRT) gehört gegenwärtig zu den vielschichtigsten Anwendungen ionisierender Strahlung in der Krebsbehandlung. Dabei kommen hochenergetische Photonenfelder mit zeitlich veränderlichen Intensitätsverteilungen zum Einsatz, um die Konformität in der dreidimensionalen (3D) Konformaltherapie weiter zu verbessern. Besonders bei konkav geformten Tumoren in der Nähe strahlensensibler Gewebe ist dies von Vorteil, da die IMRT die Möglichkeit bietet, den Hochdosisbereich entsprechend den Konturen des Zielgebiets „nachzuzeichnen". Demzufolge kann die Belastung von Risikoorganen und Normalgewebe ohne Abstriche in der Tumorbehandlung reduziert werden. Bei der segmentierten Multileaf-Kollimation (SMLC) resultiert die Intensitätsmodulation aus der Überlagerung mehrerer Subfelder oder Segmente, die mit Hilfe eines konventionellen Multileaf Kollimators (MLC) erzeugt werden. Auf Grund der enormen Anzahl von Freiheitsgraden verwendet man üblicherweise computerunterstützte Algorithmen, um die optimale Intensitätsverteilung zu ermitteln (inverse Planung).

Im Rahmen einer vorklinischen Testphase wurde das Rechenmodell des integrierten Helax-TMS IMRT-Moduls (V 6.0) bezüglich seiner Plausibilität untersucht sowie der Einfluss benutzerdefinierter Parameter auf das Optimierungsergebnis analysiert. In einem Phantom konnten mehrere Testfälle mit einem einzelnen Bestrahlungsfeld simuliert werden, um zwei Algorithmen („Target Primary Feasibility" und „Weighted Feasibility") miteinander zu vergleichen, wobei nur der letztgenannte eine Gewichtung verschiedener Organstrukturen zulässt. Im Falle fehlender Risikoorgane versuchten beide Algorithmen vorrangig, die Minimaldosisbedingungen der Zielgebiete zu erfüllen. Des Weiteren wurden Untersuchungen mit Mehrfeldertechniken angestellt, um klinisch relevante Situationen nachzuahmen. Dabei wirkte sich die Vorgabe einer Segmentmindestgröße und einer maximalen Segmentanzahl nicht wesentlich auf die Qualität der Bestrahlungspläne aus, während andererseits solche Limitierungen für die Effizienz der Behandlung und aus dosimetrischen Gründen sinnvoll sind. Die im System voreingestellte Iterationsanzahl und die Voxeldichte stellten sich als ausreichend heraus. Zusätzlich wurde die Notwendigkeit verdeutlicht, bei der Verwendung computerunterstützter Optimierungsverfahren die Behandlungsziele möglichst präzise festzulegen.

Bevor der ELEKTA Precise Linac für IMRT-Behandlungen eingesetzt werden konnte, mussten seine dosimetrischen Eigenschaften in der Anlaufphase des Strahls (Einschwingverhalten) und die Genauigkeit der mechanischen Komponenten untersucht werden, da in einer typischen SMLC-IMRT Anwendung häufig irregulär geformte Segmente mit geringen geometrischen Abmessungen und nur wenigen Monitor Units (MU) auftreten. Für drei Photonenenergien (6 MV, 10 MV und 25 MV) wurden die Linearität der Dosis pro MU, die Strahlsymmetrie und die Strahlhomogenität (nach IEC 60976 Standard) bei drei verschiedenen Dosisleistungen gemessen (100 MU/min, 200 MU/min und 400 MU/min). Die geforderte Stabilität bezüglich Dosislinearität ($\pm$1%), Homogenität ($\leq$3%) und Symmetrie ($\leq$103%) konnte bei allen Energien mit einer Dosisleistung von 400 MU/min erreicht werden, sofern mindestens 2 MU appliziert wurden. Nach der Installation eines Fast-Tuning Magnetrons zur Beschleunigung von SMLC-IMRT Behandlungen erfüllten sogar Segmente mit nur 1 MU die dosimetrischen Akzeptanzkriterien. Bei einer nominellen quadratischen Feldgröße von 3 cm bzw. 5 cm verursachten Abweichungen von $\pm$1 mm bei allen Energien eine Änderung des Outputs von weniger als 1%, während bei

25 MV und einer Feldgröße von 2 cm der Fehler auf 2% anstieg. Infolgedessen wurde eine Mindestsegmentgröße von 9 cm² mit wenigstens drei offenen Leaf-Paaren festgesetzt. Um die mechanische Genauigkeit des integrierten MLC beurteilen zu können, wurden Felder mit einer nominellen Breite von 2 cm an drei verschiedenen Kollimatorpositionen appliziert und die Profilbreite für jedes Leaf-Paar filmdosimetrisch vermessen. Zusätzlich wurde anhand eines zusammengesetzten Feldes der korrekte Anschluss angrenzender Segmente verifiziert. Drei Leaf-Paare mussten neu kalibriert werden, um die geforderte Präzision von 0.5 mm pro Leaf einhalten zu können.

Infolge der komplexen Planung und Applikation von IMRT-Behandlungen ist es notwendig, jeden Bestrahlungsplan vor seiner Applikation am Patienten zu verifizieren. Meist werden so genannte Hybrid-Pläne erzeugt, wobei der Patientenplan ohne eine Änderung der Intensitätsverteilung auf ein Phantom übertragen und umgerechnet wird. Ionisationskammermessungen an einzelnen Punkten sind geeignet, um die Anzahl der MU zu kontrollieren, während zweidimensionale (2D) Dosisverteilungen vorzugsweise filmdosimetrisch verifiziert werden. Für die Konversion der optischen Dichte in Dosiswerte benötigt man dabei eine sensitometrische Kurve, die möglichst wenig von Energie, Feldgröße, Phantomtiefe und Filmorientierung abhängen sollte. Dazu müssen die sensitometrischen Kurven für 6 MV, 10 MV und 25 MV auf jene Dosis normiert werden, aus der für die jeweilige Energie eine optische Dichte von 1 resultiert. So kann bei beiden Filmtypen (Kodak X-Omat V und EDR-2) jeweils eine einzige Kurve für alle drei Energien verwendet werden. Die normierte sensitometrische Kurve ist außerdem weitestgehend unabhängig von Feldgröße, Tiefe und Orientierung (Abweichungen ≤3%), jedoch können beim Einsatz verschiedener Entwicklungsmaschinen Unterschiede von bis zu 20% entstehen.

Für die patientenspezifische Qualitätssicherung wurde ein Protokoll erarbeitet, in dem auch klinische Akzeptanzkriterien festgelegt sind. Während sich die Verifikation einzelner Felder wegen der häufig auftretenden steilen Dosisgradienten als kritisch herausgestellt hat, konnte die Methode der Hybrid-Pläne praktikabel und zuverlässig umgesetzt werden. Um die Handhabung weiter zu vereinfachen, wurden eigene IMRT Verifikationsphantome entwickelt. Mit Hilfe eines intern entwickelten Software-Pakets konnte das mathematische Konzept des γ-Index eingeführt werden, das eine quantitative Auswertung von 2D-Dosisverteilungen ermöglicht. Es beruht auf einer Kombination von Dosisdifferenzen und geometrischen Abweichungen, für die als Kriterien üblicherweise 3% bzw. 3 mm zugelassen werden, wobei ein γ-Index größer als 1 eine Überschreitung der kombinierten Kriterien anzeigt. Ein IMRT-Bestrahlungsplan wird klinisch akzeptiert, sofern alle folgenden Bedingungen erfüllt sind: absolute Abweichung der MU ≤3%, weniger als 10% der Messfläche mit einem γ-Index größer als 1, mittlerer γ-Wert ≤0.6 und maximaler γ-Wert ≤2. Ansonsten wird die Verifikation wiederholt oder ein neuer Plan erstellt.

Schließlich werden typische Fallstudien verschiedener Tumorentitäten präsentiert (Prostata, Paraspinale Tumoren und HNO) und ausführlich diskutiert. Die Beispiele entstammen realen Patientenbehandlungen und zeigen sehr deutlich die Vorteile und Möglichkeiten der IMRT: konkav geformte Hochdosisregionen, Schonung von Risikoorganen in der Nähe des Zielgebiets, sogar wenn sie (zumindest teilweise) vom Tumor umgeben sind, Schonung von Normalgewebe, Erhöhung der Tumordosis und Anwendung simultan integrierter Boost-Techniken. Derzeit werden weltweit in verschiedenen Institutionen Studien durchgeführt, um den klinischen Nutzen der IMRT nachzuweisen.

DANKSAGUNG

TABLE OF CONTENTS

CHAPTER 1

PURPOSE AND STRUCTURE OF THIS THESIS

The work presented in this thesis is focussed on two main items. At first, to implement intensity modulated radiotherapy (IMRT) based on segmental multileaf collimation (SMLC) at the Radiotherapy Department of the Medical University of Vienna, including extensive performance evaluations of the equipment for IMRT delivery. At second, to develop an effective verification method of IMRT treatment plans in dedicated phantoms and to define appropriate acceptance criteria for patient specific quality assurance (QA) together with a consequential decision protocol.

In IMRT, photon fields of time-variable intensity patterns are used to further increase the conformity of three-dimensional conformal radiotherapy (3D-CRT). Especially for concavely shaped targets with sensitive structures in their direct vicinity, IMRT has the potential to "paint" the high dose region following the target outline, thus reducing the dose load to organs at risk (OAR). In the SMLC approach, the intensity modulation is accomplished by superimposing several sub-fields or segments, individually shaped by a multileaf collimator (MLC).

Due to the vast number of degrees of freedom, the optimal intensity distribution is hardly possible to be found manually by trial-and-error. Instead, computerized optimization algorithms have been developed to automate the search process. However, the mathematical functionality of such optimization procedures is not straightforward and the derived results are frequently non-intuitive for the user. Thus, the plausibility of the applied algorithm and the influences of user-defined parameters on the optimization outcome have to be investigated within the scope of a pre-clinical test phase. For the treatment planning system (TPS) under investigation (Helax-TMS), the evaluation is described in CHAPTER 3.

The sequencer included in the optimization module of Helax-TMS translates the ideal fluence patterns to MLC segments, best possibly approximating the desired dose distribution. Prevalently, these sub-fields are very irregularly shaped and likely to be small in terms of field dimensions and number of monitor units (MU). As the delivery of such segments poses a major challenge to the capacity of a linear accelerator (Linac), its dosimetric performance during the beam start-up phase and

the precision of the mechanical components have to be checked extensively, before the Linac is clinically used for SMLC-IMRT treatments. In CHAPTER 4 the inspection of an ELEKTA Precise accelerator with three available photon beam qualities is described.

The planning system and its performance are closely linked to the Linac, as the dosimetric and mechanical characteristics of the treatment machine have to be taken into account. Although the combination of the Helax-TMS system with an ELEKTA Linac to plan and deliver intensity modulated radiotherapy is not unique [Adams *et al* 2004, Martens *et al* 2002a], such a thorough investigation of the preferences and limitations of the specified technical equipment has not been described elsewhere.

The second emphasis in this thesis is placed on the development of a patient specific QA procedure. Due to the complex nature of IMRT planning and delivery, it is necessary to verify each treatment plan before its first application onto the patient, despite of the extensive pre-clinical commissioning programme. In general, hybrid IMRT plans are created, i.e., the patient plan is transferred to a phantom and recalculated with unmodified fluence patterns. To check the calculated number of MU, single point ionization chamber measurements are appropriate, while relative dose distributions are verified preferably by film dosimetry. The procedure can be carried out either for each single beam or the entire treatment plan.

For the evaluation of film measurements a sensitometric curve for the conversion of optical density to dose is needed. In CHAPTER 5 the generation of a normalized sensitometric curve is described, providing the user with dose values in a relative scale. Due to its dosimetric characteristics it is well-suited for the application in an IMRT verification programme. Additionally, only one unique sensitometric curve is necessary for the three available photon beam energies.

The final aim of the development is to define a standard protocol for the patient specific verification, giving quantitative information about possible deviations in terms of number of MU and relative dose. Besides the design of dedicated verification phantoms, the central part of CHAPTER 6 deals with the implementation of a mathematical concept to quantitatively evaluate two-dimensional dose distributions, embedded in an in-house developed software package. Furthermore, the specification of acceptance criteria in order to appraise the verification results and the postulation of corresponding clinical consequences are discussed.

In CHAPTER 7 patient case studies are elaborately discussed, presenting three tumour entities frequently treated by intensity modulated radiotherapy. This chapter is supposed to clearly demonstrate the advantages and possibilities of IMRT by means of concrete examples, taken from actual treatments at the Medical University of Vienna.

Finally, a summary is given in order to outline the applied methods and to highlight the main results and clinical consequences derived within this thesis.

CHAPTER 2

GENERAL INTRODUCTION TO INTENSITY MODULATED RADIOTHERAPY (IMRT)

The following chapter is giving a brief overview of the main issues in the large field of intensity modulated radiotherapy. It will concentrate primarily on methods and materials utilized for IMRT in the Radiotherapy Department of the Medical University of Vienna. Thus, the introduction is not intended to be exhaustive. The reader may find further details in pertinent books providing comprehensive information about IMRT [Palta and Mackie 2003, Webb 2001].

Additionally, it has to be mentioned that within this thesis the term "dose" is always regarded as physical dose. Biological effects and modelling are not taken into account as they are beyond the scope of this work. However, there are several reports dealing with biological items in combination with intensity modulated radiotherapy [e.g., Alber *et al* 2003, Fowler *et al* 2004, Stavrev *et al* 2003, Vaarkamp and Krasin 2001].

2.1 DEFINITION OF IMRT

Besides surgery and chemotherapy, the application of radiotherapy belongs to the most effective treatment methods of cancer. In external beam radiotherapy, solid tumours are irradiated by high voltage photon and/or electron beams generated by linear accelerators (Linacs) or by collimated radiation fields of cobalt-60 sources. The primary goal in radiotherapy is to maximize the dose delivered to the tumour, while keeping the dose to critical organs and normal tissue as low as possible. Therefore, multiple beams from different directions are applied and superimposed at the location of the tumour.

In the early stage of radiotherapy treatments, only square or rectangular fields were available. The methodology was significantly improved by using additional blocks brought into the radiation fields. Thus, the beam shapes could individually be conformed to the respective projections of the target. This so-called conformal

radiotherapy (CRT) was further facilitated by the advent of multileaf collimators (MLC), as time efforts and workload were drastically reduced. Except for particular cases where blocked "islands" within the beams are needed, the MLC concept has replaced the construction and application of individual blocks in modern radiotherapy [Georg 1997a].

The intensity modulated radiotherapy (IMRT) has been established as a special form of CRT in the recent years. Thereby, the geometrically shaped fields are separated to bixels or beamlets with varying intensity levels to achieve a new degree of conformity. In contrast to CRT, it is possible to generate concavely formed high dose volumes by the application of IMRT. This is especially useful if organs at risk (OAR) are partly or even completely surrounded by the tumour. In such cases, it is possible to decrease the dose to the critical organ(s) without losing tumour control. Figure 2.1 (a) illustrates the development from conventional radiotherapy to IMRT, while an example of a typical IMRT fluence distribution is shown in Figure 2.1 (b).

(a)

(b)
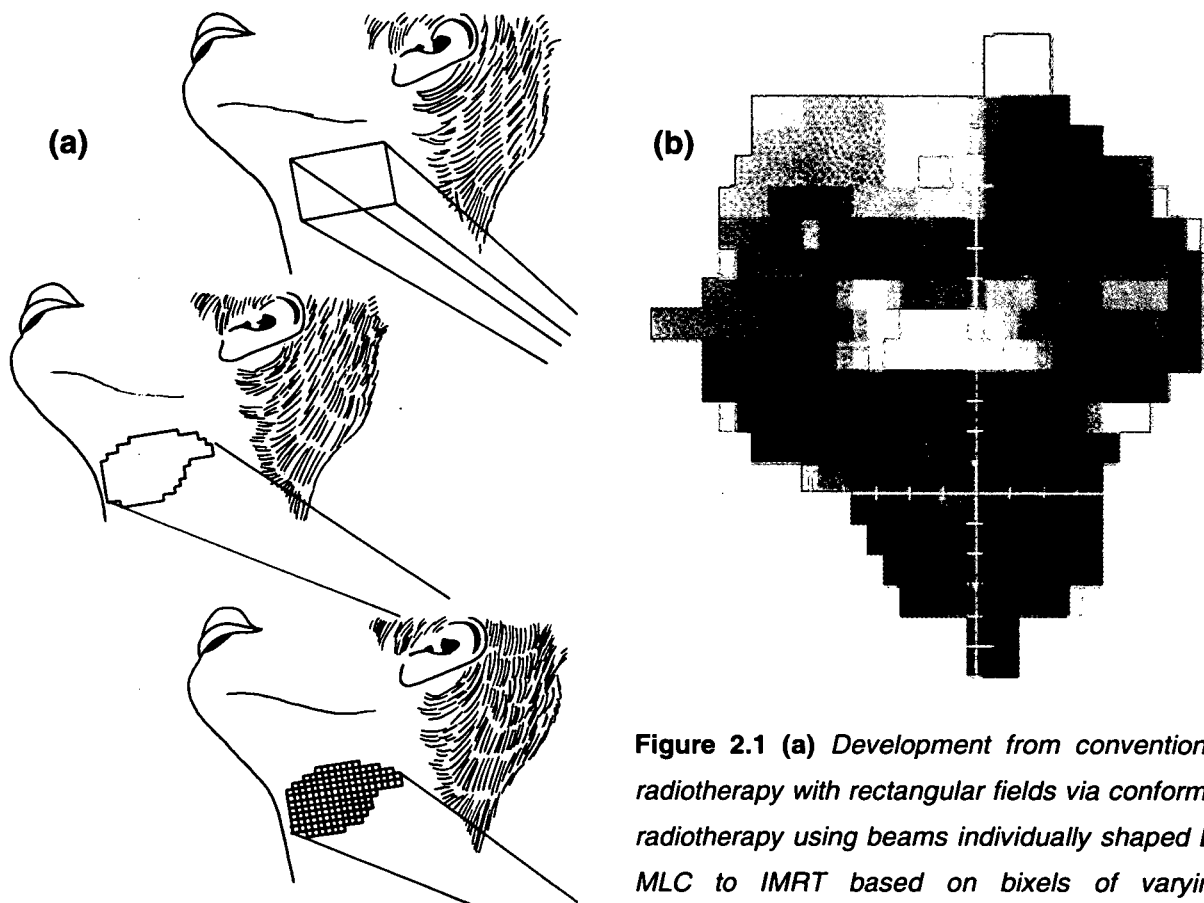
Figure 2.1 (a) *Development from conventional radiotherapy with rectangular fields via conformal radiotherapy using beams individually shaped by MLC to IMRT based on bixels of varying intensities.* (b) *Typical fluence pattern in an IMRT treatment beam, where the greyscale is proportional to intensity.*

5

However, modern IMRT is more than just the use of non-uniform intensities in radiation fields. In fact, intensity modulated distributions were being produced many decades ago, when considering simple blocks and wedges, or compensator filters in order to correct for missing tissue. While a block creates a binary intensity distribution with the primary fluence either being present or absent (except for a certain amount of transmission), a gradient of intensity is generated by a wedge in its slope direction. The examples are illustrated in Figure 2.2 (a) and (b).

According to the definition from the Intensity Modulated Radiation Therapy Collaborative Working Group (2001), modern IMRT is characterized by the search for the optimum beam fluence, which can be performed inversely by various computer optimization techniques or manually in a forward planning process, yet excluding simple modulators like blocks and wedges. The crucial part in IMRT is the determination of physically deliverable modulated beam fluence profiles, resulting in a dose distribution that most closely matches the desired one.
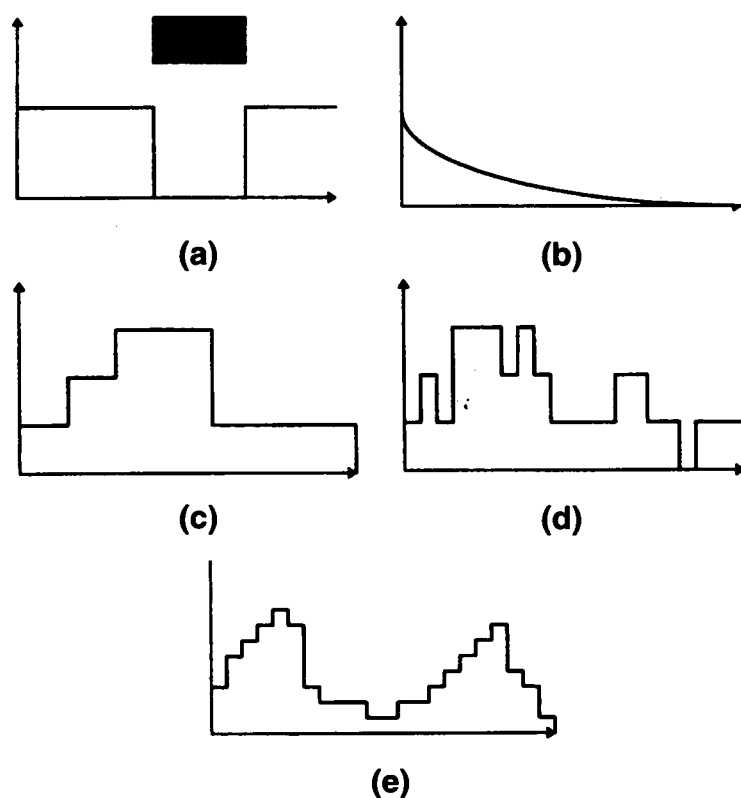
Figure 2.2 *Intensity profiles of different complexity, with the abscissa representing spatial distance.* **(a)** *Block leading to a binary "on-off" distribution.* **(b)** *Gradient profile in wedge slope direction.* **(c)** *Full modulation with coarse spatial and intensity scale.* **(d)** *Full modulation with fine spatial and coarse intensity scale.* **(e)** *Full modulation with fine spatial and intensity scale.*

In Figure 2.2 (c) to (e) typical fluence profiles of fully intensity modulated beams are presented. There are two parameters that can be defined, the spatial resolution and the number of intensity levels. In Figure (c), a coarse spatial scale is used and only four intensity levels are applied (including zero). Figure (d) displays a profile with the same intensity scale but a fine spatial resolution, while in Figure (e) the number of intensity levels is increased to nine and a fine spatial scale is used. By default, in many IMRT planning systems 0.5 cm spatial resolution and ten intensity levels are applied.

2.2 INTENTIONS OF IMRT

Due to the complex nature of IMRT planning and delivery, it is neither possible nor reasonable to apply IMRT treatments to every case indicated for radiotherapy. However, there are certain intentions which can be pursued successfully by the use of IMRT. They are summarized in the following list.

- To increase the conformity of the high dose volume, which is especially useful when irradiating concavely shaped targets, as the dose load to normal tissue can be reduced.
- To minimize the exposure to adjacent or proximate OAR, without decreasing the dose delivered to the target (see case study 1 in section 7.1)
- To increase the treatment dose in the tumour, while respecting dose limits of OAR ("dose escalation"). As an example case study 2 in section 7.2 is presented.
- To perform a simultaneous integrated boost (SIB), i.e. to apply different dose levels within the target. By only one treatment plan, the delivery of different fraction doses to certain volumes is possible. The method is further explained by case study 3 in section 7.3.
- A combination of the above mentioned goals is also possible and sometimes necessary.

2.3 IMRT DELIVERY METHODS

2.3.1 Scanned beam

Providing computer-controlled scanned beams the Scanditronix Racetrack Microtron System enabled the implementation of the first modern IMRT delivery technique [Brahme 1987]. By controlling the beam-steering magnets, the angle and intensity of the electron beam striking the X-ray target is affected. Thus, elemental bremsstrahlung beams are produced and located according to pre-calculated scan patterns. However, since the full width at half maximum of the 50 MV photon beam is in the range of several centimetres, only a limited resolution can be achieved. As described by Karlsson *et al* (1998), the technique can be used in a modified way to create intensity modulated high energy electron beams.

2.3.2 Tomotherapy

2.3.2.1 Serial Tomotherapy

This IMRT method resembles the technique used for the acquisition of computer-tomographic (CT) studies, i.e., the dose is delivered by narrow fan beams rotating around the patient [Mackie *et al* 1993]. A commercially available system has been developed by NOMOS (Nomos Corporation, Sewickley, US) and is called Peacock MIMiC (Multileaf Intensity Modulating Collimator). The fields are collimated to 2 cm in longitudinal direction and 20 cm in perpendicular, in which the intensity modulation is accomplished by a special binary mini-MLC attached to the Linac head, as shown in Figure 2.3.

Its leaves are driven in and out while the gantry is rotating, resulting in beamlets of different intensities. The complete treatment is performed serially by irradiating adjoining axial slices. Thus, particular attention has to be paid to the accuracy of couch motion in order to prevent under- or overdoses in the abutment regions. An error of 1 mm in table positioning can sum up to 25% deviation in dose

delivery [Dogan *et al* 2000]. Additionally, the number of MU needed for tomotherapy IMRT treatments is about seven to ten times higher compared to 3D conformal radiotherapy. Nevertheless, up to date the majority of IMRT deliveries worldwide have been performed by this method.
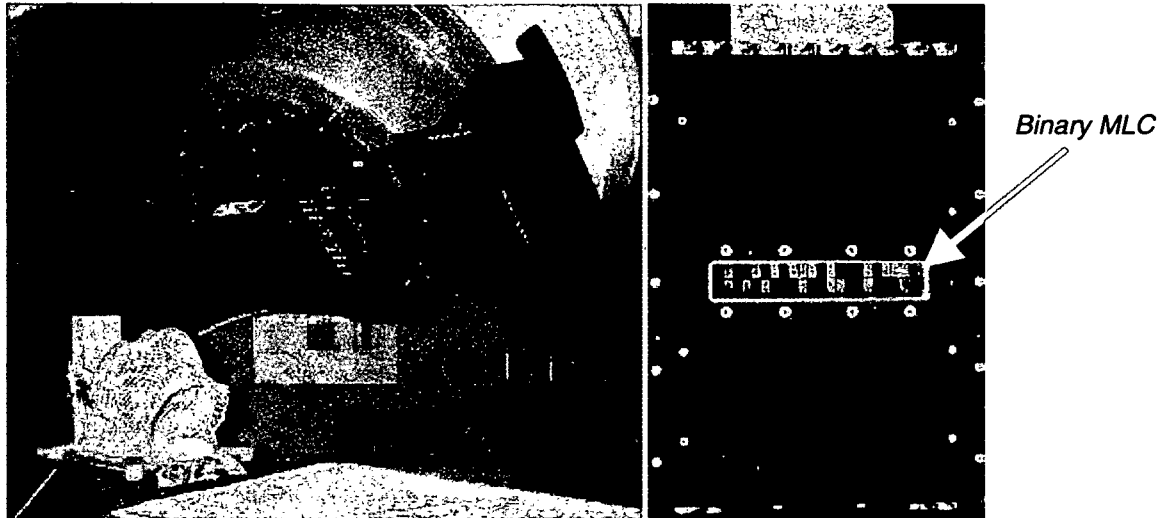
Figure 2.3 *The PEACOCK MIMiC tomotherapy system mounted to a Linac (left image), with a detailed view of its binary MLC (right image). The leaves step in and out while the gantry is in motion, yielding fan beams of varying intensity.*

2.3.2.2 Helical Tomotherapy

An advanced approach to the fan beam IMRT technique is the so-called helical tomotherapy. A low-energy megavoltage Linac and a temporally modulated collimator system are mounted on a CT-like gantry, through which the patient is moved continuously during the treatment. This helps to overcome the dosimetric uncertainties described above. In addition, a diagnostic CT system can be integrated in order to simultaneously acquire a verification study of the patient positioning [Ruchala *et al* 1999]. The machine configuration and its application are illustrated schematically in Figure 2.4.
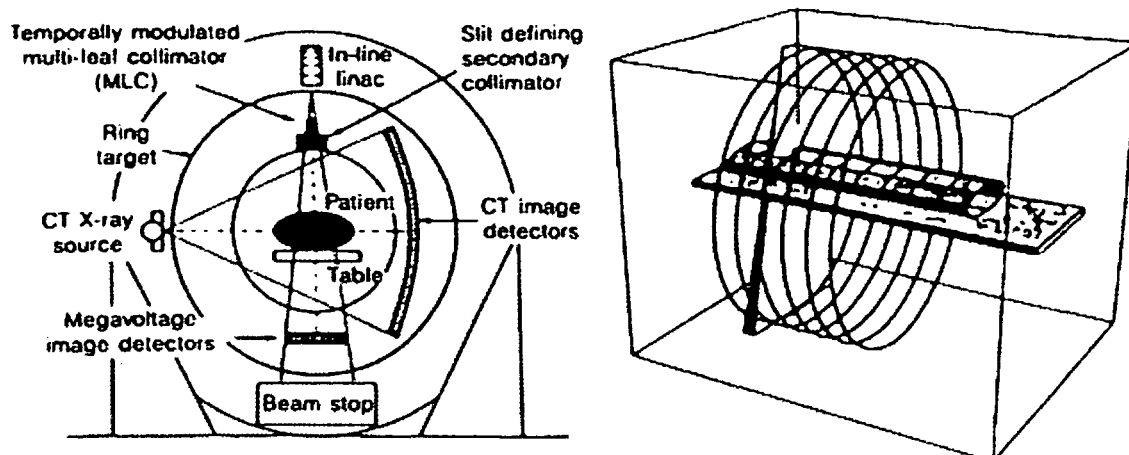
Figure 2.4 *Schematical machine configuration of a helical tomotherapy unit (left image) and application of a spiral scan (right image). The patient is moved continuously in longitudinal direction while the gantry is rotating, preventing dosimetric uncertainties in slice abutment regions.*

2.3.3 Conventional Multileaf Collimator

2.3.3.1 Dynamic Multileaf Collimator (DMLC)

In the DMLC-IMRT or "sliding window" delivery mode, the leaves of a conventional multileaf collimator are used to generate time-variable cone beams [Yu *et al* 1995a]. With fixed gantry positions, the leaves are moving while the radiation beam is on. The desired intensity distribution is accomplished by varying the position, size, and speed of the opening formed by each leaf pair. Special algorithms are needed to translate the intensity profiles to leaf movements which can be mechanically performed [Spirou and Chui 1994, Bortfeld *et al* 1994a]. When using the DMLC-IMRT approach, special interest has to be put on quality assurance of the MLC system. In addition to positional accuracy, the travel speed of each leaf has to be checked within the routine maintenance programme, since a deviation would dramatically affect the machine output as well as the delivered dose distribution. Furthermore, due to the dynamic mode dose discrepancies can arise when resuming a treatment after an interruption, if either caused by a technical failure or needed for patient care.

2.3.3.2 Segmental Multileaf Collimator (SMLC)

The SMLC technique represents another way of delivering intensity modulated beams by a conventional multileaf collimator [Galvin *et al* 1993]. For a fixed gantry angle, the radiation field consists of a series of MLC shapes, which are called segments or subfields. By superposition of these irregularly formed segments the desired fluence patterns are generated. In contrast to the dynamic mode, the phases of leaf motion and radiation are not executed simultaneously but sequentially; i.e., after irradiating the MU prescribed for the first segment, the beam is turned off and the leaves move to shape the second segment. The next MU are applied, before the beam stops again and the third segment is formed by the MLC, etc. Thus, the SMLC-IMRT delivery is also called "step-and-shoot" or "stop-and-shoot".
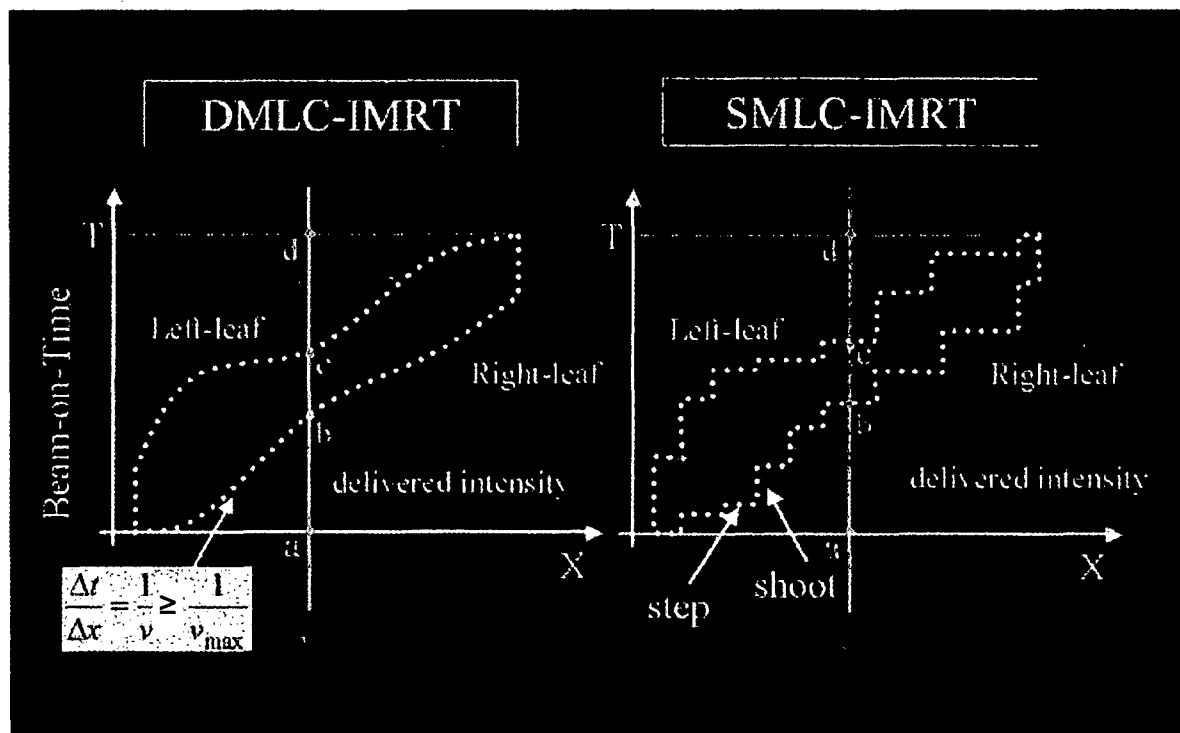
Figure 2.5 *Positions (white dotted lines) of a single leaf pair versus beam-on time for DMLC (left chart) and SMLC (right chart) deliveries. The resulting intensity profiles are delineated as red lines. Due to continuous leaf motions, a smooth curve is generated by DMLC, while the step and shoot phases in the SMLC mode can only produce discrete intensity levels. However, the delivered dose will be smoothed out due to radiation transport and scatter, as long as the spatial resolution is chosen not too coarse. On the other hand, in the DMLC approach the generation of arbitrary intensity profiles is limited by the maximum leaf motion speed, as indicated in the formula.*

In Figure 2.5, the positions of a single leaf pair generating a desired intensity profile are delineated versus the beam-on time. The left side illustrates the continuous leaf motion and the resulting smooth intensity profile when using the DMLC technique. On the right side, the corresponding case is demonstrated for a SMLC delivery. Here, the horizontal lines in the leaf positions indicate the "step" phases, where the beam is off and the leaves move to shape the next segment. Consequently, the vertical lines represent the "shoot" phases with the leaves kept stationary while the beam is on. Although the generated intensity profile evidently consists of discrete levels, the delivered dose will be smoothed out due to radiation transport and scatter, as long as the spatial resolution of the leaf sequence is chosen not too coarse [Bortfeld *et al* 1994b].

At the Medical University of Vienna, IMRT treatments are delivered by the SMLC technique, as it offers the following advantages:

- No additional treatment hardware components are needed, since the conventional MLC can be used.
- The generation of intensity patterns is traceable as it arises from the superposition of individual subfields.
- For the same reason, portal verifications of intensity patterns are feasible.
- It is easy to resume an interrupted treatment.
- Only a relatively simple accelerator control system is necessary.
- Both, forward and inverse planning is possible to get SMLC sequences.
- Compared to tomotherapy and DMLC deliveries, the smallest number of MU is needed.

For very complex cases, the number of segments can increase drastically. Therefore, the most commercially available treatment planning systems offer the possibility to limit the number of segments per beam and to merge similarly shaped subfields, in order to maximize treatment efficiency without significantly compromising the dose distribution. Furthermore, in SMLC-IMRT segments of small spatial dimensions (<3 cm) and/or with a small number of MU (<3 MU) are likely to be generated. Thus, extensive dosimetric studies of such fields have to be carried out during the Linac commissioning procedure, see CHAPTER 4.

2.3.3.3 Intensity modulated Arc Therapy (IMAT)

The IMAT delivery method poses the third option to use a conventional MLC for the generation of intensity modulated beams and was developed by Yu (1995b). Whereas in tomotherapy fan beams are rotated around the patient, in IMAT multiple irregularly shaped cone beams are applied while the gantry is in motion. The dose is delivered by superimposing arcs, within each the MLC opening is modified continuously. Based on the optimization results, the leaf movements are prescribed as a function of gantry angle in such a way that the accumulated intensity modulation creates the desired dose distribution as closely as possible.

2.3.4 Physical modulator (compensating filter)

Placed in radiation fields in order to provide intensity modulated fluence profiles, physical modulators generally are designed by 3D treatment planning systems [Jiang and Ayyangar 1998, Basran et al 1998]. The required thicknesses are calculated along ray lines by using effective attenuation coefficients for the filter material and dose-ratio parameters for the effective depths. Usually, metal alloys are used to fabricate the modulators which can get shaped in different ways. One method is milling out the required surface from a metal block by a computer-controlled machine. Alternatively, the hot alloy is poured into a foam mould, with its shape representing the negative copy of the desired surface, created by a micro-processor controlled cutter. Another method is based on the use of metal granulate material, being filled into foam moulds [Frenzel 2000].

By the application of physical compensators in IMRT, higher spatial resolutions perpendicular to leaf motion direction is achievable, as compared to MLC based delivery methods. Due to the continuous nature of modulated beams, matchline discrepancies cannot occur. However, the manufacturing process for physical modulators is found to be cumbersome and time-consuming. Additionally, for each gantry position the treatment room has to be entered in order to manually change the compensator filter, leading to prolongated patient treatment times. For these reasons, the clinical implementation of compensator based IMRT deliveries

reveals as relatively impractical and inconvenient, both from the patient's point of view as well as from the personnel's.

2.3.5 Robotic Linear Accelerator

The use of robotic linear accelerators is the most recent method applied to deliver intensity modulated treatment beams and is still under development [Webb 1999, 2000]. A small x-band Linac is mounted on an industrial robot, providing beamlets with any orientation relative to the target volume. The treatment is specified by the trajectory of the robot and the number of MU delivered at each robotic orientation. Although this IMRT technique offers the largest flexibility, it is not (yet) widely available and needs further research to determine its clinical benefit.

2.4 COMPUTER OPTIMIZATION

In conventional 3D conformal radiotherapy, one tries to find the best possible treatment plan that is physically deliverable by a procedure called "forward planning", i.e., the planner defines beam number and directions, beam qualities, weights, modifiers (e.g. wedge filters), and draws individual apertures for each field. Based on this configuration, the resulting dose distribution is calculated and evaluated by dose-volume-histograms (DVH) and isodose line maps. In order to maximize the dose to target and/or to minimize the exposure of organs at risk, it may be necessary to change the initial set-up. Again, dose calculations are performed and the results reviewed. This iterative trial-and-error method is repeated until a satisfactory dose distribution has been found, both from the medical as well as from the physical point of view.

Although the forward planning process can also be used to generate a simple kind of intensity modulated radiotherapy treatment plans, e.g. when delivering SMLC-IMRT with only a few segments per beam, in general the number of degrees of freedom is too large for a human planner to find the optimal fluence distribution, since each beam can be separated into hundreds of beamlets. Due to the rapid development of computer technologies in the past two decades, the treatment

planning systems have become capable of performing such optimization processes within clinically tolerable times. Hence, there are several commercial optimization modules available which can properly fulfil the task of "inverse planning" to generate complex IMRT dose distributions. Usually, the planner only predefines the number and directions of beams as well as their energies, while the most important part is the determination of clinical goals. Based on these, the IMRT module tries to find a set of fluence patterns, which generates the dose distribution optimally approximating the desired one. After evaluating the results, the clinical constraints may need to be adapted before a second run of the optimization module is started, of which the outcome has to be reviewed again. This procedure is redone until a satisfying solution has been found. Thus, it is obvious that inverse planning using computer optimization modules still needs a certain number of iterations performed by the human planner, rather than being a simple "plug and play" method. In the following, the different computer optimization techniques will be roughly described, with the main emphasis on the definition of objective functions, the actual optimization algorithms, and the leaf sequencing.

2.4.1 Objective Functions

The "objective function" (also "score function" or "cost function") can be considered as mathematical translation of the clinical goals which are supposed to be achieved by the IMRT treatment. Its value is regarded as degree of quality of the respective treatment plan. During the optimization procedure the objective function is going to be minimized or maximized, depending on its definition. It can be based on biological criteria and/or physical criteria, on the latter of which this thesis will concentrate. These criteria can be described by measurable physical quantities, as there are for example absorbed dose and volume.

In radiotherapy, the ideal dose distribution would be characterized by 100% dose to the tumour without any exposure to critical structures. Of course, even with IMRT this is not achievable since the optimization can only redistribute but not reduce the integral dose, but it can be used for the definition of a simple physical objective function, which is the mean square deviation between the calculated dose distribution and the ideal prescription in the entire volume. While this "least-squares

optimization" method is based on the minimization of quadratic objective functions, linear objectives or objective functions with linear terms can be used for the maximization of mean target doses and/or the minimization of mean doses to critical structures [Rosen *et al* 1991].

As explained by Bortfeld (1999), the clinical relevance of the optimization techniques mentioned above is significantly increased by the introduction of constraints. The least-squares method can be improved by minimizing the mean square deviation between actual and prescribed dose only in the target volume as well as by the application of individual constraints for organs at risk. The simplest way is to limit the dose to critical structures by a maximum threshold value [Niemierko 1992]. However, if the OAR is in close vicinity to the tumour, the strict fulfilment of the constraint can negatively affect the target coverage. Hence, the requirement can be relaxed by the use of a "weighting factor" (also "penalty factor" or "importance factor"), which defines the relative importance of the respective constraint [Hristov and Fallone 1998]. As delineated in Figure 2.6 (a), a small weighting factor permits some overdose beyond the threshold value, which is clinically possible if only relatively mild complications are to be expected. However, if an overdose would cause severe consequences, a large factor has to be determined in order to keep the dose below the required limit, which is shown in Figure 2.6 (b).
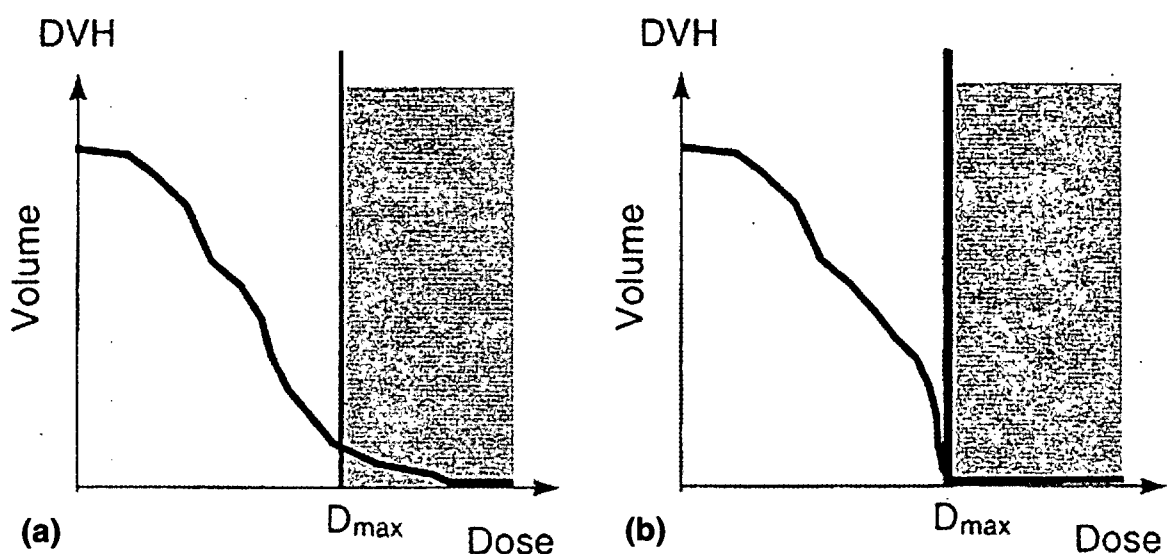
Figure 2.6 *Application of maximal dose constraints in critical structures.* (a) *Using a small penalty factor permits some overdose beyond the threshold value D_{max}.* (b) *A large penalty factor forces the optimization to keep the dose below the required limit.*

16

The maximal dose constraint is not appropriate when sparing an organ at risk that exhibits a large volume effect, as it is found in the lungs, for example. Their complication probability does not only depend on the dose level, but also on the respective affected volume. In such cases the use of DVH constraints is indicated [Spirou and Chui 1998, Gustafsson 1994a]. They can be illustrated as points with the coordinates (D_{max}, V_{max}) in the histogram, as depicted in Figure 2.7; i.e., the volume enclosed by the isodose surface of D_{max} has to be kept below the required value V_{MAX}. In most cases, the application of multiple DVH constraints for each structure is necessary to achieve satisfying results.
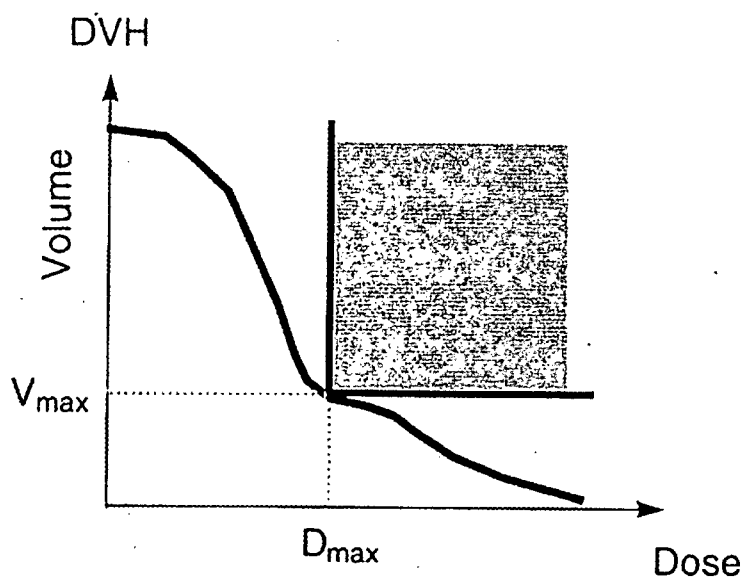
Figure 2.7 *Structures showing large volume effects are more effectively spared by the use of DVH constraints. They prevent the curve from exceeding the point (D_{max}, V_{max}).*
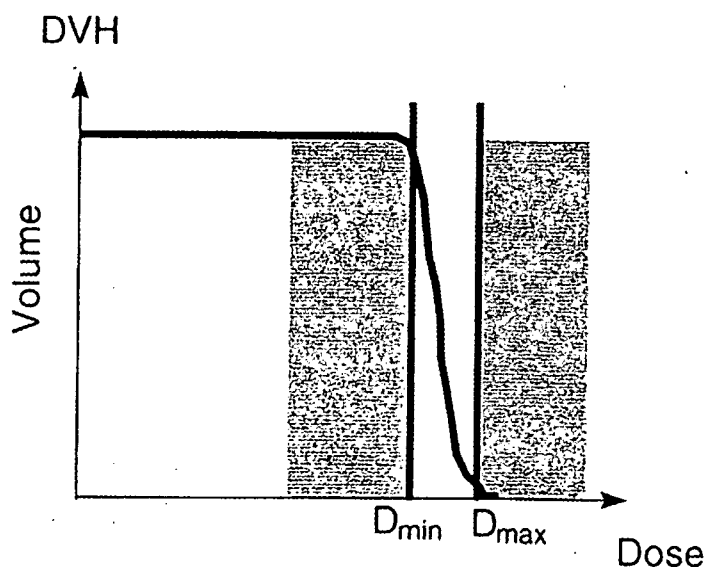
Figure 2.8 *Application of minimum and maximum dose constraints for target volumes. By limiting the dose to a certain interval, the target dose inhomogeneity is controlled. The degree of violation may be regulated by penalty factors.*

The introduced concept of DVH constraints is also applicable for target volumes, for which usually minimum and maximum dose constraints are defined. They force the tumour dose to a certain interval and are consequently limiting the target dose inhomogeneity, see Figure 2.8. Modern treatment planning systems also allow the specification of a third constraint within the dose interval, requiring a minimum volume (e.g. 95%) covered by the so-called prescription isodose surface.

2.4.2 Optimization Algorithms

Between the inverse treatment planning problem in IMRT and the image reconstruction process applied in computer tomography (CT) a certain analogy is obvious. In CT, from measured x-ray projections of the patient under a large number of angles the underlying density distribution in transverse slices is calculated. The corresponding task in IMRT is to determine the beam profiles for a number of angles, yielding a desired dose distribution. Thus, the two procedures can be considered as mirror images of each other. As a consequence the analogy has been used to develop direct solutions of the inverse problem in IMRT treatment planning [Cormack 1987, Bortfeld *et al* 1990]. However, by these analytical methods beam profiles with negative intensities are likely to be generated, which evidently are not applicable physically. This problem arises from the fact that a single voxel cannot be irradiated without "unintentionally" delivering dose to other voxels that should be subtracted to reach the ideal distribution. The negative intensities may be removed by simply resetting them to zero or by adding a constant beam profile in order to yield nonnegative values. However, due to these modifications the resulting dose distribution will not correspond to the ideal (i.e. prescribed) one anymore.

In fact, a true inverse solution is physically impossible for the most cases. Thus, the direct calculation methods have not been established in modern IMRT treatment planning, which is mainly based on iterative procedures nowadays, as described in the following sections. Still, the analytical solutions can help to find an initial guess for optimization iterations.

2.4.2.1 Deterministic Algorithms

In this category, the modifications of beam profiles in an iteration step are defined in a deterministic way without any random components. A widely used representative of this type is the GRADIENT TECHNIQUE [Spirou and Chui 1998, Gustafsson *et al* 1994b]. Exemplarily, in Figure 2.9 an objective function is displayed of which the minimum corresponds to the optimal treatment plan, as it is the case when using the mean square deviation between actual and prescribed dose. On the x-axis, the intensity of one beam element (bixel) is plotted, which is just a small fraction of the whole optimization search space with typically around 10,000 bixels. With x_0 being the value of the initial guess when starting the optimization, the new (and improved) value x_1 is found in the first iteration by subtracting an amount which is proportional to the gradient of the objective function at x_0. Analogously, x_2 is found by the calculation of the gradient at x_1 in the second iteration, etc. As the trend of the objective function becomes more and more flat, the step size per iteration decreases correspondingly, until the process is stopped when arriving at the minimum where the gradient and consequently the step size are zero.
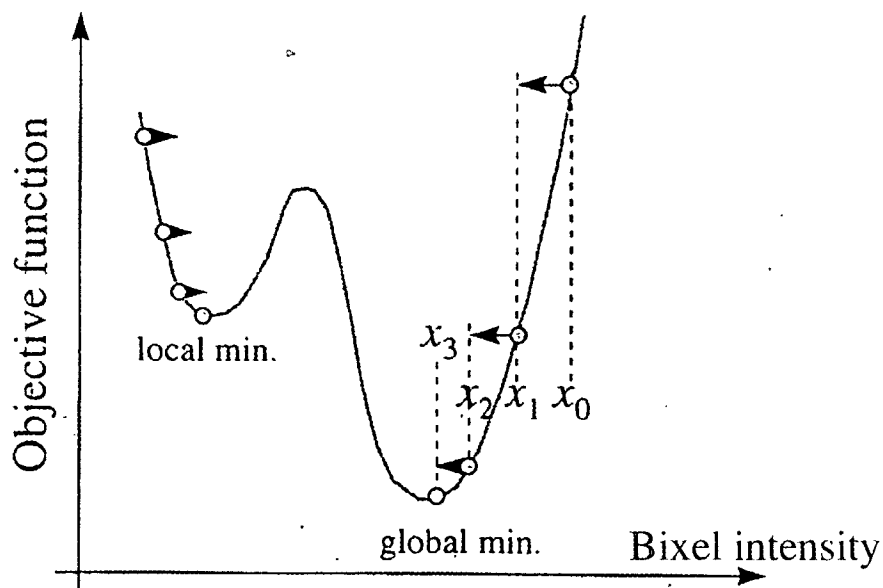
Figure 2.9 *Principle of the gradient optimization technique. The curve indicates the graph of an objective function plotted versus the intensity of a single bixel, with the optimal treatment plan corresponding to the global minimum. When starting from x_0 the algorithm iteratively follows the gradient until the latter becomes zero at x_3. However, if the procedure is started at the left-hand side, the algorithm gets trapped in a local minimum that does not represent the optimal solution.*

The main advantage of the gradient technique is its calculation speed, as typically 100 iterations suffice to approximate the minimum. On the other hand, there is an inherent possibility to miss the optimal treatment plan, because the algorithm may be trapped in a local minimum of the objective function, as it is shown on the left side of Figure 2.9. Since here the gradient is zero, there is no chance to escape and to reach the global minimum. However, the relevance of these local minima has been described as not critical by Bortfeld (1999), when optimizing only the beam intensities. First of all, it has been proven that for least squares objective functions based on minimal and maximal dose constraints local minima do not exist [Deasy 1997]. Second, by using analytical methods in order to derive an initial guess for the iteration process, the starting point will be set not too far from the global minimum, avoiding the appearance of local minima on the optimization path. And finally, in many cases the value of an objective function at local minima does not significantly differ from its value at the global minimum, providing good results even though the algorithm has been trapped.

Since the objective functions can show very flat minima in some cases, the solutions may be non-unique, with many different beam profiles generating the same quality of the treatment plan. This aspect is addressed by the so-called MAXIMAL ENTROPY optimization, which chooses the beam profiles characterized by maximal entropy, practically corresponding to maximal smoothness [Wu and Zhu 2001]. The mathematical implementation is similar to the gradient method. However, the maximal entropy optimization is based on multiplicative instead of additive corrections of bixel intensities, with the factors depending primarily on the ratio of prescribed and actual doses.

In the MAXIMAL LIKELIHOOD optimization, the maximal entropy procedure has been extended by a penalty technique in order to consider constraints in a flexible way [Llacer 1997]. Both, the entropy and likelihood optimization methods need a number of iterations which is in the same order of magnitude as for the gradient technique, however they are slightly slower.

For optimization problems with linear objectives and constraints LINEAR PROGRAMMING algorithms are available [Rosen *et al* 1991]. These are mathematically investigated in detail, with multiple different applications. However, it is often difficult or impossible to express clinical criteria in a linear form. Thus, the linear optimization approach is not widely used in IMRT calculations.

2.4.2.2 Stochastic Algorithms

In these algorithms, the beam profile intensities are modified iteratively by randomized steps in the search space. The main advantage of this technique is the possibility to escape from local minima. In this category the most widely used algorithm is the so-called SIMULATED ANNEALING method [Webb 1991, Morrill *et al* 1991]. Originally, the term annealing has been used for a procedure by which materials are rapidly heated before being slowly cooled down in order to reach an optimal crystal state. Analogously to this technical process beam profiles in a treatment plan can be optimized. The average size of random steps per iteration is determined by the "temperature", which also controls the probability that a worse plan is accepted temporarily. This may occur if a random step leads to a higher value of the objective function than the previous one. Due to this behaviour the simulated annealing algorithm offers two ways out of local minima, which are both illustrated in Figure 2.10. It can climb up the nearest hill to reach the next deeper valley (2) or it can escape by tunnelling through the hill (1), which simply corresponds to a relatively large modification step.
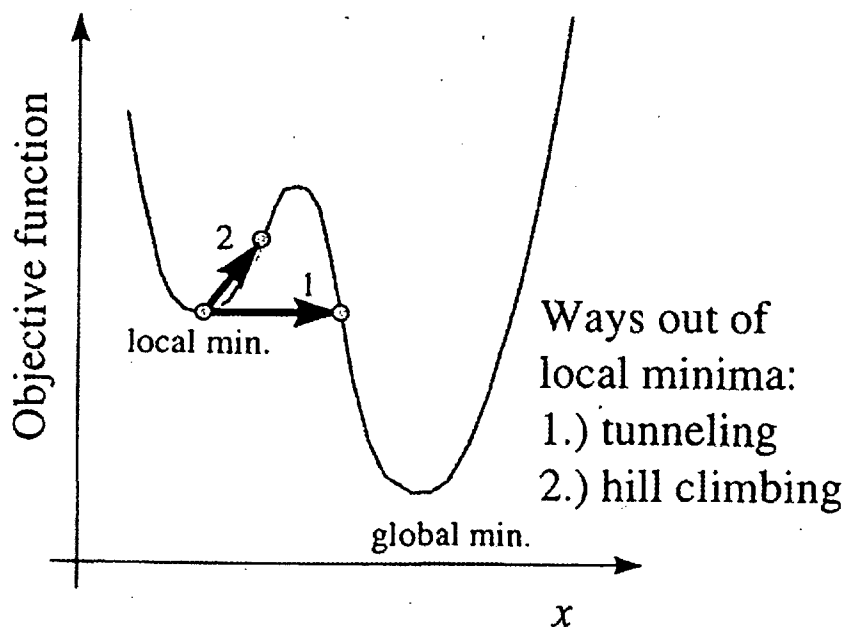
Figure 2.10 *Using stochastic algorithms, offers the possibility to escape from local minima by two ways. With a large modification step the algorithm can tunnel trough the hill (1), or it can climb up the nearest peak by temporarily accepting worse plan solutions (2).*

During the first iterations the temperature is high, enabling large steps through the search space and providing a significant probability for the acceptance of worse treatment plans (compared to previous solutions). This helps to find the coarse

direction towards the global minimum. With the optimization iterations proceeding, the temperature decreases steadily, resulting in smaller steps and lower probabilities for hill climbing and tunnelling. In the final phase at a very low temperature, the simulated annealing method resembles the gradient technique, i.e., the algorithm moves downhill towards the closest minimum, which is the global one in most cases.

Apart from the possibility to leave local minima with a certain probability, the simulated annealing optimization is very slow compared to the gradient technique, as the number of iterations necessary to reach the minimum is larger by orders of magnitude. This is explainable by the random nature of the search process, since a lot of iterations are done in wrong directions until the algorithm tends towards the final solution. The problem is addressed by the so-called FAST SIMULATED ANNEALING [Mageras and Mohan 1993], in which the temperature is cooled down more quickly to reduce the number of iterations. Additionally, artificial large steps have to be applied occasionally during the optimization to prevent an increasing risk of getting trapped in local minima. However, even the fast simulated annealing approach cannot reach the gradient methods in terms of calculation speed.

In GENETIC ALGORITHMS the natural process of evolution is simulated [Ezzell 1996]. Each treatment plan is considered as an individual whose fitness is defined by certain criteria. During the optimization procedure reproduction operators are employed, with the fertility depending on the fitness. Although in analogy to the simulated annealing method many bad treatment plans are generated temporarily, the optimal solution may be found by these simple rules. However, the application of genetic algorithms in IMRT is still under development.

2.4.3 Leaf Sequence Generation

If a conventional MLC is used to deliver IMRT treatments, the ideal beam profiles calculated by optimization modules have to be translated into leaf prescriptions. Various algorithms are available to perform the process of leaf sequencing, in which either MLC shapes for SMLC-IMRT [e.g., Galvin et al 1993, Bortfeld et al 1994b] or trajectories for DMLC-IMRT [e.g., Spirou and Chui 1994, Dirkx et al 1998] are determined. The main challenge for sequencing algorithms is to find leaf configurations by which the optimal dose distribution is resembled as closely

as possible, being practically realizable at the same time; i.e., contiguous leaf prescriptions have to be generated that do not violate any mechanical restrictions of the local MLC. In SMLC-IMRT, the algorithm should also tend to minimize the number of segments in order to keep the beam-on time and the number of MU as low as physically achievable. Additionally, the MLC shapes ought to be smooth as far as possible and must not under-run a certain opening size, which helps to avoid dosimetric uncertainties. Sequencing algorithms of high quality also try to minimize the "tongue-and-groove" effect, described in the following section.

2.4.3.1 Tongue-and-groove Effect

In order to minimize interleaf leakage, the vertical sides of adjacent leaves in commercial multileaf collimators show various stepped designs. As exemplarily depicted in Figure 2.11 (a), the leaves interlock like tongue and groove, thus significantly reducing leakage radiation [Georg 1997a]. However, at the edges of irregularly shaped segments either the tongue or the groove may get projected into the open part of the field, leading to under-dosed match-lines between adjoining segments. In Figure 2.11 (b), the resulting fluence profile is illustrated with a single leaf pair open, while in (c) the sum of separate exposures from retracting adjacent leaves is displayed, where the tongue-and-groove effect appears at the intersection area.

This behaviour is not at all or at least not sufficiently taken into account by the dose calculation algorithms in the most treatment planning systems, leading to systematic deviations between calculated and measured dose distributions [Chui et al 1994]. The incidence of tongue-and-groove effects is yet a result of the leaf sequencing procedure and cannot be influenced by the user. Thus, it is one of the most important reasons for the application of patient specific verification programmes, as described in CHAPTER 6. On the other hand, it has been shown that for IMRT treatment plans with five or more beam directions the significance of tongue-and-groove effects will be much less dramatic than displayed in Figure 2.11 (c) [Deng et al 2001]. This is due to smearing effects of the individual fields, allowing clinically acceptable IMRT deliveries modulated by conventional MLCs.

**Cross-section
of MLC leaves**

(a)

**Fluence Profile:
Single Leaf open**

100%

(b) 14%
2%

**Fluence Profile:
Sum of separate
exposures from
retracting adjacent
leaves**

102%

28%
16%
(c) 4%

Tongue-and-groove
effect.
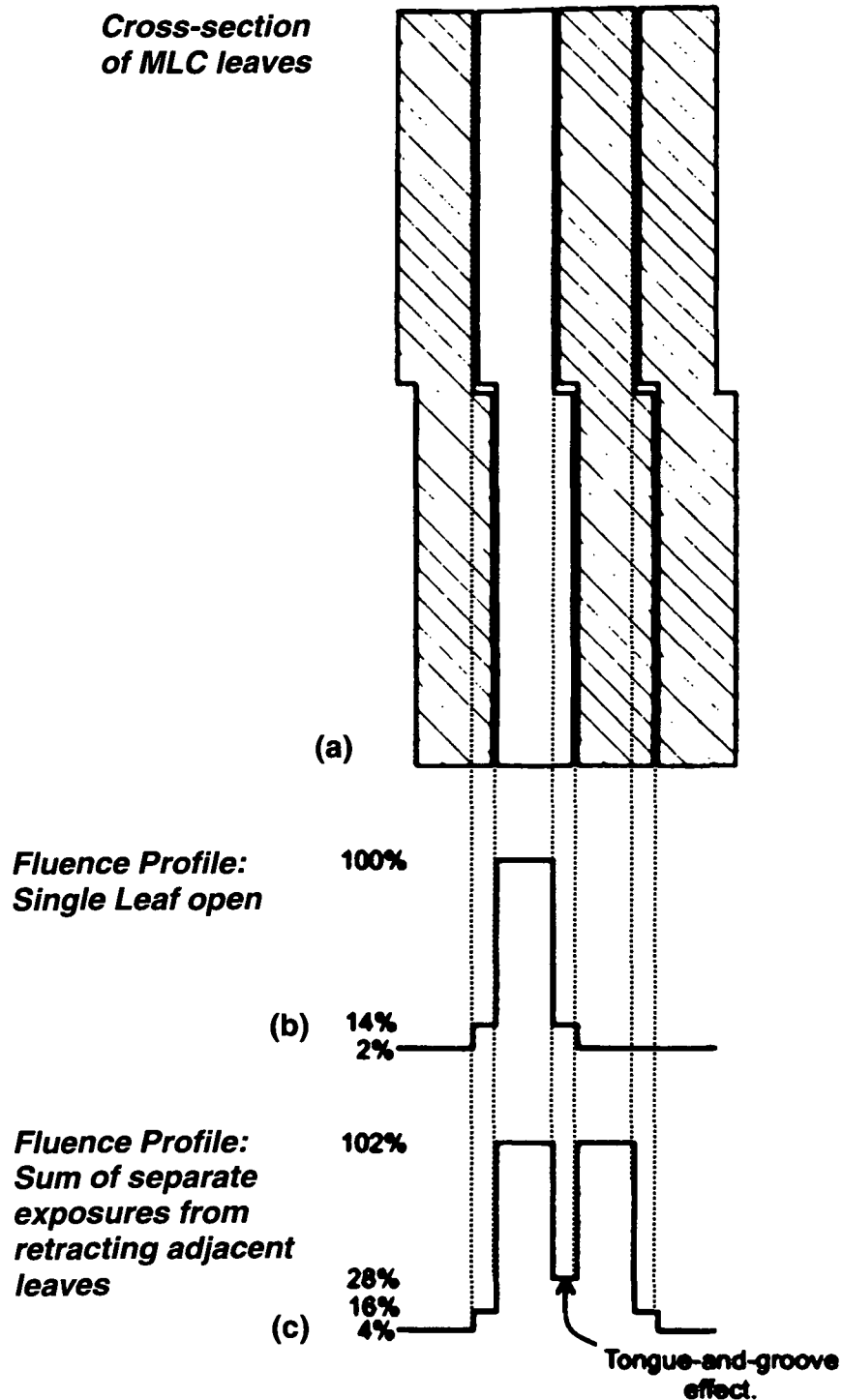
Figure 2.11 (a) *Typical cross-section of MLC leaves, showing the tongue-and-groove leaf side design to reduce leakage radiation.* **(b)** *Fluence profile of a single leaf pair opened.* **(c)** *Fluence profile generated by the sum of separate exposures from retracting adjacent leaves, with the tongue-and-groove effect appearing as under-dosed region at the leaf intersection area.*

24

2.4.4 Beam Number and Orientation

The optimization of beam incidence directions is a topic of its own. As thoroughly explained in the previous sections, the optimal beam intensity patterns have to be found within a search space comprising a large number of degrees of freedom. If in addition the beam directions are not predefined by the user but optimized by computer algorithms, the domain of search grows exponentially, leading to drastically increased calculation times which are clinically hardly acceptable, if at all. Thus, program modules optimizing the number and orientation of IMRT beams are mainly used for research purposes.

A systematic scientific investigation of this subject was carried out by Stein *et al* (1997) with the following results. The minimum required number of equiangular beams depends on the prescription dose level in the target, i.e., the larger the ratio of tumour dose and tolerance levels of the surrounding tissue, the more beams are needed in order to yield a satisfying sparing effect in organs at risk. Furthermore, target dose homogeneity is improved by adding incidence directions. The optimization of beam orientations is most valuable for a small number of beams (not more than five directions), as the benefit diminishes rapidly for higher numbers. In other words, for an exemplary configuration of seven different gantry angles it is sufficient to apply equiangular spaced beams [Bortfeld and Schlegel 1993], since the quality of the treatment plan cannot be significantly improved by the use of optimized beam directions. Generally, it is advisable to use odd numbers of beams in order to prevent opposing fields by which the intensity optimization algorithm would lose some of its dose shaping possibilities. In contrast to conventional conformal radiotherapy, IMRT beam directions through critical structures are preferable as they provide a larger flexibility to manipulate dose distributions by reducing the intensity of respective rays.

2.4.5 The Helax-TMS Optimization Solution

The treatment planning system Helax-TMS (Nucletron, Veenendaal, The Netherlands) offers an integrated optimization module for the delivery of

SMLC-IMRT. The system is able to search for optimal intensity profiles generating a desired dose distribution and to translate them to MLC sequences, while the beam number, directions of incidence, and beam qualities have to be defined by the user. In the following a brief summary of the main features in the optimization algorithm is given. The reader interested in more mathematical and software-related details may be referred to the system's documentation [Helax AB 2000].

2.4.5.1 The Objective Function

In Helax-TMS, the clinical goals of IMRT treatment plans are defined by the user via the specification of dose-volume constraints, both for target structures and OAR. However, they are not applied explicitly in the optimization, but transformed to several parameters like the mean target prescription dose $\overline{D}_i^T$, which is the mean value of minimum and maximum dose-volume constraints for a target indexed i. The importance weights of different structures are also derived from dose-volume constraints, if the algorithm is driven in the "target primary feasibility" mode, while they can be defined by the user in the "weighted feasibility" mode.

The objective function F that has to be minimized is determined as a subtraction of two terms, representing the Target(s) and the Critical structures (OAR), respectively:

$$F(D) = T(D) - C(D) \tag{2.1}$$

with D being the calculated dose distribution:

$$D = \bigcup_i \bigcup_j D_{i,j} \tag{2.2}$$

for each volume of interest (VOI) with index i, containing a number of dose calculation voxels indexed j. To obtain a sufficient number of voxels in VOI of different size, they are distributed according to the quasi-random method [Press and Teukolsky 1989, Niemierko and Goitein 1990], with a default number of 1500 per volume.

The target and critical structure terms in (2.1) can be separated into sums of individual volumes:

$$T = \sum_{i=1}^{T'} T_i , \qquad C = \sum_{i=1}^{C'} C_i \qquad (2.3)$$

where T' and C' indicate the number of targets and critical structures involved in the optimization, respectively. The summands T_i are proportional to the mean square deviation between actual dose and mean target prescription dose:

$$T_i \propto w_i^T \sum_j v_{i,j} (D_{i,j} - \overline{D}_i^T)^2 \qquad (2.4)$$

with w_i^T being the importance weight of target i and $v_{i,j}$ the volume of dose voxel (i,j).

For critical structures, the goal is to reduce the dose as much as possible compared to $\overline{D}$, which is the maximum value of mean target prescription doses $\overline{D}_i^T$ among all targets. For the definition of C_i in the quadratic objective function two possibilities have to be considered:

$$C_i \propto p \cdot w_i^C \sum_{j|D_{i,j}<\overline{D}} v_{i,j} (D_{i,j} - \overline{D})^2 - w_i^C \sum_{j|D_{i,j}>\overline{D}} v_{i,j} (D_{i,j} - \overline{D})^2 \qquad (2.5)$$

In the desired case of $D_{i,j}$ being smaller than $\overline{D}$, a positive contribution to C_i is added, thus decreasing the value of the objective function according to (2.1). Correspondingly, the negative term in (2.5) is applied if $D_{i,j}$ exceeds the level of $\overline{D}$, leading to an increase in the objective function. The relative importance weights of respective critical structures are represented by the factors w_i^C. In addition, the so-called penalty coefficient p has been introduced to the first term in (2.5), providing a controlled reduction of the critical structure contribution to the objective function if target requirements are not fulfilled. In case of intersecting volumes of different types, the corresponding voxels are accounted for only in the target term, but not in the critical structures.

2.4.5.2 The Optimization Algorithm

The optimization method implemented in Helax-TMS is based on the gradient of the objective function, which is used to determine the search direction for an improved solution in an iterative way. It is mainly based on the methods described by Gustafsson *et al* (1994b, 1995), with slight modifications necessary in a clinical implementation. Before starting the actual optimization procedure, an initial variable estimation has to be performed. The beam cross-sections are subdivided to bixels, in which the intensity variables are set to unity if their relative contribution to the target dose is larger than 3%, otherwise the variable is set to zero. If a bixel delivers less than 1%, it is completely excluded from the optimization process to enhance calculation speed. Finally, the beam weights are re-scaled in order to achieve a sufficient dose level in the target(s).

The optimization workflow consists of two nested loops. In the minor loop, ten consecutive iterations are performed using the same value of the penalty coefficient p. Furthermore, during the minor loop head scatter is not re-calculated and the modulation matrix is not converted into MLC segments, as the modifications are assumed to be of small magnitude. Only at the end of the minor loop (i.e. after ten iterations), a full dose calculation is performed, including segment generation and head scatter calculation. Subsequently, the major loop is entered in which the penalty coefficient p is adjusted, depending on the violation of target requirements. In many cases, p will be smaller than unity and is further decreased in the major loop in order to limit the impact of critical structures to the objective function. However, if the target constraints are well fulfilled, the penalty coefficient may also be increased to direct the emphasis towards the organs at risk.

The optimization engine driving the actual search for new and improved solutions is the so-called L-BFGSB algorithm, which has been developed by Byrd *et al* (1995). It is a limited memory, variable metric (or quasi-Newton) algorithm and relies on the calculation of (exact) first order derivatives (i.e. the gradient) of the objective function, whereas the second order derivative is estimated from the use of the m latest calculated gradients. In the Helax-TMS implementation m has been set to nine.

The optimization procedure is terminated if either the maximum number of iterations is reached or the maximum calculation time is exceeded, which are set by

28

default to overall 100 iterations and three hours, respectively. However, also the optimization engine itself can stop the process, if in case of convergence the numerical termination criterion is fulfilled, which in fact is very rare. More frequently, the abnormal termination occurs, indicating that the objective function still can be reduced while the optimization engine is unable to find a search direction towards an improved solution. This is due to the fact that the gradients can only be calculated approximately, with generally negligible errors. However, close to an optimal solution the error magnitude starts to play a role, possibly leading to an abnormal termination.

The gradient calculation can be separated in two distinct parts, which are the objective function gradient with respect to the dose distribution and the dose distribution gradient with respect to the optimization variables. The gradient is determined for each variable independent of the others. Thus, it is possible to isolate the calculation to one particular variable x:

$$\frac{\partial F}{\partial x} = \sum_i \sum_j \frac{\partial F}{\partial D_{i,j}} \frac{\partial D_{i,j}}{\partial x} \tag{2.6}$$

While the determination of $\partial F / \partial D_{i,j}$ for all voxels (i,j) is necessary only once per iteration and can be performed in a straightforward manner [cf. (2.4) and (2.5)], the calculation of $\partial D_{i,j} / \partial x$ turns out to be very complex, calling for two approximations. The patient is assumed to consist of water equivalent material only and the treatment head scatter is supposed to be constant. It has to be noted that these assumptions are just applied in the gradient computations, but not in the actual dose calculations.

2.4.5.3 The Leaf Sequence Generation

In the Helax-TMS implementation, the conversion of a calculated modulation matrix into a sequence of MLC segments is mainly based on the description by Bortfeld *et al* (1994b). It is performed each time the minor loop is completed, thus providing an optimization progression that is compatible with the local collimator equipment.

29

The modulation matrix is always orientated the same way as the MLC, with the bixel size in the direction perpendicular to leaf movement corresponding to leaf width, while in the movement direction the default bixel size of 5 mm may be changed by the user before starting the optimization. To facilitate the leaf position determination, the continuous modulation in the matrix is sampled into a number of equispaced modulation levels J, with a distance of Δm:

$$\Delta m = \frac{m_{MAX}}{J} \tag{2.7}$$

where m_{MAX} is the maximum modulation value in the respective matrix. The number J is set to 10 by default, but may be edited by the user as well. In Helax-TMS the bixel values are modified to the nearest level, therefore they can either be increased or decreased, keeping the sampling bias always below $\Delta m / 2$. From the discretized modulation matrix, for each leaf pair the positions are identified by a method resembling the "sliding window" technique, i.e., the opening between the right (leading) leaf and the left (trailing) leaf is sweeping across the area to be modulated by single steps.

In the next phase, the individual leaf positions are re-organized and composed to MLC segments. By matching as many instances of adjacent leaf pairs as possible, it is feasible to maximize the field size per segment, which is necessary for dosimetric reasons, as described in section 4.4. The number of segments will be minimized simultaneously, enhancing the treatment efficiency, while in addition the influence of tongue-and-groove effects (see section 2.4.3.1) can be considerably reduced. Most important, the segments have to be physically deliverable taking into account the local MLC restrictions, as there are:

- minimum and maximum positions of a single leaf
- minimum separation between the leaves in a leaf pair
- minimum separation between a leaf in one leaf bank and an adjacent leaf in the opposing leaf bank or maximum over-travel
- maximum separation between two adjacent leaves in one leaf bank
- maximum separation between any two leaves in the same leaf bank

In the final phase, the algorithm attempts to reduce the number of segments in order to follow the user-defined maximum number per beam. If two or more segments are sufficiently equivalent, i.e., if the difference between the same leaf in two segments and the sum of differences between leaves in two segments are not bigger than certain values set by the user, they are replaced by a single segment with a relative weight equal to the sum of relative weights of the superseded segments. Furthermore, segments with geometrical dimensions smaller than required by the user will be deleted. If afterwards the number of segments is still too large, the smallest ones are discarded, where in this case the term "size" is defined as the open area times the relative weight. Finally, the weights of the remaining segments are refined and the jaws positioned at the outermost limits of the open area for each segment.

2.5 HISTORY OF IMRT

before **1960**	primitive IMRT with blocks, wedges and compensators
1960	gravity oriented devices
1982	mathematical solution for wedged and blocked one-dimensional intensity modulation (IM)
1988	general concept of inverse planning for IM
1989	simulated annealing proposed for optimization
1991	principle of segmented field delivery
1992	principle of dynamic MLC delivery
	serial tomotherapy delivery for IMRT
1993	conceptual design of helical tomotherapy
1994	clinical application of segmented field delivery
	dynamic field delivery in clinical application
1995	concept of intensity modulated arc therapy (IMAT)
2000	robotic Linac for IMRT
since **2000**	publications on clinical experiences and outcome of IMRT and commercial "turn-key" solutions available
2001	IMAT in clinical application

Table 2.1
Milestones in the historical development of intensity modulated radiotherapy

In Table 2.1, the milestones in the historical development of intensity modulated radiotherapy are listed, based on Georg (2003) and Webb (2001). Obviously, most of the techniques applied in modern IMRT have been practically introduced within the nineteen nineties, mainly based on mathematical concepts derived in the eighties. Nowadays, the main focus is put on the refinement of the presented concepts as well as on the improvement of their clinical efficiency and dosimetric steadiness.

2.6 PRACTICAL CONSIDERATIONS

As previously mentioned, the term IMRT stands for much more than just the application of non-uniform beam profiles. In fact, the entire treatment chain in radiotherapy is affected and has to be adapted to the needs of IMRT as described by Ezzell *et al* (2003) and displayed in Figure 2.12:
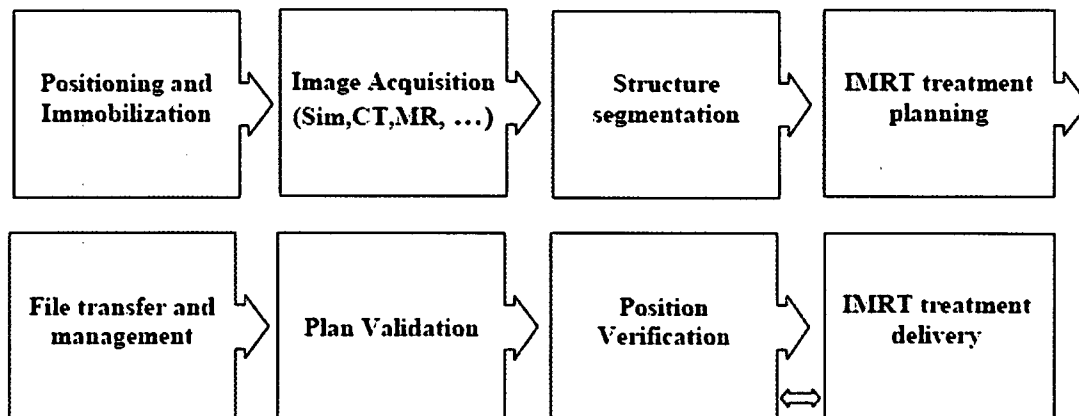
Figure 2.12 *Schematical overview of the IMRT treatment chain. Although similar items are also found in conventional CRT, the workflow had to be extended to meet the complex demands of IMRT.*

Prior to image acquisition, special interest has to be paid to patient positioning and immobilization. IMRT treatment plans are typically characterized by the appearance of steep dose gradients, especially in the vicinity of organs at risk. Thus, even small geometrical differences between the actual and the planned patient position may result in significant overdoses to critical structures. Furthermore, the benefit of IMRT can be maximized by reducing the geometrical safety margin around

target structures. This is yet allowable only if the patient is immobilized rigidly, which is achievable by the use of body-frames and fixation masks. In addition, stereotactic localizers and markers help to provide a reproducible patient positioning (see also sections 7.2 and 7.3).

In IMRT, the segmentation of organ structures plays a crucial role. The target(s) have to be defined as precisely as possible to enable the sparing of neighboured OAR. They are often separated to sub-volumes being irradiated to different dose levels. Ideally, this task is performed by a team of members of different oncological faculties, based on international recommendations of several groups, as for instance for the head and neck region [e.g., Gregoire and Maingon 2004, Gregoire *et al* 2003a, 2003b]. For the delineation of critical structures, there is the strict requirement to prevent intersections of clinical target volumes (CTV) and OAR, since a certain voxel can only belong to either the tumour or the critical organ. However, for planning target volumes (PTV) overlaps are allowable and even frequently unavoidable as safety margins are simply needed for geometrical reasons according to ICRU reports 50 and 62 [International Commission on Radiation Units and Measurements 1993, 1999]. In order to facilitate these segmentation efforts, enhanced methods in image acquisition are needed. The application of multi-modality imaging, mainly including computed tomography (CT), magnetic resonance imaging (MRI), positron emission tomography (PET), single photon emission computed tomography (SPECT), and ultrasound (US) is strongly advisable, depending on the respective tumour site. In modern treatment planning systems, the generated images of different types can be fused manually or automatically, combining the maximum information from the benefits of each imaging modality.

As thoroughly explained in the previous sections, the IMRT treatment planning procedure significantly differs from conventional methods in many aspects. The user has to enter constraints, either minimum and maximum or arbitrary dose-volume values, from which the optimization process can derive an objective function and start the searching for an optimal plan solution. However, the translation of medical requirements to simple numbers probably is one of the most delicate features in IMRT, as the complexity of biological correlations between different organ structures can never be sufficiently covered by two-dimensional DVH. Thus, it is important for

the user to find a general relationship between the mathematical values entered to the system and the actual outcome which has to be re-translated to clinical terms. It can only be managed by experience and needs to be done separately for different tumour entities.

Another interesting issue is the method of dose calculations used within the optimization procedure. Apparently, for iterative planning methods as widely performed in IMRT a compromise has to be found between calculation speed and accuracy. Thus, commercially available optimization modules are generally based on pencil beam (PB) calculations [Laub *et al* 2001] with path length corrections accounting for varying density. The more precise superposition/convolution (SC) methods still are too slow to be clinically applied in optimization calculations, although they provide improved dosimetric reliability particularly in lung cases, but also in head-and-neck treatments [Scholz *et al* 2003]. However, procedures are being developed that utilize the speed of PB algorithms, yet achieve the accuracy of optimizing based upon SC algorithms via the application of dose correction matrices [Siebers *et al* 2002]. At least, modern treatment planning systems offer the possibility to recalculate IMRT plans by SC methods after the performance of PB optimizations.

Compared to conventional 3D-CRT, IMRT treatment plans are generally characterized by an increased dose inhomogeneity within the target(s). Although the intensity modulation in principal would have the ability to decrease the target dose heterogeneity, the latter usually is enlarged in clinical cases. This is caused by the influence of OAR, which can only be substantially spared if a larger dose range in the target(s) is accepted. Frequently, the DVH indicates the prescribed dose level covering not the whole target but some percent less. In such cases, the locations of under-dosed regions and the amount of under-dosing have to be considered, as there certainly is a difference if a cold spot is found at the edge of the target or in the centre of the tumour. However, it is a medical decision whether the appearance of hot and cold spots is clinically acceptable, which needs to be made individually for each patient case. On the other hand, it has to be noted that despite of the intensity modulation in photon beam radiotherapy certain dose distributions are not achievable for physical reasons, since the integral dose can only be redistributed rather than reduced.

Due to the relatively inefficient use of MU in IMRT compared to conventional radiotherapy, the beam-on time is increased by a factor between roughly 1.5 and 10, depending on the IMRT delivery technique applied. Since the accelerator head leakage contribution is proportional to the number of MU, it is enlarged by the same amount. This has to be considered in the treatment room shielding design [Mutic *et al* 2001] and for the estimations of whole body doses to which the patients are exposed during IMRT treatments. However, due to its energy dependence the secondary radiation portion can be minimized by choosing beam qualities of less or equal 10 MV [Followill *et al* 1997].
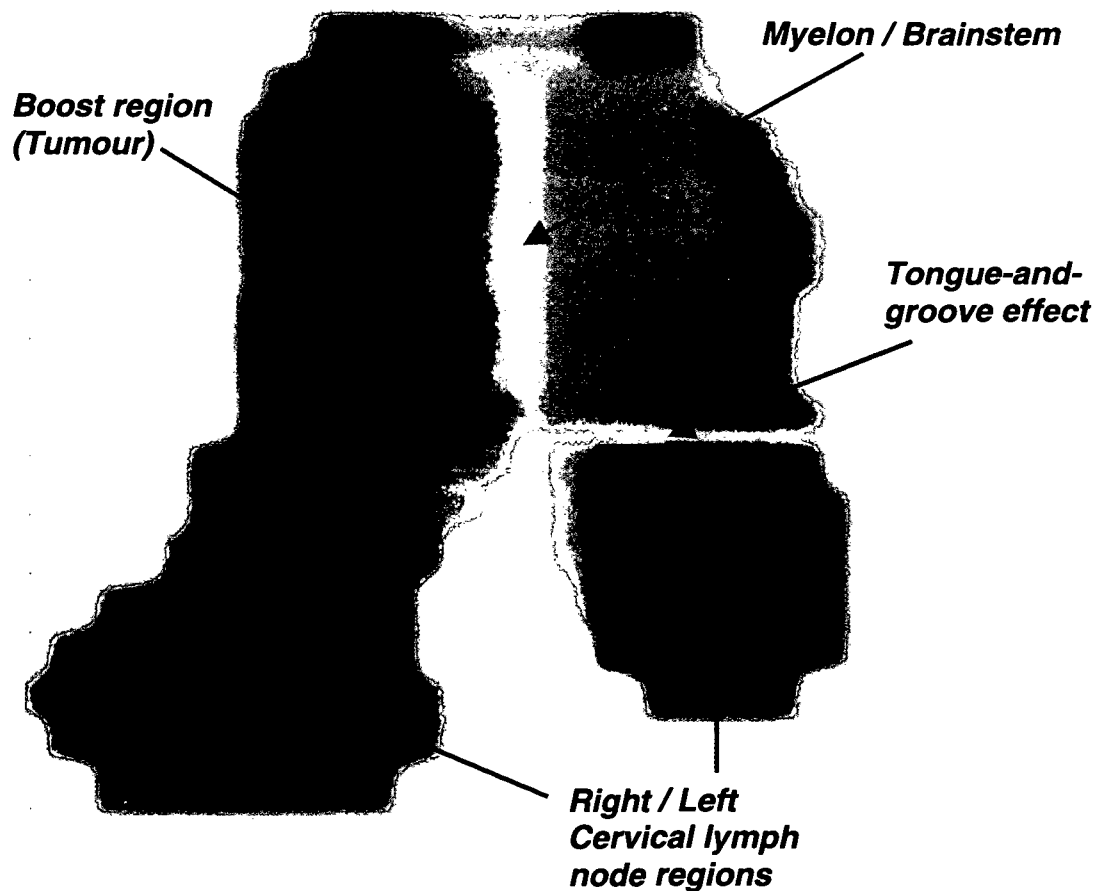
Figure 2.13 *Orthogonal film exposure taken from the anterior field of a head-and-neck treatment, which was performed as simultaneous integrated boost. 60 Gy were applied to the tumour, while the large target was irradiated up to 50 Gy, including the ambilateral cervical lymph node regions. The sparing of myelon and brainstem is visible as relatively bright area, while the horizontal stripe is generated as dosimetric artefact due to the tongue-and-groove effect. The image is digitally re-mastered in order to maximize relative contrast.*

To complete this chapter, an orthogonal film exposure of a typical IMRT beam is presented in Figure 2.13, in which some of the issues described in the sections above can be identified. The image has been digitally re-mastered in order to maximize relative contrast. It is taken from the anterior field of a head-and-neck treatment, which was performed as simultaneous integrated boost technique at the Medical University of Vienna. Thus, the tumour itself was defined as boost region, while the target also included the cervical lymph node regions right and left, with the larger volume on the tumour's side. On the other side, the influence of the tongue-and-groove effect can be detected as small under-dosed stripe. However, that did not harm the patient's treatment as it was the only beam affected by such an artefact at this position. Finally, the sparing of myelon and brainstem is visible as relatively bright zone in the centre.

Currently, clinical studies are performed in several institutions around the world to demonstrate the benefit of IMRT, which is at present one of the most complex treatment options in modern radiotherapy.

CHAPTER 3   is based on

PRE-CLINICAL EVALUATION OF AN INVERSE PLANNING MODULE FOR SEGMENTAL MLC BASED IMRT DELIVERY

Dietmar Georg[1] and Bernhard Kroupa[1,2]

[1] Division of Medical Radiation Physics, Department of Radiotherapy and Radiobiology, Medical University of Vienna, Waehringer Guertel 18–20, A-1090 Vienna, Austria

[2] Atomic Institute of the Austrian Universities, Stadionallee 2, A-1020 Vienna, Austria

Abstract:

Phantom tests are performed for pre-clinical evaluation of a commercial inverse planning system (Helax-TMS, V 6.0) for segmented multileaf collimator (MLC) intensity modulated radiotherapy (IMRT) delivery. The optimization module has available two optimization algorithms: the target primary feasibility and the weighted feasibility algorithm, only the latter allows the user to specify weights for structures. In the first series, single beam tests are performed to evaluate the outcome of inverse planning in terms of plausibility for the following situations: oblique incidence, presence of inhomogeneities, multiple targets at different depths, and multiple targets with different desired doses. Additionally, for these tests a manual plan is made for comparison. In the absence of organs at risk, both the optimization algorithms are found to assign the highest priority to low dose constraints for targets. In the second series, tests resembling clinical relevant configurations (simultaneous boost and concave target with critical organ) are performed with multiple beam arrangements in order to determine the impact of the system's configuration on inverse planning. It is found that the definition of certain segment number and segment size limitations does not largely compromise treatment plans when using multiple beams. On the other hand, these limitations are important for delivery efficiency and dosimetry. For the number of iterations and voxels per volume of interest, standard values in the system's configuration are considered to be sufficient. Additionally, it is demonstrated that precautions must be taken to precisely define treatment goals when using computerized treatment optimization. Similar phantom tests could be used for a direct dosimetric verification of all steps from inverse treatment planning to IMRT delivery.

3.1 INTRODUCTION

Intensity modulated radiotherapy (IMRT) is based on a non-uniform fluence distribution incident on the patient. Compared to 'conventional' conformal radiotherapy in which geometrical field shaping alone is applied with a uniform intensity across the field, a new degree of conformity can be achieved. Although IMRT treatment planning can be accomplished as well in a (time-consuming) trial and error forward process, modern IMRT is directly associated with computer optimization techniques to determine the fluence distribution across the target volume. These optimization modules calculate the intensity profile from clinical objectives (physical

doses or biological parameters) entered into the system [e.g., Bortfeld *et al* 1990, Niemierko *et al* 1992, Spirou and Chui 1998].

For IMRT based on computerized treatment plan optimization or inverse planning there are in-house developed and commercial systems in use at present. Among these systems, there are substantial differences in the mathematical formulation of clinical objectives as well as in the optimization/search processes [e.g., Bortfeld and Schlegel 1993, De Gersem *et al* 2001, De Neve *et al* 1999, De Wagter *et al* 1998, Gustafsson *et al* 1994b, 1995, Kallman *et al* 1992, Llacer *et al* 2001, Xing and Chen 1996]. It is even expected that their number increases and in updated software of commercial systems some algorithms will be replaced by others. Additionally, leaf sequencing methods which convert fluence maps into deliverable MLC settings or leaf trajectories, taking into account the mechanical restrictions of MLCs, become integral parts of treatment planning systems (TPSs) and are even considered during optimization [Ahnesjo and Aspradakis 1999, Bar *et al* 2001, Langer *et al* 2001, Potter *et al* 2002, Seco *et al* 2001]. IMRT delivery can be accomplished with numerous modalities, ranging from physical compensators to robotic linacs. They have been summarized in recent literature [Webb 2001, IMRT Collaborative Working Group 2001].

Computerized treatment plan optimization and inverse planning is an entirely new tool in radiotherapy. In a recent report of an IMRT collaborative working group, it has been highlighted that new techniques for commissioning and acceptance testing need to be developed. For conventional conformal radiotherapy, these tests concentrate mainly on dose calculation accuracy, which is not sufficient for optimization tools used in IMRT [Fraass *et al* 1998, Van Dyk *et al* 1993].

More complex dose calculation algorithms, such as pencil beam or superposition/convolution algorithms, are unknown to most users. There is a potential danger that, in a similar way, optimization algorithms for IMRT basically remain 'obscure'. Before using computerized treatment plan optimization, users are encouraged to learn to drive their system, to know its limitations and the influence of the system's configuration on the outcome of the optimization.

The aim of the present note is to describe a method for pre-clinical evaluation of an inverse planning system (Helax-TMS, V 6.0) for the segmented MLC IMRT delivery technique. Phantom tests are designed on the one hand to verify the

plausibility of the outcome of computerized treatment plan optimization and on the other hand to determine the impact of the system's configuration on the outcome.

3.2 MATERIALS AND METHODS

3.2.1 Treatment planning system and phantom

The TPS under investigation is Helax-TMS V 6.0 (Nucletron). For each optimization process, the user can choose between two algorithms which 'create' the objective function to be minimized: (i) the weighted feasibility and (ii) the target primary feasibility. Both methods derive their objective function from dose volume constraints for target(s) and organs at risk (OAR) based on the same mathematical formulae. However, the weighted feasibility allows relative weights to be defined for each OAR according to their importance while the target primary feasibility does not offer such a possibility but calculates relative importance factors internally. The optimization includes full head scatter and phantom scatter modelling as well as leaf sequencing. Hence the outcome is directly deliverable. Besides optimization for IMRT, the TPS under investigation offers further optimization options, e.g., wedge angles and beam weights for 'conventional' treatment plans. For more details on the IMRT optimization algorithm the reader is referred to literature [Helax AB 2000].

For all subsequent tests the fluence profiles of beams are optimized while the treatment geometry (gantry angle, collimator angle, table angle, etc) is defined by treatment planner.

All tests are performed using the pencil beam algorithm although the TPS in use offers the possibility of performing dose calculations with the more accurate collapsed cone convolution algorithm [Ahnesjo 1989]. However for IMRT optimization, the pencil beam model is used and the optimization result can only be recalculated with the collapsed cone algorithm. The effect of dose calculation accuracy on inverse planning has been the subject of a recent publication [Jeraj et al 2002].

The planning system investigated is running on an alpha station 500 (open VMS 6.2, processor DEC-alpha 500 MHz). Beam data used for dose calculations

refer to 6, 10, and 25 MV photon beams provided by an Elekta Precise linear accelerator. The mechanical limitations of the MLC (e.g., minimal leaf opening, maximum leaf overtravel) are parts of the system's configuration as well.

For the segmental MLC delivery technique the following IMRT parameters can be specified by the user in Helax-TMS: maximum number of intensity levels, maximum number of segments per beam, maximum number of iterations, minimum segment size, minimum number of leaf pairs opened per segment and number of voxels per volume of interest (VOI). The last four parameters are part of the system's configuration and cannot be easily set for each patient while the first two can even be defined individually for each beam per patient.

All subsequent tests are performed with a polystyrene multipurpose phantom (MPP). This solid MPP is a copy of the 'EC MPP' described by Bridier *et al* (2000). This phantom consists of various layers and includes inhomogeneities as well as inserts for dosimetric equipment and can be arranged in different set-ups. The outer dimensions are 20×20×20 cm^3. It is CT scanned in various configurations and CT data are transferred to the planning system for direct dosimetric verification. However, dosimetric measurements are not considered in the present work.

3.2.2 Single beam arrangements

Four specific test cases, each with a single beam arrangement, are carried out in a first stage. Test 1 is aimed at compensating for missing tissue (or oblique incidence), test 2 at compensating for inhomogeneities in lung and air, test 3 at delivering different doses in a ratio 3:2:1 to three different target volumes located at same depth and test 4 is designed to deliver the same dose to three target volumes located at different depths. For each test, target volumes of 1 cm thickness are defined in the MPP. For tests 1 and 2, the target length is 10 cm while the width is 8 cm and 7.5 cm, respectively. For tests 3 and 4, each target is 4×7.5 cm^2 with a 0.5 cm spacing. Tests 1–3 are performed in an isocentric set-up with the target centres located at depths of 3.3 cm for test 1, 10 cm for test 2 and 7 cm for test 3. Target depths in test 4 are 4 cm, 7 cm and 10 cm, with the phantom surface at 93 cm. Figure 3.1 illustrates tests 1–4.
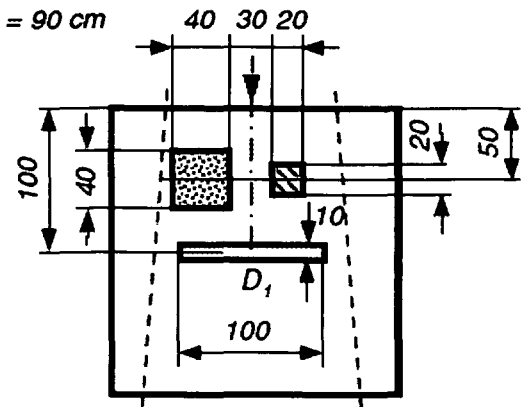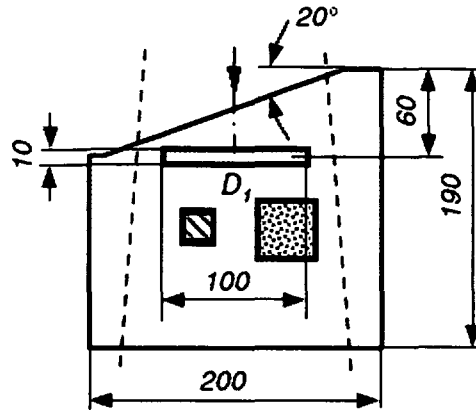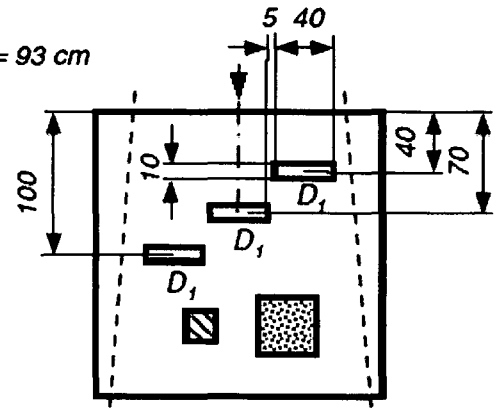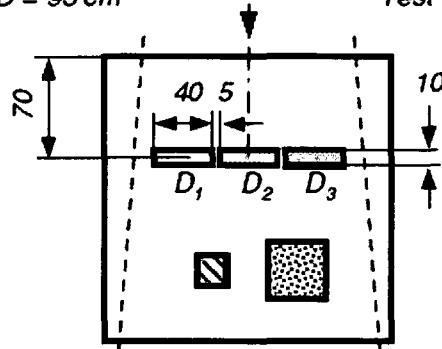
Figure 3.1 *Schematic illustration of the tests performed with a single beam to verify the plausibility of the outcome of inverse planning using either the target primary or the weighted feasibility algorithm. All dimensions are in mm. (For further explanation see text.)*

All tests are performed with the weighted feasibility and the target primary feasibility. Additionally, a manual plan based on human intelligence is made for comparison. The goal of tests 1, 2, and 4 is to deliver a dose between 94% and 106% of the target mean dose to 100% of the target volume. In test 3, target 1 should receive a dose between 106% and 94%, target 2 a dose between 71% and 63%, and target 3 a dose between 35% and 31%, when normalized to the mean dose in target 1.

In order to provide enough degrees of freedom, tests 1–4 are performed without constraints in terms of segment size and segment number. The number of intensity levels is however restricted to 10 and 1500 voxels per VOI are used for the optimization. The maximum number of iterations is limited to 100. No dose constraints are set for the 'outline structure'.

3.2.3 Multiple beam arrangements

Two tests resembling clinical relevant configurations are performed with multiple beam arrangements. Test 5 is meant to deliver a simultaneous boost. Target 1 is a cylindrical volume 8 cm in diameter and 10 cm in length, and three equally spaced beams are used. The boost target 2 is a cylinder as well, having a diameter of 4 cm and a length of 6 cm. The following dose prescription is used: 97% of boost target 2 should be covered at least with the 95% isodose surface and no more than 3% of the boost volume should receive doses higher than 105%. Additionally, 97% of target 1 should be covered with at least the 75% isodose surface. All isodose levels are normalized to the mean dose in boost target 2.

In test 6, a critical OAR is located near a concave target and five equally spaced beams are used for this arrangement. The OAR is a cylinder 4 cm in diameter and 10 cm in length. The target is half a 'doughnut' with an inner radius of 3 cm and an outer radius of 6 cm. The target to OAR distance is 1 cm. The following dose prescription is used for optimization: 97% of the target volume should be covered with at least the 95% isodose and no more than 3% of the target should receive doses higher than 105% when normalized to the mean target dose. For the OAR, the following dose constraints are defined: no more than 3% of the OAR should receive 90% of the prescribed dose and less than 50% of the OAR should receive doses higher than 50%.

For both tests, no dose constraints are set for the 'outline structure'. Figure 3.2 illustrates tests 5 and 6 resembling clinical settings. Both tests are performed for the three photon beam qualities (6, 10, 25 MV) available and for both optimization algorithms. For these clinical test configurations, a first run is performed without a limitation in terms of segment number and segment size, in a second run they are repeated with the following limitations: smallest segment size 9 cm^2 with at least three leaf pairs involved in forming a segment, maximum number of segments per beam, 15. The number of intensity levels is 10 and the number of voxels per VOI is 1500. In additional tests the last two figures are varied as well.

120°

126

40

80
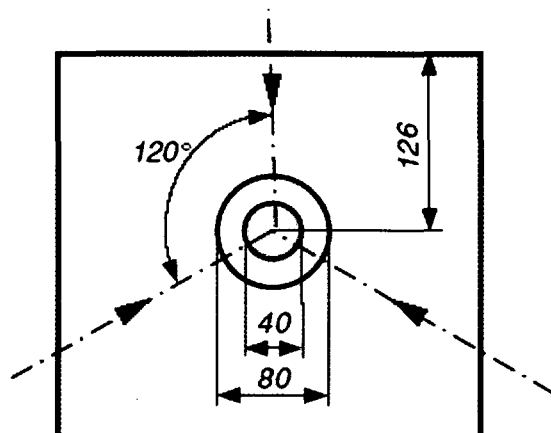
☐ Boost PTV 2

☐ PTV 1

VOI	Dose	Volume
Boost PTV 2	95 %	> 97 %
	105 %	< 3 %
PTV 1	75 %	> 97 %

72°

160

30 40

10
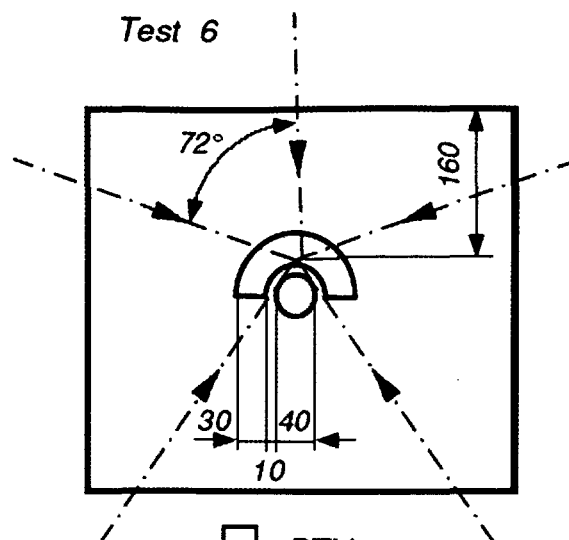
☐ PTV

☐ OAR

VOI	Dose	Volume
PTV	95 %	> 97 %
	105 %	< 3 %
OAR	50 %	< 50 %
	90 %	< 3 %

Figure 3.2 *Schematic illustration of the two clinical orientated tests. Beam incident directions are indicated by dotted lines. Test 5 resembles a simultaneous boost technique and test 6 is aimed at demonstrating the capability for conformal avoidance. All dimensions are in mm. (For further explanation see text.)*

3.3 RESULTS

3.3.1 Single beam arrangements

Table 3.1 summarizes the results of test 1 (missing tissue/oblique incidence) for a 6 MV photon beam for both optimization methods and a manual plan. Small parts of the target receive doses less than the minimum dose constraint (94%) for both computerized optimization algorithms. The isodose level fully encompassing the target is slightly higher for the weighted feasibility as compared to the target primary feasibility. Target volumes receiving higher doses than the maximum dose constraint (106%) are small and of the same order of magnitude for both optimization methods.

The same holds for the maximum dose in the target. However, using a simple wedged beam technique the manual plan could fulfil all constraints.

	Weighted feasibility	Target prim. feasibility	Manual plan
Volume D < 94 %	2 %	3 %	0 %
Minimum Dose	91 %	90 %	94 %
Volume D > 106 %	7 %	5 %	0 %
Maximum Dose	117 %	115 %	106 %

Table 3.1 *Summary of the results for the missing tissue/oblique incidence test (test 1) for a 6 MV photon beam. The minimum dose value refers to the isodose level fully encompassing the target and the maximum dose value refers to the maximum dose observed in the target.*

In Figure 3.3 profiles are shown for IM beams at 6 MV for test 2, perpendicular to the inhomogeneities through the central target plane (isocenter at 10 cm depth). For comparison, the same dose profile is presented for an unmodulated beam. The dotted lines indicate the desired dose level between 94% and 106%. Although both algorithms could fulfil the test, the dose profile obtained using the weighted feasibility algorithm is flatter compared to the one obtained with the target primary feasibility.

Figure 3.4 shows profiles for a manually optimized and the two inversely planned IM beams for test 3 at 25 MV through the central target plane (isocenter at 7 cm depth). The manually 'optimized' solution is obtained with three individually shaped and weighted segments taking into account depth-dose characteristics and output factors for the respective segments. The segment number for the two inversely planned solutions is 13 each. All three plans are able to deliver the desired dose to target 1 but only the inversely planned solutions are nearly able to completely fulfil the demands for target 2. As shown in Figure 3.4, a small volume of target 2 located near target 1 receives too high doses with the weighted feasibility while a small volume of target 2 near target 3 is overdosed by the target feasibility algorithm. With the manually obtained solution, overdosed areas are also present in target 2. Both the manual plan and the target feasibility algorithm overdose substantial parts of target 3. Although an overdosage is also present with the weighted feasibility

algorithm, this algorithm performed best for this test. The dose profile throughout target 1 is flatter than for the target primary feasibility and a steeper dose gradient between targets 2 and 3 is obtained.
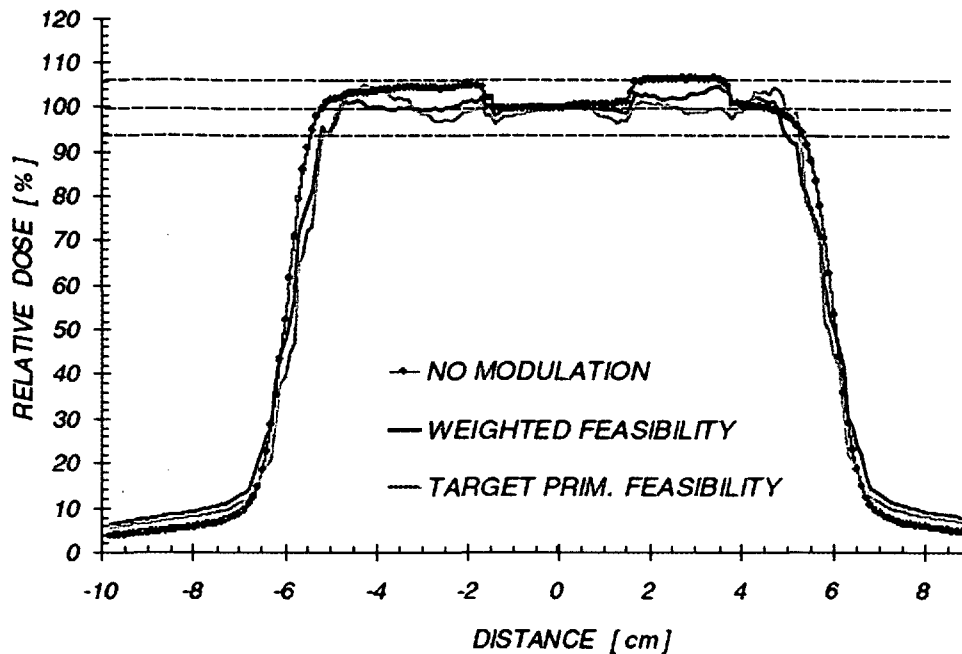
Figure 3.3 *Examples of dose profiles for test 2 for IM beams at 6 MV, perpendicular to the inhomogeneities through the central target plane. For comparison, a dose profile is presented for an unmodulated beam. The dotted lines indicate the desired dose level.*
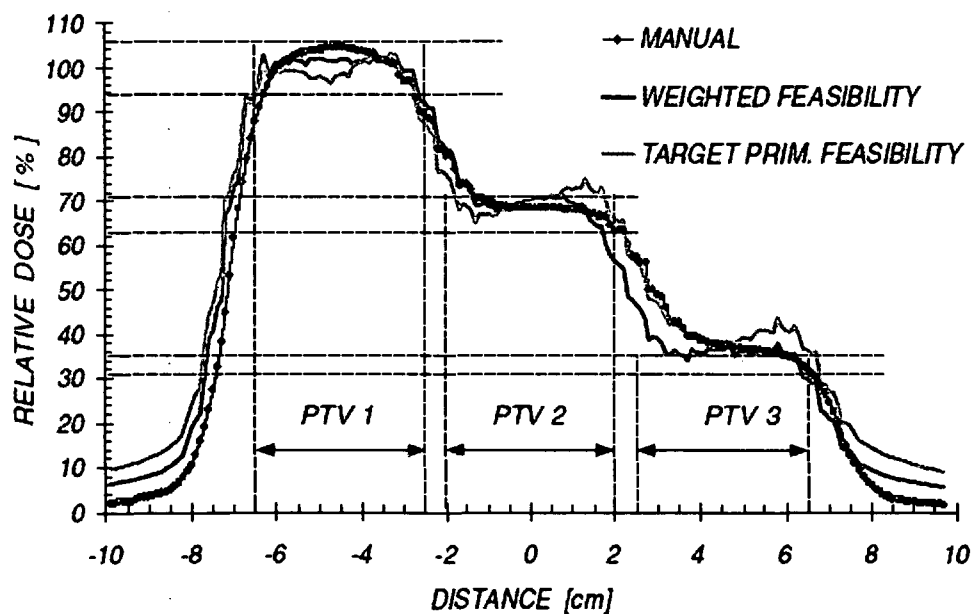
Figure 3.4 *Example of dose profiles through the central target plane for a manually optimized and the two inversely planned IM beams for test 3. Profiles refer to a 25 MV photon beam. The locations of the three targets and the respective desired dose levels are indicated by the dotted lines.*

Figure 3.5 shows isodose distributions in an axial plane for test 4 for a manually optimized and two inversely planned IM beams at 25 MV. Again, depth

dose and output factors are considered during the manual optimization and beam weighting procedure. The weighted feasibility algorithm tends to underdose outer parts of targets at 4 cm and 10 cm depth while the desired dose is delivered to the central target at 7 cm depth. This underdosage is smaller for the manually optimized plan. With the target primary algorithm, only the outer parts of the target located at 10 cm depth are partly underdosed while all other constraints are fulfilled.

WEIGHTED   MANUAL   TARGET PRIMARY
FEASIBILITY   FEASIBILITY
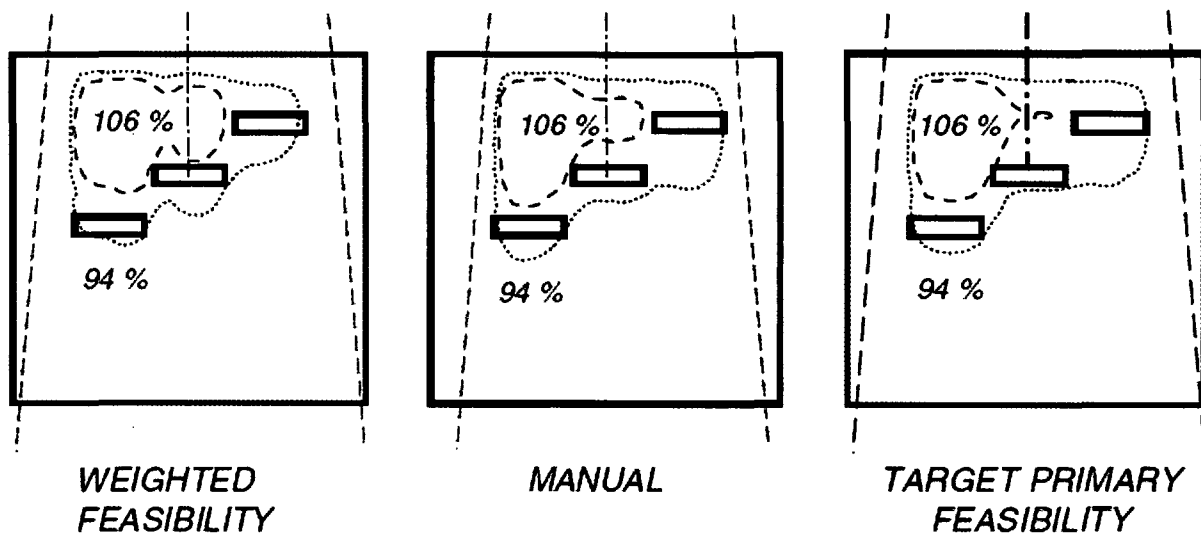
Figure 3.5 Examples of isodose distributions in an axial plane for test 4 (multiple targets at different depths) for a manually optimized and two inversely planned IM beams using 25 MV photon beams.

3.3.2 Multiple beam arrangements

Figure 3.6 (a) to (c) shows the isodose distribution in a coronal plane for the integrated boost test configuration obtained with the weighted feasibility at 25 MV. The respective DVH constraints used for the optimization are shown in the tables. By using a 'hot-spot' constraint for the boost volume only, the inverse algorithm fulfils this demand but places large hot spots in PTV 1 (see Figure 3.6 (a)). This can be avoided by using 'hot-spot' constraints for both boost PTV 2 and PTV 1 (see Figure 3.6 (b)). Although large hot-spot regions are avoided and the DVH constraints for both PTVs are fulfilled, the desired high dose (95%) volume is fairly large and not tailored around PTV 2. In order to get this isodose as close as possible around PTV 2, another constraint must be set. Boost PTV 2 is located in PTV 1 and, hence,

a high dose region constraint must be set for PTV 1 as well. By allowing a high dose volume in PTV 1 corresponding to volume ratio PTV 2/PTV 1, the high dose region follows the boost volume closely (see Figure 3.6 (c)).

□ PTV 1
□ boost PTV 2

— ·· — 75 %　　———— 95 %　　- - - - 105 %

(a)　　　　　　　　　　(b)　　　　　　　　　　(c)

VOI	Dose	Volume
Boost	95 %	> 97 %
PTV 2	105 %	< 3 %
PTV 1	75 %	> 97 %

VOI	Dose	Volume
Boost	95 %	> 97 %
PTV 2	105 %	< 3 %
PTV 1	75 %	> 97 %
	105 %	< 3 %

VOI	Dose	Volume
Boost	95 %	> 97 %
PTV 2	105 %	< 3 %
	75 %	> 97 %
PTV 1	105 %	< 3 %
	95 %	< 20 %
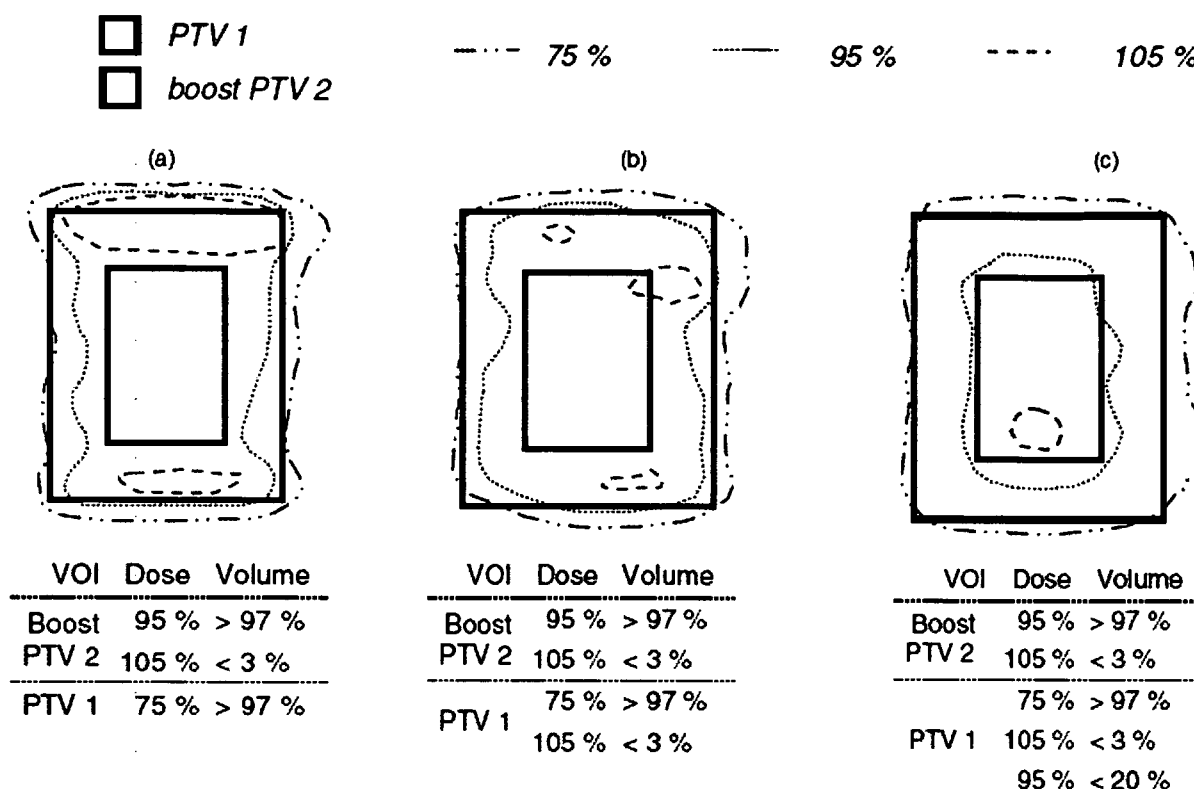
Figure 3.6 *Isodose distribution in a coronal plane for the integrated boost test configuration obtained with the weighted feasibility at 25 MV. The DVH constraints used for the optimization are shown in their respective tables.*

Figure 3.7 shows DVHs for target and OAR for test 6 obtained with the weighted feasibility algorithm using 25 MV photon beams. The dotted line refers to a treatment plan without any restrictions. In order to deliver this treatment, 110 segments are needed. The solid line represents DVHs for a plan using the same energy and DVH constraints but restrictions in terms of segment number and size. By using such restrictions the number of segments is reduced to 61 without compromising dose distributions.

When performing test 5 without limitations, 62 segments are needed for treatment delivery while only 32 are needed when restricting segment number and size again. The differences in DVHs for both boost PTV 2 and PTV 1 are smaller than those displayed in Figure 3.7.
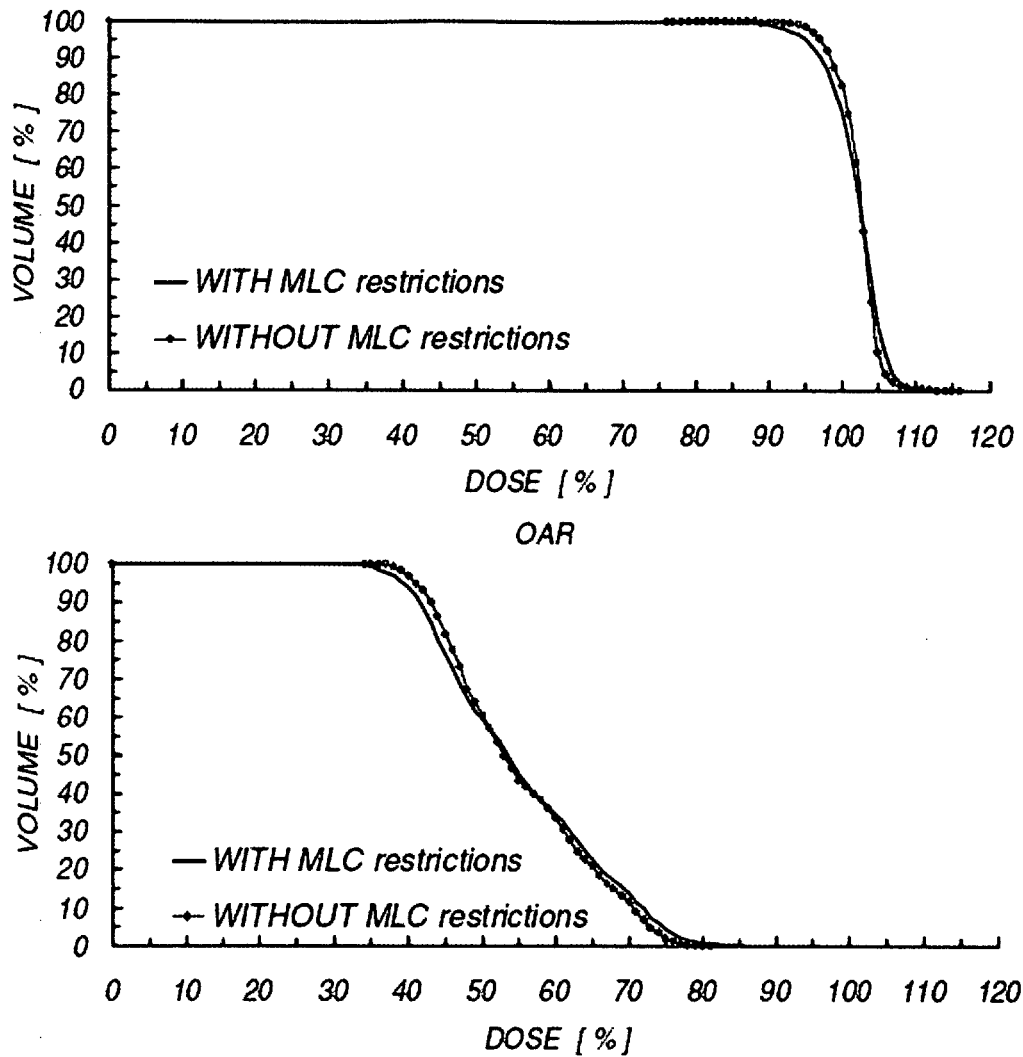
Figure 3.7 *DVHs for target and OAR for test 6 with a concave target and an OAR in the close vicinity, obtained with the weighted feasibility algorithm using 25 MV photon beams. The dotted line refers to a treatment plan without any restrictions, the solid line to a plan with limitations in terms of segment number and segment size.*

For clinically orientated tests 5 and 6, preliminary testing is performed also with the target primary feasibility algorithm (results not presented). Especially for test case 6 with an OAR near the target, the weighted feasibility algorithm provided much better conformity. The differences between the two optimization methods for test 5 (without an OAR) are less pronounced.

3.3.3 Reproducibility, system configuration and speed

All tests are repeated at least three times (up to five times) for the same energy. Differences for the repeated tests are present but found to be very small and negligible. They can be explained by the quasi-random distribution of voxels used during optimization.

Additionally, tests are repeated allowing more than 100 iterations, more than 10 intensity levels, and more than 1500 voxels per VOI during optimization. All these parameters are found to have no or little effect on the outcome of optimization processes for the TPS in use, but increased the time needed for inverse treatment planning.

For clinical tests 5 and 6 using multiple beam arrangements, the dose calculation process including optimization and segmentation takes ~30 min, for single beam arrangements <10 min. These calculation times depend largely on the available computer and are most probably shorter for more modern hardware.

3.4 DISCUSSION AND CONCLUSION

Although single beams will not be used in a clinical IMRT application, the proposed tests can be used to evaluate the outcome of computerized treatment plan optimization in terms of plausibility. The single beam arrangement tests described are designed to check inverse planning tools for situations commonly encountered in radiotherapy: missing tissue, inhomogeneities, different target doses, and different target depths. If needed, combinations of these four tests can be performed or other inhomogeneities (e.g. bone) can be used. These tests have been performed for all three available photon beam qualities. All results presented refer to one energy only but are representative for the other energies as well.

In the present study, single beam tests are mainly intended to investigate the differences between the target primary feasibility and the weighted feasibility algorithm in the absence of constraints for OAR. The strict fulfilment of DVH constraints used for the optimization is not given highest priority when evaluating single beam tests. Firstly, a single beam does not provide the same degree of

50

freedom for the segmented MLC technique as multiple beams. Secondly, other parameters such as target size, target location, mutual distance of targets, etc, have a great influence on the optimization outcome. For example, if target volumes are too thin (e.g. 2 mm), the distribution of voxels used during optimization becomes a critical parameter for the test. On the other hand, if test targets are too thick (e.g. 5 cm), the depth-dose characteristics of photon beams will not allow narrow dose constraints to be set when using only one beam. Additionally, the photon beam energies available can have an impact, too. Therefore, test configurations 1–4 contain compromises in all these aspects.

Both optimization algorithms, target primary feasibility and weighted feasibility, assign highest priority to the low dose constraint for targets, i.e. to cover the target volume with the prescribed minimal dose, the maximum dose constraint is a secondary goal. This is reflected by the results presented in Table 3.1 and Figure 3.4, where low dose constraints are fulfilled in a better manner than high dose constraints.

As mentioned above, an OAR cannot be assigned a 'weight' by the planner using the target primary algorithm where weights are managed internally. But even in the absence of an OAR, both algorithms behave differently, see results for single beam arrangements. This can probably be explained by the starting parameters used in the optimization algorithms when DVH constraints are used to create the objective function. However, the detailed reason is beyond the scope of this study.

When looking at Figure 3.5, one might conclude that the target primary feasibility algorithm is the better optimization option when considering targets only. By repeating test 4 with the weighted feasibility algorithm but using more strict constraints on the desired dose (e.g. D_{MIN} = 97% and D_{MAX} = 103%), the initial constraint (D_{MIN} = 94% and D_{MAX} = 106%) could also be fulfilled. Using such kinds of 'fictive' but more stringent constraints in order to achieve the desired goal is typical when using computerized optimization tools.

The assignment of relative importance factors or weights for structures is considered to be very important for clinical applications. Although the assignment of equal weights to all structures is found to be sufficient for the rather simple tests 5 and 6, it is the authors' opinion that in the case of multiple OAR and/or targets (e.g. head and neck regions), some flexibility of the system is lost if the relative

importance of structures cannot be specified by the user. For all these reasons, the weighted feasibility algorithm is recommended for clinical applications.

The crucial influence of constraint setting is demonstrated in test 5, see Figure 3.6. Considerations obvious for an experienced treatment planner, such as the avoidance of hot spots outside the target, are not necessarily obvious for a computerized optimization module. Precautions must be taken to precisely define treatment goals in terms of constraints. The outcome of computerized treatment plan optimization depends largely on the input ('garbage in – garbage out').

By restricting the number of segments and the segment size to certain acceptable numbers in the system's configuration, as demonstrated in test cases 5 and 6, treatment efficiency is largely influenced. Additionally, dosimetric uncertainties of small size segments, e.g. due to the influence of leaf calibration on output factors, can be avoided [Sharpe *et al* 2000]. However, these advantages have to be weighted against a possible gain in the dose distribution in the case of unrestricted delivery. Moderate restrictions are found to be acceptable for multiple beam arrangements in clinical situations but more rigorous restrictions might result in less favourable dose distributions.

In IMRT, the common method to normalize dose distributions to a pre-defined normalization point (e.g. the isocenter) is no longer recommended. The prescribed dose to the target is usually given by a certain dose interval. Therefore, an arbitrary point in the target will get a dose value inside the required interval (if the optimization can fulfil the constraints). As a consequence, demanding a fixed dose to the normalization point (e.g. 100%) may necessitate rescaling of the whole optimized plan. To avoid this, it is preferable to use a volume-based normalization method. The TPS under investigation allows the user to normalize dose distributions either to minimum, maximum, mean, or median doses of a pre-defined VOI. In the present study, all dose distributions are normalized to the mean dose in a specific target and all results presented are valid for this type of normalization only. For clinical applications, the normalization type becomes even more critical. When interpreting DVHs with relative dose values displayed on the abscissa, the normalization type and the method of dose prescription must be considered in order to safely apply IMRT.

In summary, simple tests have been performed for pre-clinical evaluation of an inverse planning module for the segmental MLC IMRT delivery technique. These

tests are aimed at verifying the outcome of inverse planning procedures in terms of plausibility and at evaluating the impact of the system's configuration on the outcome, which in turn influences treatment delivery and dosimetry. Selecting appropriate parameters for inverse planning needs to be investigated before it can be clinically implemented with confidence. Pre-clinical testing of an entirely new planning tool as described can be valuable for that purpose. Additionally, phantom tests carried out using the MPP can be directly used to verify the whole chain from inverse treatment planning to IMRT delivery, e.g. by using films, TLDs and ionization chambers. However, the presentation of results on dosimetric verification is beyond the scope of this note.

CHAPTER 4

DOSIMETRIC AND MECHANICAL EVALUATION OF THE LINEAR ACCELERATOR DEDICATED TO HIGH PRECISION RADIOTHERAPY

4.1 INTRODUCTION

The treatment machine under investigation is the travelling wave linear accelerator PRECISE (ELEKTA Oncology Systems, Crawley, UK). It is the company's most modern Linac type and is able to deliver segmental MLC based IMRT. It provides three qualities of photon beams (6 MV, 10 MV, and 25 MV) which can be shaped by the integrated multileaf collimator. Figure 4.1 illustrates the simplified design of the Linac head [Elekta Oncology Systems Ltd. 2002].
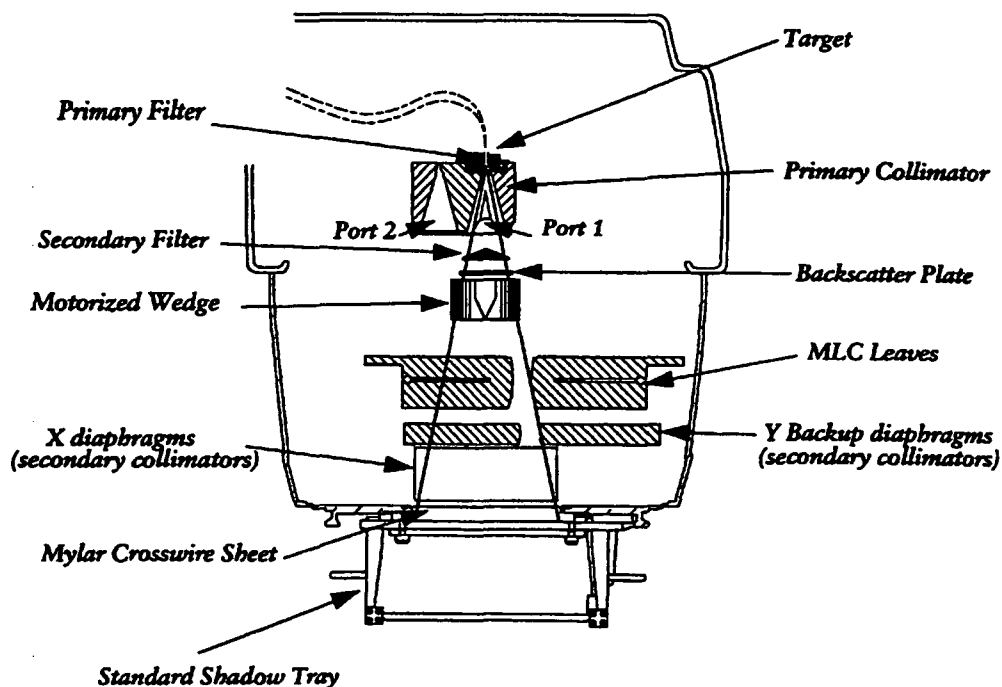
Figure 4.1 *MLC treatment head of the Elekta Precise Linac. The secondary collimation in Y-direction is accomplished by 40 leaf pairs in combination with backup diaphragms, minimizing both leaf transmission and interleaf leakage.*

Apparently, the Y-jaws are designed as backup diaphragms moving in parallel to the leaves in order to minimize leaf transmission as well as interleaf leakage [Georg *et al* 1997b]. These diaphragms are always locked to the outermost leaves which is also true for segmental MLC based IMRT. Thus, for each individual segment the four jaws are positioned to shape the smallest possible rectangle encompassing the open field area. The only exception arises from the mechanical limitation of the X-diaphragms driven perpendicularly to leaf motion direction as they cannot cross the collimator midline, which has to be considered in the planning system.

The MLC consists of 40 leaf pairs and is a so-called "single-focussed" device, i.e., the leaves move along a straight trajectory and do not follow the divergence of the beam, while the leaf ends are rounded to decrease penumbra width. The leaves are made of Tungsten, showing a thickness of 7.5 cm and a nominal width of 1 cm projected to the isocenter. Their positions are not verified mechanically but by optical markers on top of the leaves which are registered by a special video camera. In fact, the projected shadow of a single leaf is slightly larger (about 1.1 cm) due to its tongue-and-groove design helping to reduce interleaf leakage, as described in section 2.4.3.1. This leads to small overlap areas between two adjacent leaves and creates some dosimetric uncertainties since this effect is not implemented in the Helax-TMS dose calculation algorithm.
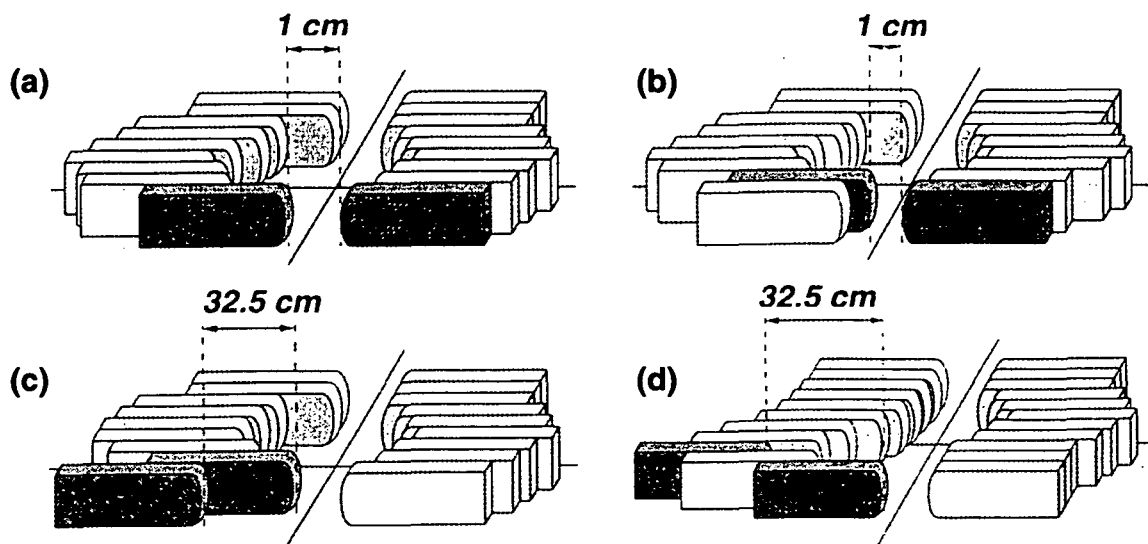
Figure 4.2 *Mechanical restrictions of the Elekta Precise multileaf collimator.* (a) *Minimum possible separation between opposing leaves.* (b) *Minimum possible separation between adjacent opposing leaves.* (c) *Maximum possible separation between adjacent leaves in the same leaf bank.* (d) *Maximum separation between any leaves in the same leaf bank.*

For both, conventional 3D conformal radiotherapy and IMRT delivery, a maximum field size of 40×40 cm^2 can be used. The leaves can over-travel the collimator midline by 12.5 cm providing large flexibility for irregularly shaped segments. However, there are some mechanical restrictions, which are schematically illustrated in Figure 4.2 [MDS Nordion 2001]. They are incorporated in the leaf sequencing algorithm of the Helax-TMS optimization module ensuring physical deliverability of generated segments without violating any mechanical limits.

When creating treatment plans for segmental MLC based IMRT, the optimization algorithm frequently produces segments smaller than 10 MU. As usually the accelerator calibration and fine-tuning is done at 200 MU it is not possible to assure a linear dosimetric performance from the very first MU without verifying the beam start-up behaviour. Even for the same type of Linac (e.g. PRECISE) each unit acts as an "individual" and therefore needs to be validated. For all photon beam energies available the dose linearity with number of delivered MU has to be investigated. Additionally, the beam geometry in terms of flatness and symmetry is of major interest as a potential start-up instability would effect the treatment negatively [e.g., Buchgeister and Nusslin 1998, Cheng and Das 2002].

Since in SMLC-IMRT the geometrical dimensions of single segments can be quite small (<3 cm), the mechanical accuracy of gantry and couch rotation, jaw positioning and leaf calibration plays an important role. Certainly, the requirements of IMRT treatments are stronger than in conventional 3D-CRT, both for segmental and dynamic MLC based delivery [LoSasso *et al* 1998]. Hence, measurements to investigate the precision of mechanical components have to be done when commissioning a Linac for IMRT, but also periodically as part of the routine quality assurance programme.

4.2 DOSIMETRIC START-UP PERFORMANCE

4.2.1 Dose per MU linearity

For exposures of 1-10, 20, 30, 40, 50, 100, and 200 MU, the dose per MU was measured with an ionization chamber (type 31002, PTW, Freiburg, Germany) connected to an UNIDOS electrometer (PTW). In a polystyrene phantom, the chamber was positioned at a depth of 10 cm with a source-to-surface distance (SSD) of 90 cm (i.e. in the isocenter). Gantry angle and collimator angle were set to 0°, where a field size of 20×20 cm^2 was chosen. For each MU setting, the mean value of three measurements was calculated and normalized to unity at 200 MU. In Figure 4.3 (a) to (c), the results for the available photon beam qualities (6 MV, 10 MV, and 25 MV) at different dose rate settings (100 MU/min, 200 MU/min, and 400 MU/min) are displayed. The error bars represent one standard deviation.

For 6 MV, deviations up to 4% are detected only for 1 MU exposures, whereas in segments with 2 MU or more the dose linearity is within ±1% of the expected value for all dose rate settings. For 10 MV this is only true at a dose rate of 400 MU/min while lower dose rate settings show a slightly decreased stability below 4 MU. This contradicts the findings of Hansen *et al* (1998) who suggested using a low pulse repetition frequency for very short segments. It may be explained by the Linac fine-tuning and calibration procedure that is always performed at 400 MU/min, representing the standard setting for patient treatments at the local radiotherapy department. For the 25 MV beam quality the dose linearity is within ±1% from the very first MU, except for the lowest dose rate (±2%).

4.2.2 Beam geometry

To investigate the dosimetric beam geometry, the linear ion chamber array LA 48 (PTW) was used. It consists of 47 liquid-filled ion chamber elements with an area of 4×4 mm^2 and a centre-to-centre distance of 8 mm. It offers the great advantage to obtain complete beam profiles at once, unlike a single ionization chamber which has to scan through the beam.
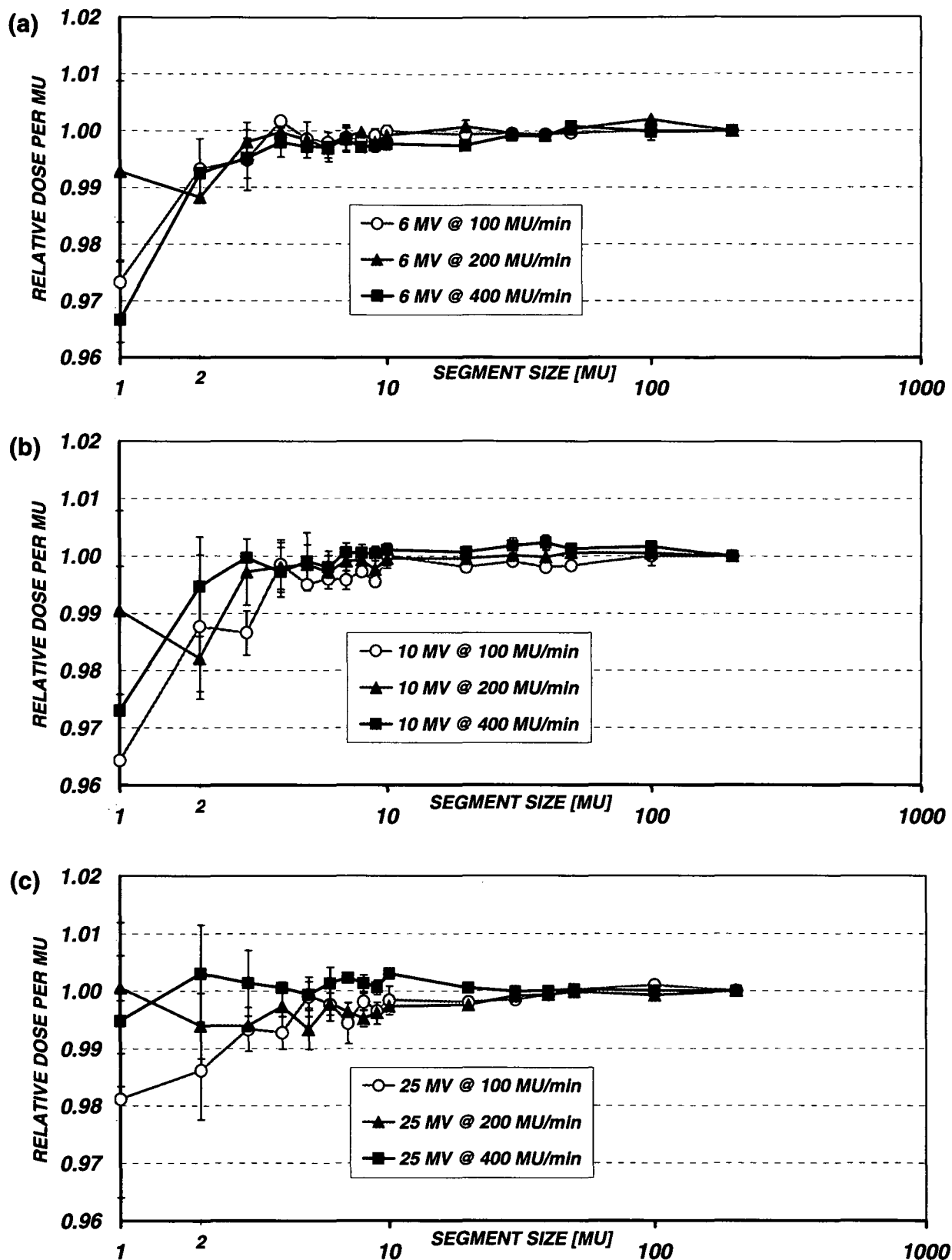
Figure 4.3 *Relative dose per MU as a function of segment size, normalized to unity at 200 MU, respectively. Data are shown for beam qualities of* **(a)** *6 MV,* **(b)** *10 MV, and* **(c)** *25 MV, at three different dose rate settings each. The values represent averaged results of three measurements, with the error bars corresponding to one standard deviation.*

All measurements were performed in an MP3 water phantom (PTW). The ion chamber array was connected to a MULTIDOS dosimeter (PTW) with ME48 extender (PTW) which expands the MULTIDOS to 48 channels. The data were transferred to a PC and evaluated with special software (MEPHYSTO, PTW).

The LA48 array has been found to be well suited for measurements of beams with steep dose gradients, as frequently occurring in IMRT [Martens et al 2001a, 2001b]. In the latter publication it is recommended to validate the calibration factors provided by PTW and to assess the magnitude of dark current before starting profile measurements.

4.2.2.1 Calibration factors of LA48 array

Within the MEPHYSTO-Software, PTW provided relative calibration factors for each of the 47 ion chamber elements. In order to check the stored values, profiles obtained by the LA48 array were compared to measurements with a single ion chamber scanning through the beam.

With the LA48 mounted in the MP3 water phantom, profiles were measured along the major axis in gun-target direction at a depth of 10 cm. For a source-to-surface distance of 90 cm the field size of a 6 MV beam was set to 40×40 cm^2, keeping each of the 47 chamber elements within the high dose region. Three measurements were performed and the mean values calculated.

Under the same conditions, profiles were obtained by a single ionization chamber (31002, PTW) with a sensitive volume of 0.125 cm^3. The scanning steps were set to 8 mm in order to resemble the positions of the chamber array elements. Again, three measurements were performed and averaged.

Normalized to 100% on central beam axis, the profiles show very good agreement. For the 47 positions, the average difference between LA48 and single chamber is 0.46% with a maximum value of 1.13%. When only considering the 27 inner positions which are relevant to measure a 20×20 cm^2 field, the average deviation even decreases to 0.22% with a maximum of 0.59%. Therefore, no changes to the provided calibration factors were needed, in agreement with Martens et al (2001b).

4.2.2.2 Dark current of LA48 array

In multiple measurement sessions the dark current of the linear chamber array was investigated. Again in accordance with Martens *et al* (2001b), the dark current shows some variability with time and absorbed dose. Nevertheless, related to the high dose region of a beam at 100 MU/min the amount of dark current is always found to be in the magnitude of a few per mill. Since for the quantification of beam symmetry and beam flatness the high dose region is relevant, the dark current can be regarded as negligible.

4.2.2.3 Measurements of beam symmetry and flatness

For exposures of 1, 3, 5, 10, and 100 MU the beam symmetry and beam flatness were determined with the linear ion chamber array LA48 mounted in the water phantom MP3. The measurement configuration was similar to the set-up used for validating the calibration factors, i.e. a source-to-surface distance of 90 cm and a measuring depth of 10 cm, just the field size was changed to 20×20 cm². Profiles were obtained both in Gun-Target direction (G-T) and orthogonally (A-B). Similar to dose linearity, measurements were performed for three beam qualities (6 MV, 10 MV, and 25 MV) and three dose rate settings (100 MU/min, 200 MU/min and 400 MU/min). To analyse the profile data, definitions according to the IEC 60976 standard [International Electrotechnical Commission 1989] were used by the MEPHYSTO-software:

$$FLATNESS = \frac{D_{MAX} - D_{MIN}}{D_{MAX} + D_{MIN}} \cdot 100\% \qquad (4.1)$$

where D_{MAX} and D_{MIN} are the maximum and minimum dose values within the flattened region (80% of field size). For an ideal profile the flatness would be 0%.

$$SYMMETRY = MAX\left(\frac{D(x)}{D(-x)}\right) \cdot 100\% \qquad (4.2)$$

where x and $-x$ are positions symmetrical to the central beam axis within the flattened region, while $D(x)$ and $D(-x)$ are the corresponding dose values. For an ideal profile the symmetry would be 100%.
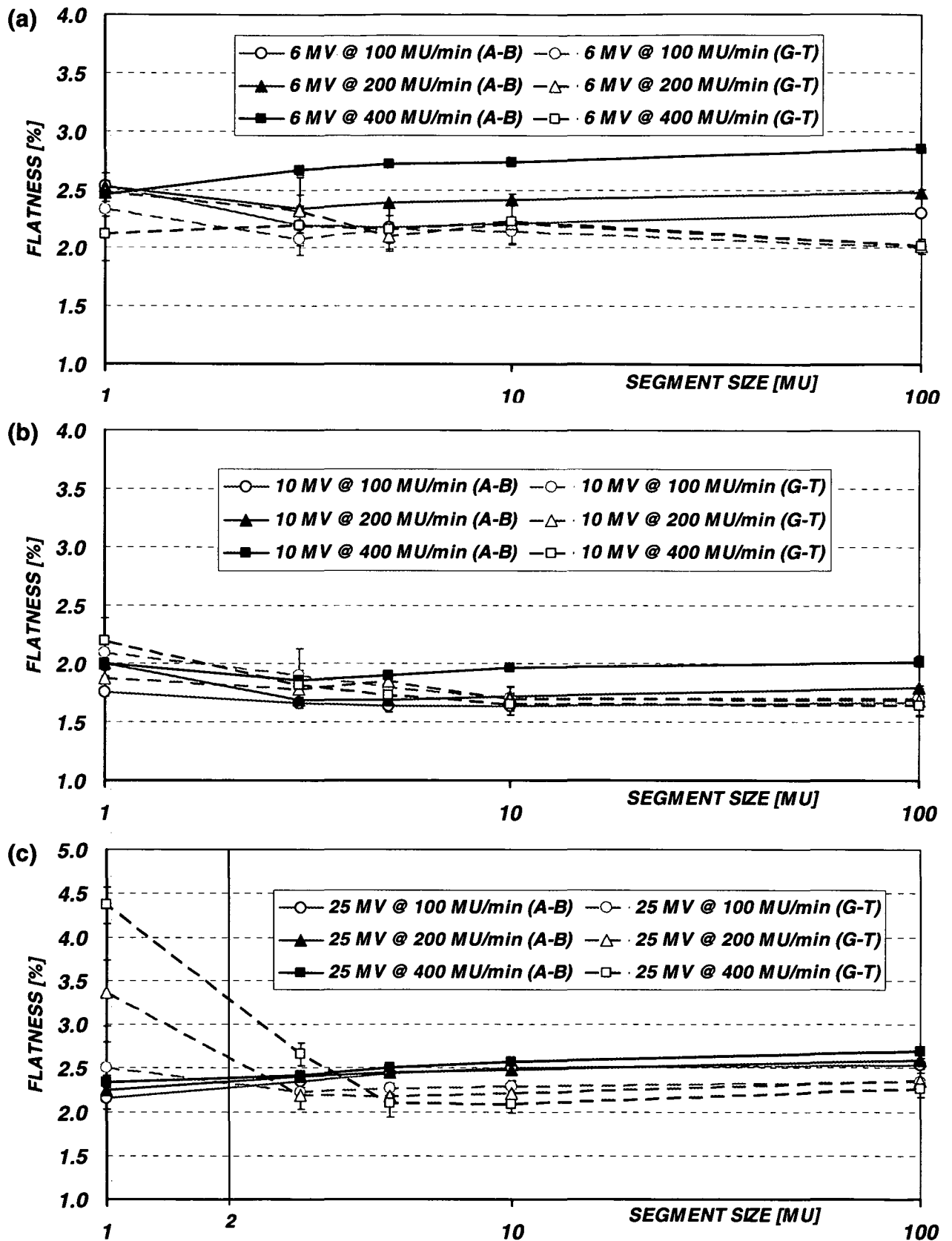
Figure 4.4 *Beam flatness measured in gun-target direction (G-T) and orthogonally (A-B) as a function of segment size. Data are shown for beam qualities of* **(a)** *6 MV,* **(b)** *10 MV, and* **(c)** *25 MV, at three different dose rate settings each. The values represent averaged results of three measurements, with the error bars corresponding to one standard deviation.*
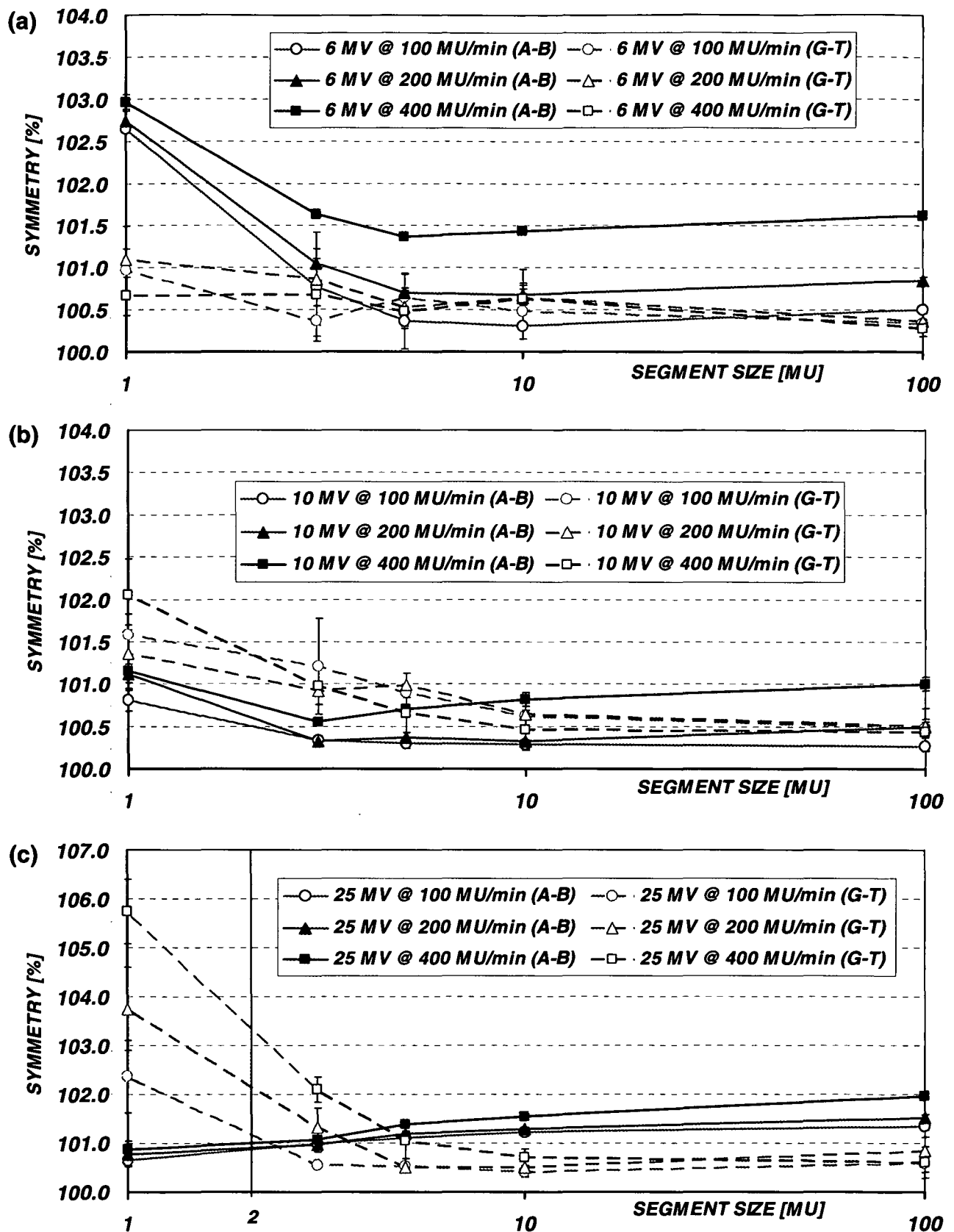
Figure 4.5 *Beam symmetry measured in gun-target direction (G-T) and orthogonally (A-B) as a function of segment size. Data are shown for beam qualities of* **(a)** *6 MV,* **(b)** *10 MV, and* **(c)** *25 MV, at three different dose rate settings each. The values represent averaged results of three measurements, with the error bars corresponding to one standard deviation.*

For each MU setting three profile measurements were performed, beam flatness and symmetry were calculated following formulae (4.1) and (4.2), respectively, and averaged. Figure 4.4 represents beam flatness vs. segment size, beam symmetry is displayed in Figure 4.5. The error bars represent one standard deviation.

For 6 MV and 10 MV photon beams the flatness is very stable, even for 1 MU exposures. This parameter is found to be within a range of 1.5% to 3%, for both directions (G-T and A-B) and independent of dose rate. For the 25 MV beam quality this is only true for profiles in A-B direction. In G-T direction, the beam flatness is nearly constant at a dose rate of 100 MU/min, while at 200 MU/min and 400 MU/min its values increase up to 4.5% for 1 MU segments, exceeding the 3%-level at an interpolated segment size of about 2 MU.

The results for beam symmetry are very similar. The 6 MV and 10 MV beams are found to be symmetrical within 100% to 102% for the whole range of segment sizes. The only exception is shown for the 6 MV photons in A-B direction where the symmetry rises to 103% for 1 MU exposures. Again, no significant dose rate dependence can be detected. The 25 MV beam is very stable in A-B direction, but in orthogonal direction increasing symmetry values for segments smaller than 3 MU are documented, probably because the electron beam is bent in this direction [Martens et al 2001a]. Here, the beam symmetry depends on dose rate and reaches a maximum of 106% at 400 MU/min for an exposure of 1 MU in which the 103%-level is exceeded at an interpolated value of about 2 MU.

4.2.3 Clinical consequences

The determination of beam flatness and beam symmetry did not show any evidence of dose rate dependence, except for the 25 MV beam quality in segments smaller than 3 MU. From measurements of dose per MU linearity, the dose rate setting of 400 MU/min turned out to be even slightly more stable than exposures at lower dose rates. It was therefore decided to concentrate on the highest dose rate investigated which also corresponds to the default setting stored in the Linac software.

For 400 MU/min, the dose per MU was found to be within ±1% for all three photon energies when delivering segments with 2 MU or more, as shown in Figure 4.3 (a) to (c). The requested range of ±1% represents a very strict limit but helps to provide an accurate dosimetry. Concerning the dosimetric beam geometry, 6 MV and 10 MV beams showed good stability and fulfilled the desired constraints for the whole range of measured segment sizes, i.e. maximum flatness of 3% and maximum symmetry of 103%. For the 25 MV beam quality, the same behaviour was observed for profiles obtained in A-B direction, while in G-T direction the beam was found to be less stable. However, at an interpolated value of 2 MU the beam geometry exceeded the desired limits just marginally, as illustrated by Figure 4.4 (c) and Figure 4.5 (c).

Summarizing the above findings, it was concluded that the requested stability in terms of dose linearity and dosimetric beam geometry is achievable for 6 MV, 10 MV and 25 MV photon beams at a dose rate of 400 MU/min, when delivering segments with 2 MU or more. Since the planning system does not allow defining a minimum number of MU per segment, it was decided to erase potential segments with less than 2 MU manually. In general, this has minimal influence on the overall treatment plan, as shown by case study 3 in CHAPTER 7, but provides an optimal dose delivery.

4.3 DOSIMETRIC START-UP PERFORMANCE AFTER LINAC-UPGRADE

In the context of a general service upgrade of the PRECISE Linac the original magnetron was exchanged by a so-called "fast-tuning magnetron" (FTM). A magnetron is used to generate microwaves which are necessary for electron acceleration. The original magnetron used a mechanically driven plunger in order to tune the magnetron cavity to the optimum frequency. In contrast, in the FTM the plunger position is controlled by an electromagnetic solenoid allowing a nearly instantaneous tuning of the magnetron when the beam is switched on.

The practical outcome is a significant reduction of the beam start-up time, measured from pressing the start-button to the audible beam-on signal. With the original magnetron this time was in a range of 6 s for 6 MV beams to 8 s for 25 MV.

After the magnetron upgrade this period was cut to 3 s (6 MV) and 5 s (25 MV) which resembles the results of Budgell *et al* (2001). The shortened beam start-up time pays off especially when delivering segmental MLC based IMRT, as the beam has to be restarted after each segment, e.g. for a delivery of 60 segments the treatment time can be reduced by up to 3 min.

With the new fast-tuning magnetron, measurements of the dosimetric start-up performance had to be redone. Unfavourably, for the 25 MV beam quality it was not possible to find a stable operating point at a dose rate of 400 MU/min. Instead, two other levels were defined, 280 MU/min and 560 MU/min respectively, where the latter was chosen as default setting for this photon energy.

4.3.1 Dose per MU linearity with fast-tuning magnetron

The measurements were performed in exactly the same phantom assembly as described in section 4.2.1. For 6 MV and 10 MV a dose rate of 400 MU/min was chosen, while the 25 MV beam was investigated at both 280 MU/min and 560 MU/min. The results are presented in Figure 4.6, with the error bars corresponding to one standard deviation. In addition, the measurement results obtained with the original magnetron are displayed for comparison.
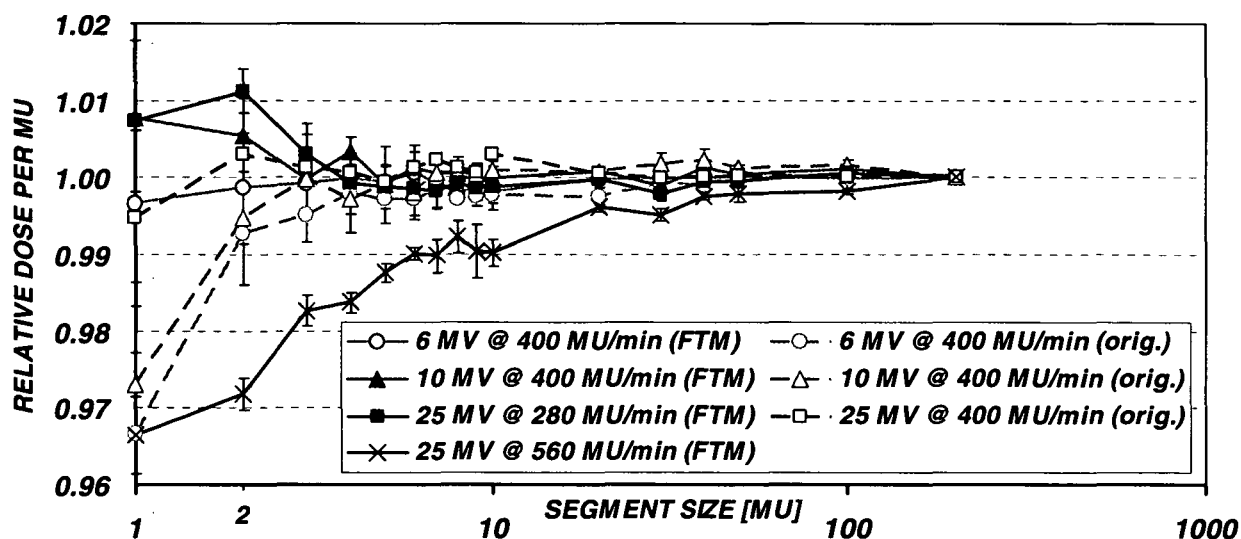
Figure 4.6 *Relative dose per MU as a function of segment size, measured after the installation of a fast-tuning magnetron (FTM) and compared to the original results (cf.* **Figure 4.3**). *Data are shown for beam qualities of 6 MV and 10 MV at a dose rate of 400 MU/min, while the 25 MV was investigated at 280 and 560 MU/min. All curves are normalized to unity at 200 MU, respectively. The values represent averaged results of three measurements, with the error bars corresponding to one standard deviation.*

Although the start-up performance with the original magnetron had emerged as very stable already, for both 6 MV and 10 MV beams the dose linearity could even be improved by the installation of the fast-tuning magnetron. Now, the values are found to be within ±1% even for exposures of only 1 MU. For 25 MV the dose linearity is significantly decreased (for the first 2 MU about 3%) when using a dose rate of 560 MU/min, while at 280 MU/min it stays within the desired limits of ±1% for the entire range of delivered segment sizes.

4.3.2 Beam geometry with fast-tuning magnetron
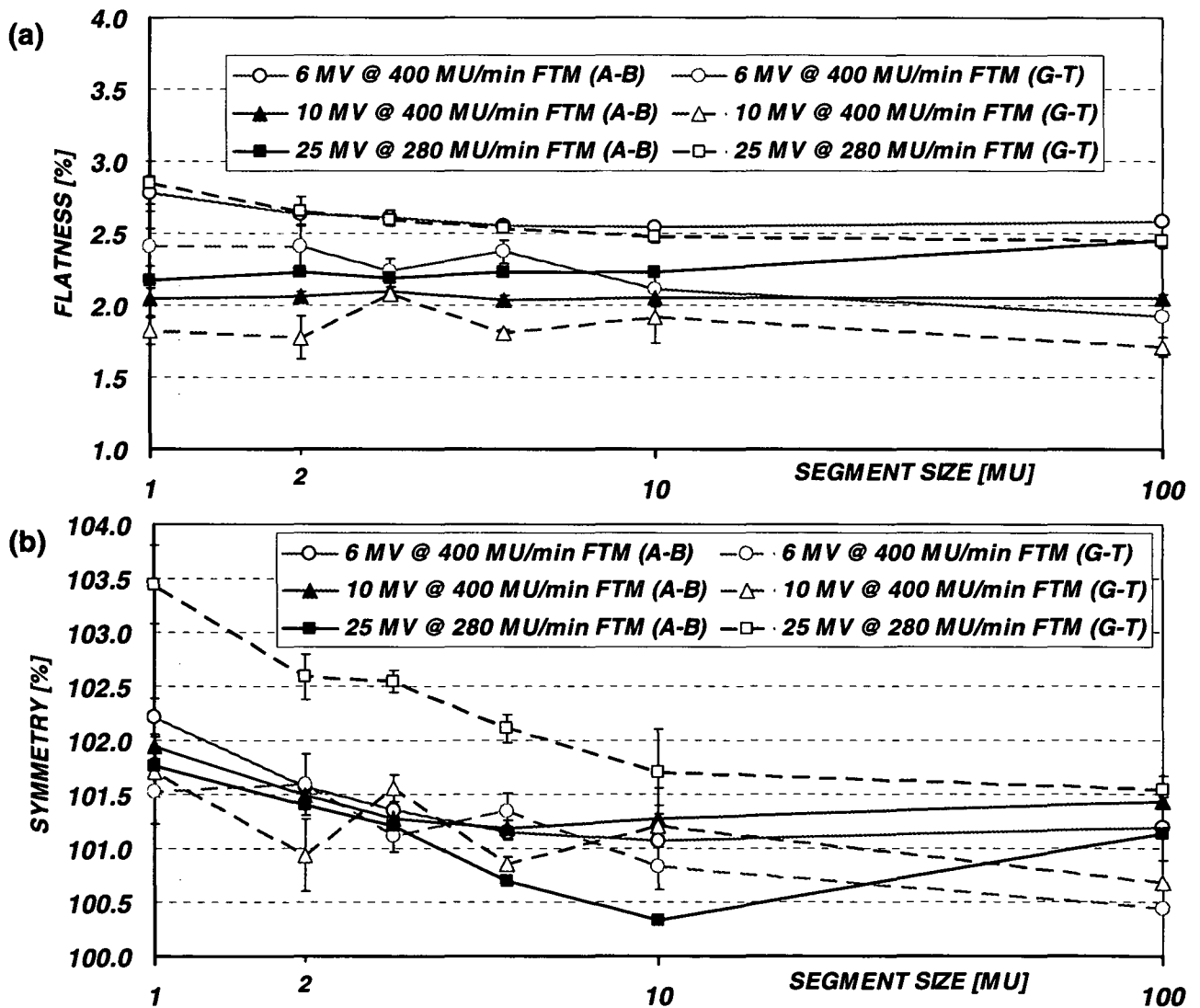
Figure 4.7 (a) *Beam flatness and* **(b)** *beam symmetry measured in gun-target direction (G-T) and in orthogonal direction (A-B) as a function of segment size, obtained after the installation of a fast-tuning magnetron (FTM). Data are shown for beam qualities of 6 MV, 10 MV, and 25 MV at 400 MU/min and 280 MU/min, respectively. The values represent averaged results of three measurements, with the error bars corresponding to one standard deviation.*

Again, measurements were carried out in exactly the same configuration as described in section 4.2.2.3, however exposures of 2 MU were investigated additionally. Following the dose linearity measurement results (Figure 4.6), the 25 MV photon beam was analysed at a dose rate of 280 MU/min only, while 6 MV and 10 MV beams were measured at 400 MU/min. The beam flatness and beam symmetry values for exposures of 1, 2, 3, 5, 10, and 100 MU are presented in Figure 4.7 (a) and (b). One standard deviation is described by the error bars.

The dosimetric beam geometry results can be summarized in a few words. At the chosen dose rate settings, the desired constraints of 3% for flatness and 103% for symmetry are fulfilled within the whole range of segment sizes, in both directions (G-T and A-B) and for each of the available photon beam energies. Only when delivering 1 MU with 25 MV, the G-T beam symmetry marginally exceeds the limit (103.4%).

4.3.3 Clinical consequences

Representing the smallest exposure the Linac is technically able to deliver, even segments with only 1 MU turned out to completely fulfil the required dosimetry levels (except for 25 MV at 560 MU/min). Thus, it was decided to only erase segments smaller than 1 MU in the planning system, occurring very rarely anyway. Additionally, it was agreed upon delivering SMLC-IMRT at a dose rate of 280 MU/min instead of the default setting of 560 MU/min if it is necessary to use the 25 MV beam quality. In this case, the loss of treatment efficiency due to the lower dose rate is much smaller than the gain achieved by shorter beam start-up times using the fast-tuning magnetron.

4.4 OUTPUT STABILITY FOR SMALL FIELD SIZES

4.4.1 Measurements of Output Factors

For the delivery of small segments (with linear dimensions <3 cm), the accelerator output significantly varies with field size. Due to unavoidable tolerances

of mechanical components in the Linac head, discrepancies between actual field size and desired field size can arise. To assess the error in dose output caused by such deviations, output factors were determined for square field sizes of 5, 3, and 2 cm which were altered intentionally by ±1 mm and ±2 mm.

Measurements were performed using a so-called "pinpoint" ionization chamber (type 31006, PTW). With its minor volume of 0.015 cm^3 it is well suited for applications in small fields whereas it overestimates the dose in large fields, where relatively more low-energy scatter is present [Martens *et al* 2000]. As the central electrode is made of steel (i.e. high atomic number), the chamber tends to over-respond due to photoelectric absorption.

The pinpoint chamber was positioned at a depth of 10 cm, with a source-to-surface distance of 90 cm. It was mounted on a computerized scanning device (MP3 water phantom, MEPHYSTO software, PTW) to allow both punctual measurements and linear beam profile scanning. The latter was needed to verify the actual field size for each beam before measuring the respective output factor. Based on these verifications, differences up to 0.8 mm were found between the set field sizes and the measured ones. Thus, adjusted values had to be entered accordingly to make the full width at half maximum (FWHM) of the obtained profiles match the required settings better than ±0.2 mm.

To measure the output factors, the chamber was positioned on the central beam axis. For each field size setting three measurements of 200 MU exposures were performed and averaged. Figure 4.8 presents output variations for 6 MV, 10 MV, and 25 MV photon beams related to nominal field sizes of 5, 3, and 2 cm, respectively. Since the standard deviations were in the order of magnitude of 1‰ no error bars are indicated.

For a reference field length of 5 cm, even a deviation of 2 mm produces output variations of only 0.5%, independent of photon beam energy. At a square field size of 3 cm, the output for 6 MV and 10 MV beams still is within ±1% for a field size range of 2.8 cm to 3.2 cm, while the 25 MV shows variations of ±2% at 2 mm and ±1% at 1 mm field size deviations. As expected, the most critical dependence is found for a nominal gap of 2 cm. When shifting the field size by 2 mm, the error in dose output increases to 1.7% (6 MV), 2.2% (10 MV) and 4.0% (25 MV), which is in good agreement with Sharpe *et al* (2000).
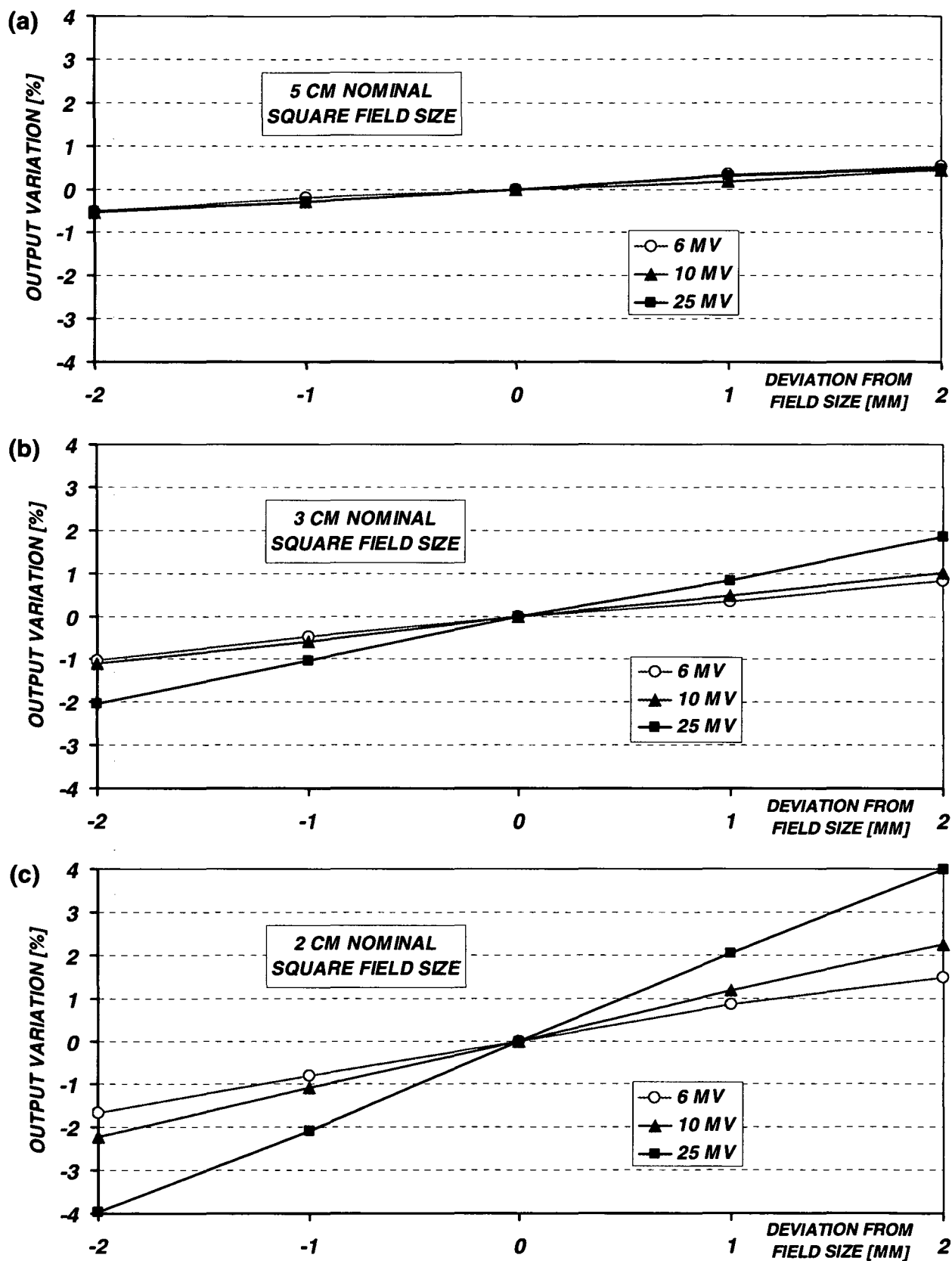
Figure 4.8 *Output variation as a function of the deviation from nominal square field sizes of* (a) *5 cm,* (b) *3 cm, and* (c) *2 cm. Data are shown for 6 MV, 10 MV, and 25 MV photon beams, respectively. The values represent averaged results of three measurements with negligible standard deviations.*

69

4.4.2 Clinical consequences

At a nominal square field size of 2 cm, a maximum mechanical deviation of 1 mm is acceptable for 6 MV and 10 MV in order to meet the required dosimetric accuracy of ±1%. However, for the 25 MV beam a tolerance level of only 0.5 mm would be necessary, which cannot be fulfilled since the field size verification measurements had shown variations up to 0.8 mm, as mentioned above. In other words, to keep the dosimetry accuracy within ±1%, square field sizes of at least 2 cm are allowed only for 6 MV and 10 MV beams, while for 25 MV photon beams square field dimensions have to be 3 cm or larger. Unfortunately, the planning system in use (Helax-TMS) only applies a single value for the minimum segment size, which is stored in a text-file and cannot be easily edited by the user. Hence, it was decided to set the minimum segment size to an area of 9 cm^2 with at least three leaf pairs opened, independent of beam energy.

For a field size accuracy of better than ±1 mm, the leaves have to perform within a tolerance level of ±0.5 mm in order to be on the safe side, when considering gravity effects and other mechanical distortions in the treatment head. Certain quality assurance procedures to check the isocenter constancy and leaf calibration, in order to assure this field size accuracy, are described in the following section.

4.5 MECHANICAL PERFORMANCE

4.5.1 Isocenter accuracy

One of the most crucial items in delivering high precision radiotherapy is the accuracy of isocenter. Ideally, rays along the central beam axis from different gantry angles meet in exactly one point (the isocenter), indicated by the room lasers. Practically, due to mechanical tolerances the isocenter is not a point rather than a small sphere. For conventional 3D-CRT, the central beam axes from different directions should meet within a sphere with a diameter of less than 2 mm, which is usually checked every three months. For high precision radiotherapy like stereotactic treatments and IMRT, the diameter of the isocenter sphere should be smaller than

1 mm and be checked daily, prior to treatments. In addition, the precision of the isocentric couch rotation has to be investigated. A simple, but very effective method to determine the isocenter accuracy is the so-called "Winston-Lutz-Test" [Lutz *et al* 1988]. A horizontal plastic needle is mounted at the top end of the treatment couch and fixed rigidly. The tip of the needle contains a small metallic pellet of 2 mm diameter which is placed at the isocenter indicated by the room lasers. In the following, radiographs are acquired by a portal imaging device or films at different gantry and couch angle combinations, with field diameters of about 1 cm. Finally, the position of the "shadow" projected by the metallic pellet is quantified relative to field edges. By this test, several important components are verified:

- Gantry rotation
- Isocentric couch rotation
- Alignment of room lasers
- If in use, the correct attachment of an additional collimator (e.g. micro-multileaf collimators or cones)

For the Winston-Lutz-Test at the local radiotherapy department, portal images are obtained for seven different combinations of gantry and couch angles and evaluated by the IVIEW software (ELEKTA). For each beam, the deviation has to be smaller than 1.5 mm, while for the average shift a maximum of 1 mm is allowed to provide an accurate treatment delivery. The results of Winston-Lutz-Tests performed over a three years period always fulfilled the above-mentioned criteria, with an overall mean deviation of 0.59±0.32 mm.

4.5.2 Leaf calibration

For MLC based IMRT delivery (segmental and dynamic), the geometrical leaf calibration is of special interest. Errors in leaf positioning do not only affect the spatial accuracy of dose distributions, but also the machine output as shown in section 4.4.1. While for dynamic IMRT treatments the leaf speed has to be checked additionally [Chui *et al* 1996], it is sufficient to investigate the static calibration precision when using the segmental MLC technique. Nevertheless, it is an extensive

procedure that has to be done both for Linac commissioning and within the framework of routine QA programmes.

The correct leaf positioning can be appropriately verified using film dosimetry. By irradiating special MLC patterns, it is possible to evaluate certain geometrical distances and to compare them to reference values. In case of discrepancies, the affected leaves or leaf pairs have to be recalibrated and verified again.

4.5.2.1 Leaf gap width measurements

Figure 4.9 *Resultant film blackening of the leaf gap width measurement. Gaps of 2 cm nominal width shaped by leaves only were irradiated consecutively at positions of -10 cm, 0 cm (i.e. collimator midline), and +10 cm. To investigate the gap size generated by leaf pairs 7 to 34, profiles were defined in leaf movement direction at the centre of each leaf pair, as indicated for leaf pair number 15.*
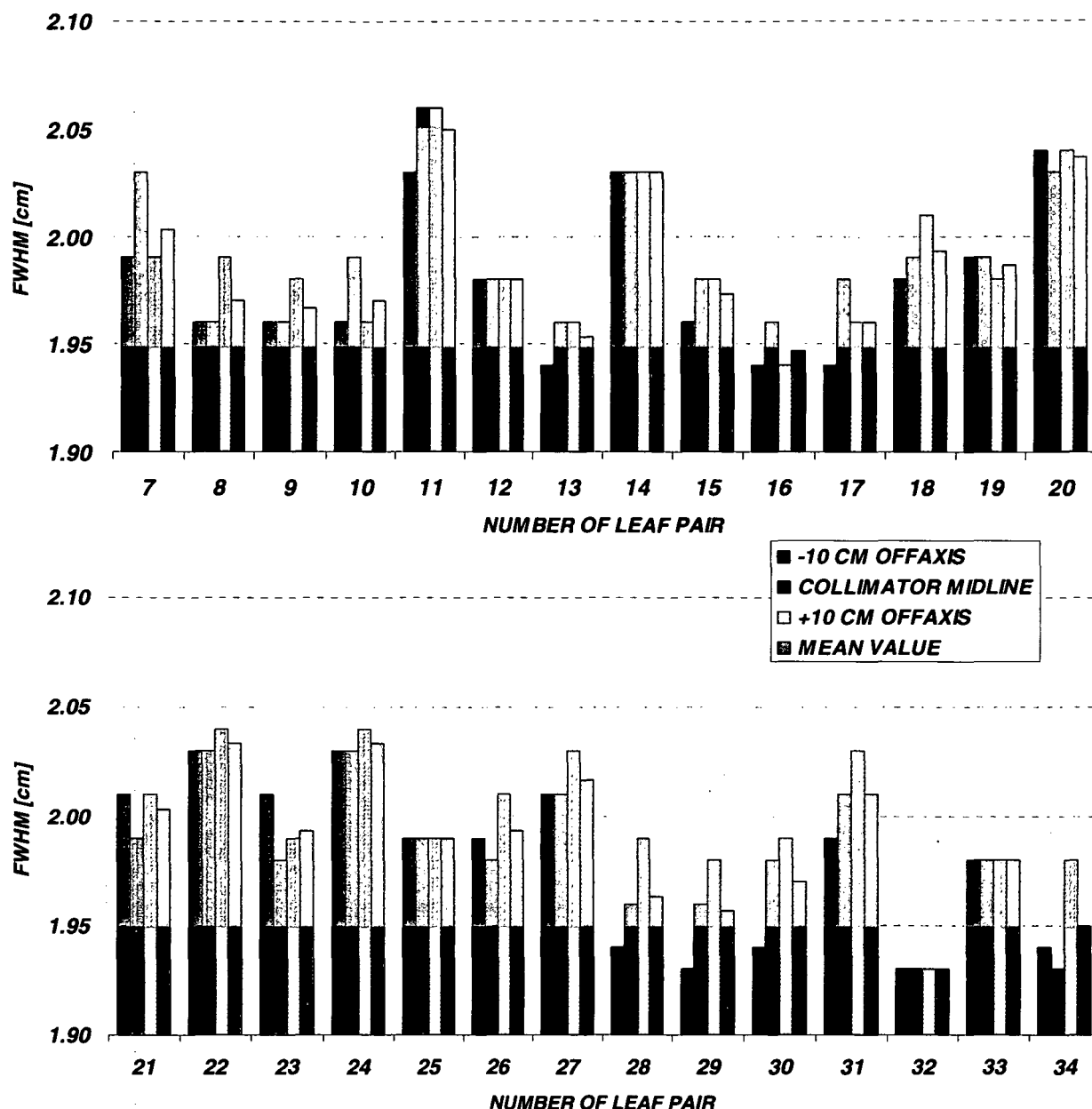
Figure 4.10 *FWHM values derived from profiles across gaps of 2 cm nominal width for leaf pairs 7 to 34, as measured by film. Data are presented for gap positions of -10 cm, 0 cm (i.e. collimator midline), and +10 cm, respectively, with the red bars indicating the mean values for each leaf pair. The tolerable variance of ±0.5 mm is marked by grey areas.*

For testing the MLC accuracy of the local PRECISE machine, leaf pairs 7 to 34 were investigated, corresponding to a field size of 28 cm in gun-target direction. The outermost six leaf pairs on each side are beyond the usual field sizes for IMRT deliveries and therefore were not taken into account. In the Linac software three gaps were defined for 6 MV beams, shaped by leaves only (i.e. without backup-diaphragms), one at the collimator midline, the others at off-axis positions of +10 cm

73

and -10 cm, respectively. The nominal gap width was set to 2 cm, across the entire field length. The beams were irradiated successively onto the same film (type EDR2, Eastman Kodak Company, New York, US) with a size of 10×12 in^2, where the SSD was set to 100 cm. Subsequently, the film was processed using a computer controlled processor (M 35 X-Omat, Kodak) and scanned by a Vidar VXR-12 plus device (Vidar Systems Corp., Herndon, US). The evaluation was performed RIT 113 software (Radiological Imaging Technology, Colorado Springs, US) based on a normalized sensitometric curve that is described in detail in CHAPTER 5. For each leaf pair, the gap width at three different off-axis positions was determined by measuring the full width at half maximum (FWHM) of the respective profile, as indicated exemplarily for leaf number 15 in Figure 4.9.

The results and the mean values over three gap positions are displayed in Figure 4.10, with the grey areas indicating the allowed tolerance level of ±0.5 mm. The overall 84 leaf gaps investigated are found to be in a range of 1.93 cm to 2.06 cm. Only two values exceed the upper criterion of 2.05 cm, while 12 gaps are smaller than 1.95 cm. When considering the mean values, results within 2±0.05 cm are obtained, except for leaf pairs 16 and 32.

4.5.2.2 Leaf abutment measurements

In a second test, adjoining segments were checked for correct abutment by means of film dosimetry. Again, gaps of 2×40 cm^2 were generated by leaves only, but with off-axis positions of +3, +1, -1 and -3 cm, respectively. This special MLC configuration yielded three abutment lines, one along the collimator midline and two lines positioned symmetrically at a distance of ±2 cm, as shown in Figure 4.11 (a). For each leaf pair, profiles were obtained in leaf motion direction across the whole field, consisting of sequential exposures of the four segments. In the following, three examples are extracted and presented in Figure 4.11 (b) to (d).

Although leaf pair 14 had shown a slightly too large gap width of 2.03 cm in section 4.5.2.1, it generated the smoothest profile in the abutment test, as illustrated in Figure 4.11 (c). The composed field exhibits a FWHM of 8.01 cm (nominal 8.00 cm) with a beam flatness of 3.22%, which is only slightly higher than in the case of a single beam.
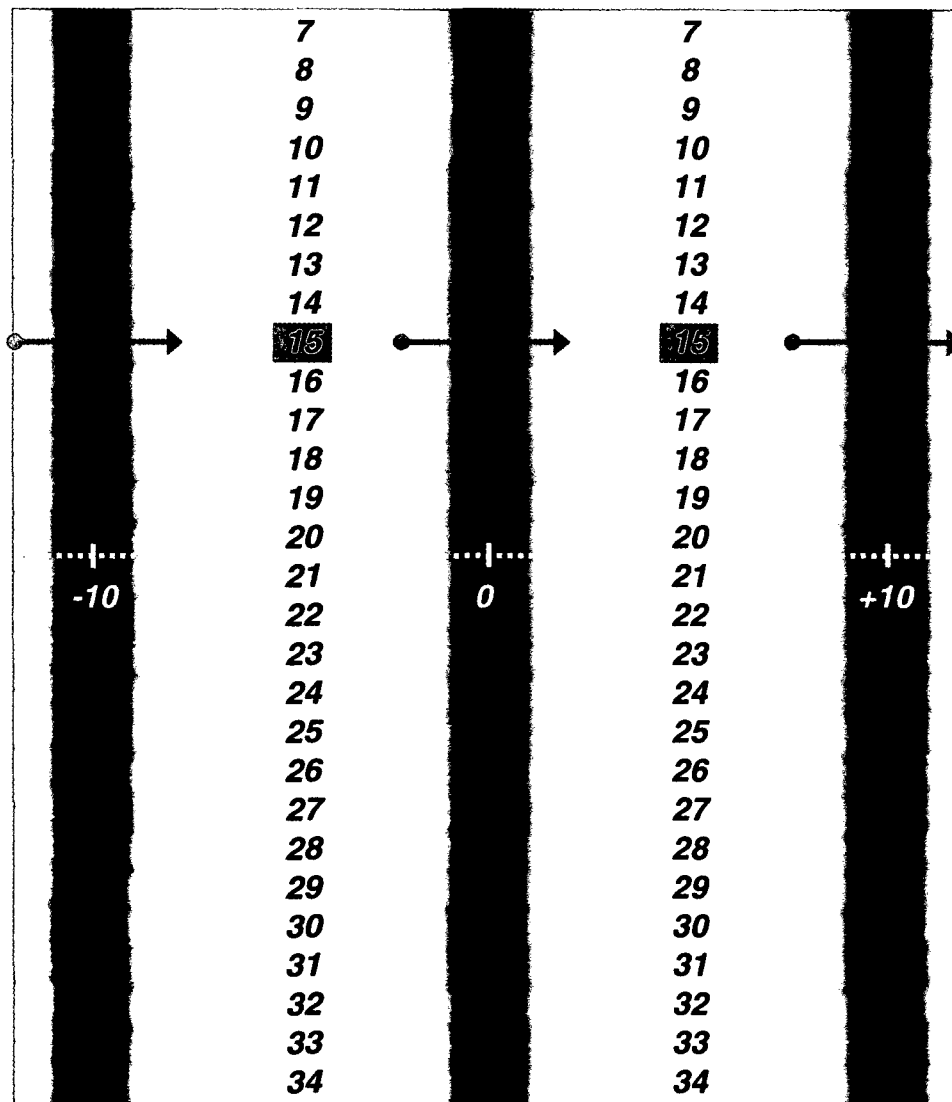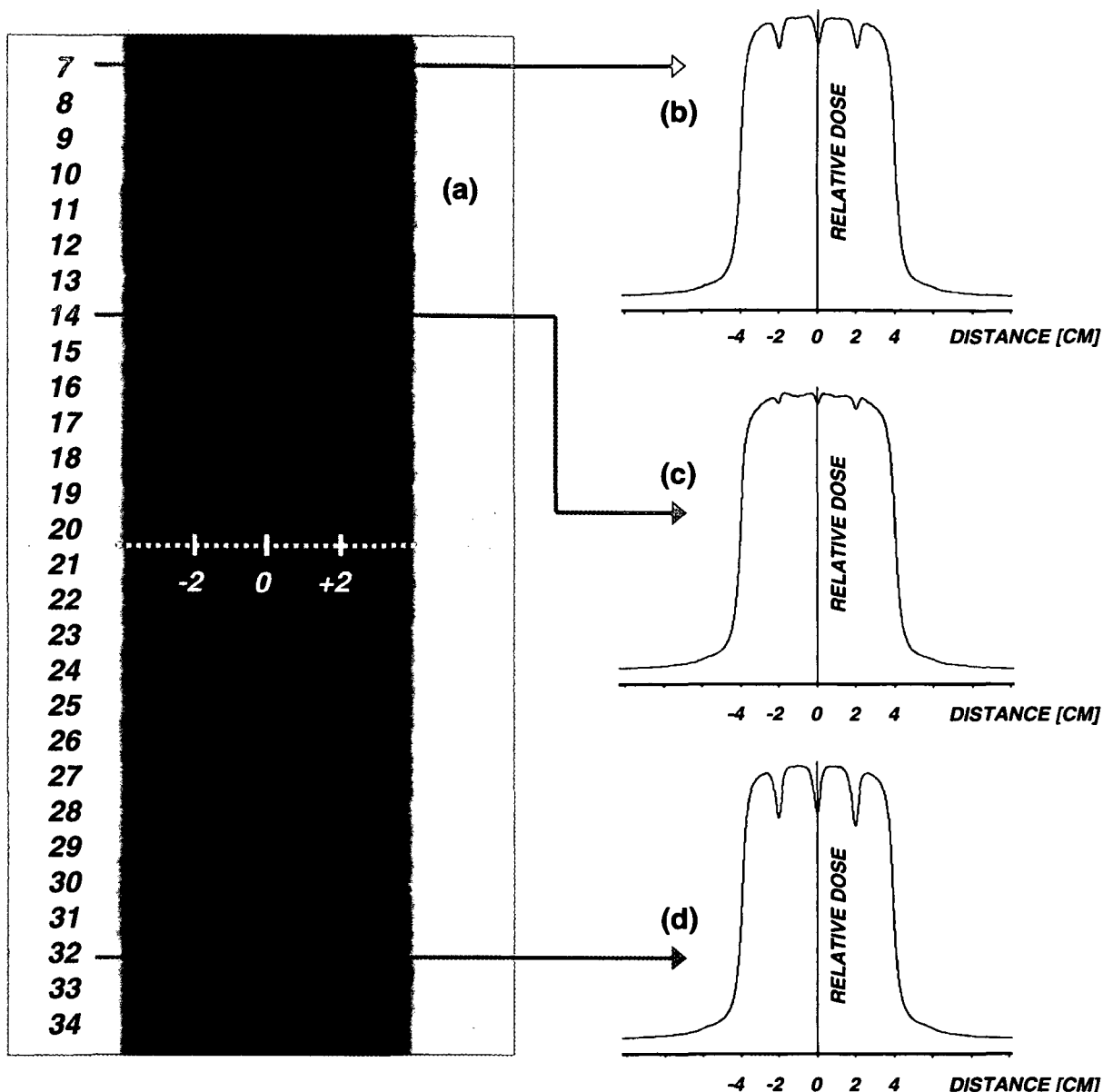
Figure 4.11 (a) *Resultant film blackening of the leaf abutment measurement. Four adjoining gaps of 2 cm nominal width shaped by leaves only were irradiated consecutively, generating match-lines at -2 cm, 0 cm (i.e. collimator midline), and +2 cm. For leaf pairs 7 to 34, profiles were defined in leaf movement direction at the centre of each leaf pair, in order to check the dosimetric steadiness within the composed field. As examples, relative dose vs. distance is displayed in* **(b)** *for leaf pair number 7, in* **(c)** *for pair number 14, and in* **(d)** *for pair number 32. To evaluate the leaf performance, beam flatness, FWHM, and maximum underdosage were derived from the profiles (see text for more details).*

When looking at leaf pair 7 displayed in Figure 4.11 (b), larger deviations from the ideal profile become obvious. While the overall field size is nearly perfect (7.99 cm), an increased flatness value of 5.95% has to be noted. This seems to be quite astonishing since that leaf pair had produced a mean gap width of 2.00 cm, as

described in the section above. An explanation may be found in the design of single-focussed leaves, for which it is not possible to generate perfectly abutting penumbra from opposing leaves. In addition, the inevitable tolerances of mechanically driven components have to be considered. However, the maximum underdosage in the abutment lines of leaf pair 7 is found to reach 9%, which is still acceptable since it is unlikely to cause significant dose errors in case of many superimposing beam segments delivered from different angles [Convery and Rosenbloom 1995]. Based on a dose gradient of about 10% per mm in the beam penumbra, a positional uncertainty of 0.9 mm may be estimated from the maximum underdosage, corresponding to roughly 0.45 mm for each leaf side.

As an example for insufficiently calibrated leaf pairs, number 32 is presented in Figure 4.11 (d). The composed field shows a beam flatness of 11.76% and a maximum underdosage of 19%, reflecting a mechanical deviation of about 1 mm for each leaf, as derived from the beam penumbra again. Thus, in combination with the poor result of the gap measurement (1.93 cm) described in 4.5.2.1, a re-calibration was required. Analogously, leaf pairs 16 and 34 had to be adjusted.

4.5.3 Clinical consequences

In summary, the ELEKTA PRECISE machine turned out to be well suited for the delivery of segmental MLC based IMRT. The isocenter accuracy is found to be significantly better than 1 mm, including gantry and couch rotations, which is checked in a daily QA procedure. For the MLC, the required precision of better than 0.5 mm holds as long as the leaves are correctly calibrated. This points out the importance of regular MLC inspections in order to meet the accuracy that is necessary for IMRT treatments.

CHAPTER 5 is based on

NORMALIZED SENSITOMETRIC CURVES FOR THE VERIFICATION OF HYBRID IMRT TREATMENT PLANS WITH MULTIPLE ENERGIES

Dietmar Georg[1], Bernhard Kroupa[1,2], Peter Winkler[1,2], and Richard Pötter[1]

[1] Division of Medical Radiation Physics, Department of Radiotherapy and Radiobiology, Medical University of Vienna, Waehringer Guertel 18–20, A-1090 Vienna, Austria

[2] Atomic Institute of the Austrian Universities, Stadionallee 2, A-1020 Vienna, Austria

Abstract:

With the clinical implementation of time-variable dose patterns and intensity modulated radiotherapy (IMRT) film dosimetry has regained popularity. Films are currently the most frequently used dosimetric means for patient specific quality assurance in IMRT. A common method is to verify a so-called hybrid IMRT plan, which is the patient specific treatment plan with unmodified fluence patterns recalculated in a dedicated phantom. For such applications the sensitometric curve, i.e., the relation between optical density (OD) and absorbed dose, should not depend critically on beam energy, field size and depth, or film orientation. In order to minimize the influence of all these variables a normalization of sensitometric curves is performed at various photon beam energies (6 MV, 10 MV, 25 MV). By doing so one unique sensitometric curve can be used for these three beam qualities. This holds for both film types investigated: Kodak X-Omat V films and EDR-2 films. Additionally, the influence of field size, depth, and film orientation on a normalized sensitometric curve is determined for both film types. For doses smaller than 0.8 Gy for X-Omat V and doses smaller than 3 Gy for EDR-2 films the field size variation of normalized sensitometric curves is much smaller than 3% for fields up to 20x20 cm^2. For X-Omat V films all differences between sensitometric curves determined at depths of 5, 10, and 15 cm are smaller than 3%. For EDR-2 films deviations larger than 3% are only observed at low net OD smaller than 0.25. The dependence of film orientation (parallel versus perpendicular) on a normalized sensitometric curve is found to be not critical. However, processing conditions have the largest influence and can result in differences up to 20% for sensitometric curves derived from films of the same batch but using different film processors. When normalizing sensitometric curves to the dose value necessary to obtain a net OD = 1 for that respective geometry and energy the large energy dependence of sensitometric curves can be almost eliminated. This becomes especially important for the verification of hybrid IMRT plans with multiple energies. Additionally, such a normalization minimizes other influences such as field size, depth, and film orientation. This method is generally applicable to both Kodak X-Omat V and EDR-2 films. In order to achieve the highest accuracy level an upper dose limit of 0.8 Gy for X-Omat V films and 3 Gy for EDR-2 films should be taken into account. However, these dose limits may vary with film reading instrument and film processor.

5.1 INTRODUCTION

In radiation therapy difficulties are associated with measurements of isodose curves in high gradient regions using conventional dosimetric tools (e.g., TLDs or ionization chambers) due to their limited spatial resolution. Radiographic film has been a valuable tool in dosimetry since the introduction of Co-60 and betatrons, especially for two-dimensional dosimetry [Granke *et al* 1954, Hettinger and Svensson 1967, Dutreix and Dutreix 1969]. It offers several advantages, such as high spatial resolution, two-dimensional information with a single irradiation, suitability for use in inhomogeneous phantoms, flexibility at curved interfaces, short immobilization time, negligible distortion of dose distributions, and cost effectiveness. Disadvantages of radiographic films are the energy dependent response due to the high atomic number of silver, film processing and film reading which do not allow on-line evaluation, and its dependence on processing conditions. However, films are widely used for acceptance testing and commissioning periodic QA as well as for pre-clinical studies of RT equipment.

With the clinical implementation of time-variable dose patterns and intensity modulated radiotherapy (IMRT) film dosimetry has regained popularity [Martens *et al* 2002b, Zhu *et al* 2002, Cadman *et al* 2002, Esthappan *et al* 2002]. Films are not only used for checking delivery equipment and treatment planning systems for quality assurance purposes but also for patient specific pre-treatment verifications. Although calculational methods have been developed for patient specific pre-treatment verification of IMRT at present, experimental methods are most commonly applied [Zhu *et al* 2002, Xing *et al* 2000, Kung *et al* 2000].

There are two approaches for experimental IMRT verification, which also can be combined. The first approach is to verify each individual beam by measuring the dose distribution at a certain depth or the fluence profile in air perpendicular to the incident beam, e.g., by using films. However, for such measurements charge couple devices or electronic portal imaging systems are an alternative to films and provide the advantage of on-line information [Xing *et al* 1999, Curtin-Savard and Podgorsak 1999, Van Esch *et al* 2001]. The second approach is to verify a so-called hybrid IMRT plan, which is the patient specific treatment plan with unmodified fluence patterns recalculated in a dedicated (homogeneous) phantom. For the latter method,

ion chambers, TLDs, or semiconductor detectors are used for absolute dose measurements while films are used to verify dose distributions in one or more relevant planes [Cadman *et al* 2002, Low *et al* 1998a, Chuang *et al* 2002].

Composite treatment plans can be evaluated by placing the film either in axial or coronal planes. For such applications the calibration curve, i.e., the relation between optical density (OD) and absorbed dose, should not depend critically on film orientation. In general, sensitometric curves of radiographic films show a nonlinear dose response and depend on beam energy, field size and depth, film emulsion, processing conditions, and film reading instrument. Concerning the influence of film orientation, many controversial results have been published. Danciu *et al* (2001) have summarized publications on all these influences in a recent paper.

When verifying composite hybrid treatment plans an analysis is made by superimposing measured and calculated dose distributions, either manually using printed isodose distributions and a light box or in a more elegant way by using software tools. For IMRT a simple subdivision in regions with high and low dose gradients and different acceptance criteria is no longer possible. An efficient and accurate quantitative dose comparison can be performed by using the γ-evaluation, which simultaneously incorporates dose and distance-to-agreement criteria [Low *et al* 1998b, Depuydt *et al* 2002]. However, methods to analyze composite treatment plans are beyond the scope of this work.

In this paper two different Kodak (Eastman Kodak Company, New York, US) films are investigated for the verification of hybrid IMRT treatment plans with multiple energies, X-Omat V films, and EDR-2 films. In order to be able to apply one unique sensitometric curve irrespective of photon beam energy a normalization is performed [Novotny *et al* 1997]. The influence of field size, depth, and film orientation on normalized sensitometric curves is determined for both film types.

5.2 MATERIALS AND METHODS

Both Kodak X-Omat V films and Kodak EDR-2 films are ready pack films with a low speed. The X-Omat V type is probably the most commonly applied film type used in radiotherapy. Its sensitometric curve is in general nonlinear. The main disadvantage of this film type is its limited dose range. A common approach to

overcome this limitation is to downscale monitor units in order to be in a dose range suitable for film dosimetry. However, this approach is not ideal when verifying IMRT treatments since there is a chance that the linac stability at very low monitor units (MU) influences the verification result. EDR-2 film is a relatively new film type. Its characteristics and applicability for IMRT dose verification have been described in recent publications [Zhu *et al* 2002, Olch 2002]. The main advantage of this film type as compared to X-Omat V film is its reduced sensitivity. EDR-2 film allows us to deliver fractional doses in the range between 1 and 5 Gy, hence standard daily fractional doses around 2 Gy can be verified without any problem.

All measurements are performed in a 30×30×25 cm^3 polystyrene phantom consisting of plates of various thickness. One plate has a special insert for a Farmer type ionization chamber. Absolute dose measurements are performed with a cylindrical ionization chamber (Farmer type NE 2571, Nuclear Enterprise) connected to a NE 2620 electrometer (Nuclear Enterprise), calibrated in an absorbed dose to water. High energy photon beams of 6 MV, 10 MV, and 25 MV, provided by an ELEKTA Precise accelerator (ELEKTA Oncology systems, Crawley, UK), are used. The linac is equipped with a MLC and is able to deliver segmental IMRT.

Sensitometric curves are determined as a function of beam energy for both Kodak X-Omat V and EDR-2 films for a field size of 10×10 cm^2. For a determination of this reference sensitometric curve films are placed perpendicular to the incident beam at a depth of 5 cm in the polystyrene phantom, at a source to surface distance of 95 cm. For each beam energy the respective "absolute" sensitometric curves are normalized to that value of the absorbed dose necessary to obtain a net OD = 1. This value is found by fitting a polynomial to measured data. In the following, this type of sensitometric curve will be referred to as a "normalized" sensitometric curve (NSC).

In a second step, the influences of field size, depth, and film orientation on normalized sensitometric curves are evaluated for both film types and all available photon beam qualities. For different geometric conditions absolute sensitometric curves are determined and normalized to that value of the absorbed dose necessary to obtain a net OD = 1 for the respective geometry. Finally, the resultant normalized dose values are compared with the normalized sensitometric curve obtained in reference conditions.

The field size dependence is determined for field sizes of 5×5 cm^2 and 20×20 cm^2 in perpendicular geometry, where films are positioned at a depth of 5 cm

using a SSD of 95 cm. In perpendicular geometry films are irradiated in the isocenter at depths of 10 cm and 15 cm for a field size of 10×10 cm^2 in order to determine the depth dependence. Additionally, films are irradiated in parallel geometry for the same field size at SSD = 95 cm by turning the gantry to 90°. In order to minimize the possible influence of air gaps film jackets are punctured at the corners prior to irradiation and a block of lead (weight 7.2 kg) is put on the top of the phantom. For films irradiated in parallel geometry, OD densities are determined at depths of 5 and 15 cm and normalized sensitometric curves are constructed. In parallel geometry films are marked with a needle at zero depth. The distance from the film edge (in air) to the phantom is about 1.5 cm.

Films are processed using a computer controlled film processor (Kodak M 35 X-Omat processor). After processing films are scanned with a Vidar VXR-12 plus scanner (Vidar Systems Corp., Herndon, US) connected to a PC. All scans are performed with a resolution of 150 dpi and a depth of 12 bit. Prior to film reading the scanner is warmed up at least for 30 min. Film analysis is performed using the RIT 113 software package (Version 3.11, Radiological Imaging Technology, Colorado Springs, US) for film dosimetry. Gray scale values are converted to OD values using a calibration film and following a calibration procedure recommended by the vendor [Radiological Imaging Technology 2001].

In perpendicular geometry all OD values presented below are averaged over a square area of 2×2 cm^2 around the central axis. In parallel geometry the area for averaging is 0.5×5 cm^2 with the long axis perpendicular to the incident beam. The centre of this rectangle is considered when referring to a certain depth in this geometry.

5.3 RESULTS

5.3.1 Reference sensitometric curves

Figure 5.1 (a) shows the net OD versus absorbed dose for a 10×10 cm^2 field size as a function of photon beam energy for EDR-2 films and X-Omat V films placed at 5 cm depth. The symbols represent measured data, the solid lines represent fitted

data. For both film types the energy dependence varies with dose. The difference between sensitometric curves is largest between 6 MV and 25 MV photon beams. It increases from 6% to 9% for X-Omat V films in the dose range between 0.3 Gy and 1 Gy. For EDR-2 films this difference decreases from about 13% at 0.5 Gy to 6% at 4.5 Gy.

(a) Absolute Sensitometric Curves for film types Kodak EDR-2 and X-Omat V

Legend:
▲ X 6 - EDR-2
◆ X 10 - EDR-2
◆ X 25 - EDR-2
△ X6 - XV
◇ X 10 - XV
○ X 25 - XV

(b) Normalized Sensitometric Curves for film types Kodak EDR-2 and X-Omat V

Legend:
— EDR-2 calc
▲ EDR-2 meas - all energies
— XV calc
◆ XV meas - all energies
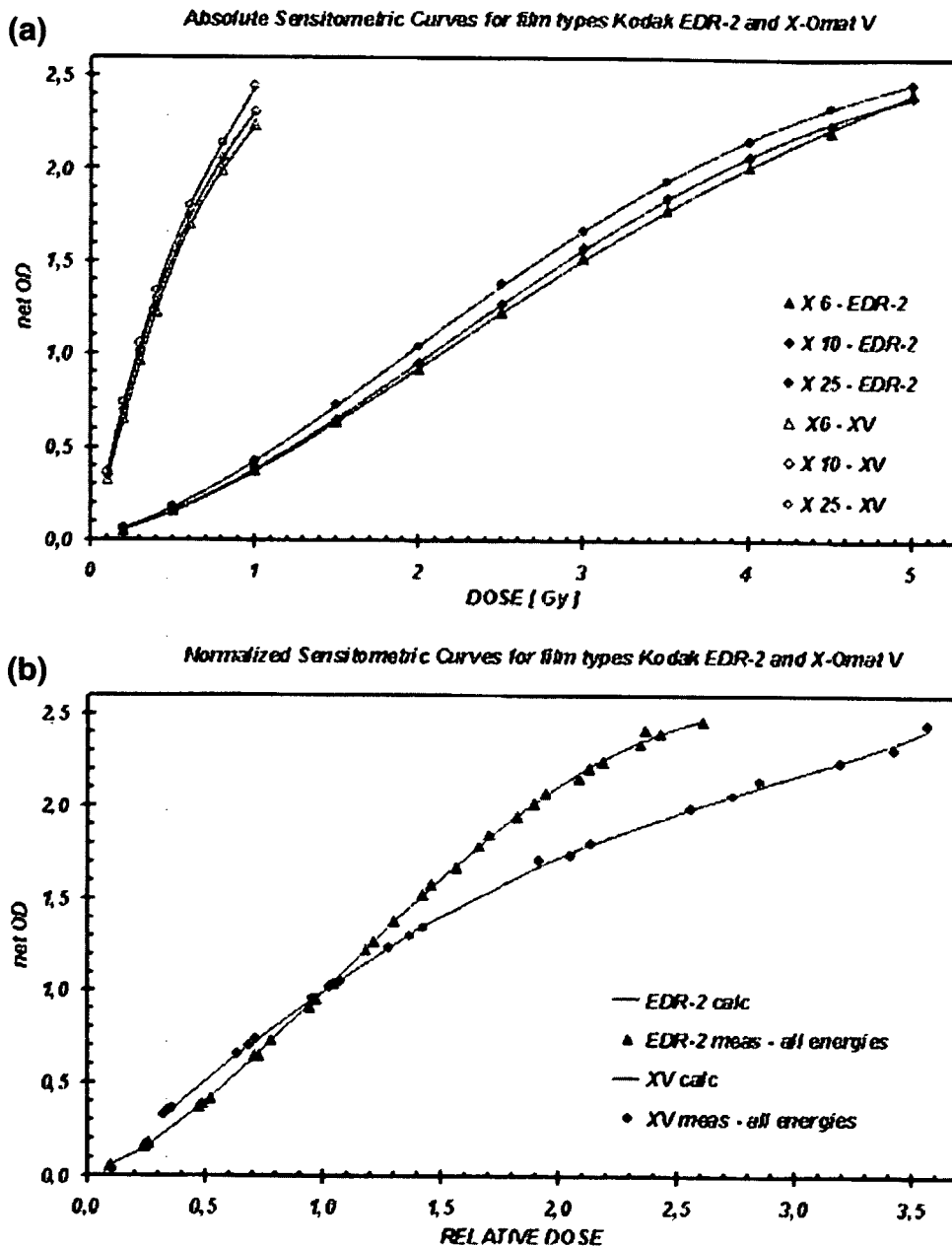
Figure 5.1 (a) *Net OD versus absorbed dose for a 10×10 cm² field size as a function of photon beam energy for EDR-2 films and X-Omat V films placed at 5 cm depth. The symbols represent measured data; the solid lines represent fitted data.* (b) *Net OD versus normalized dose for a 10×10 cm² field size as a function of photon beam energy for EDR-2 films and X-Omat V films placed at 5 cm depth. The symbols represent measured data, the solid lines represent fitted data.*

Figure 5.1 (b) shows the normalized sensitometric curves for both film types. The symbols represent all measured data given in Figure 5.1 (a), the solid lines represent fitted data using a polynomial. Note that after normalization the energy

dependence of either film type is negligible. Table 5.1 presents the absolute doses used for normalization, i.e., the values necessary to obtain a net OD = 1 in reference conditions (field size 10×10 cm^2, SSD = 95 cm, d = 5 cm) as a function of film type and photon beam energy.

Energy	X-Omat V [Gy]	EDR-2 [Gy]
6 MV	0.31	2.12
10 MV	0.29	2.06
25 MV	0.28	1.92

Table 5.1 *Absolute dose values necessary to obtain a net OD = 1 as a function of film type and photon beam energy (for reference conditions).*

5.3.2 Influence of geometry

The influence of field size on normalized sensitometric curves is shown in Figure 5.2 (a) and (b) for X-Omat V films and EDR-2 films. For both film types the influence of field size increases with relative dose. For X-Omat V films and relative doses larger than 2.7 the net OD differs by more than 3% from the reference sensitometric curve for field sizes of 5×5 cm^2 and 20×20 cm^2. The relative dose value for EDR-2 films where the field size influence cannot be neglected is about 1.7. Depending on energy, the corresponding absolute dose values are about 0.7–0.8 Gy for X-Omat V films and 3–3.5 Gy for EDR-2 films.

Figure 5.3 (a) and (b) show the influence of depth on normalized sensitometric curves for X-Omat V films and EDR-2 films. The influence of depth is less pronounced for X-Omat V films as compared to EDR-2 films. For X-Omat V films all deviations between normalized sensitometric curves determined at depths of 5, 10, and 15 cm are less than 3%. For EDR-2 films deviations larger than 3% are only observed for net OD smaller than 0.3, which corresponds to an absorbed dose value around 0.7 Gy, neglecting small variations with photon beam energy for small net OD values.

The influence of parallel beam incidence on normalized sensitometric curves is illustrated (Figure 5.4 (a) and (b)) for both film types. For EDR-2 films deviations between measured data for parallel beam incidence and the reference sensitometric curve determined from perpendicular orientation is less than 3% if the relative dose is

higher than 0.25 at 5 cm depth and higher than 0.4 at 15 cm depth. For X-Omat V films respective relative dose values are about 0.25 for 5 cm as well as for 15 cm depth. The corresponding absolute dose values are in the order of 0.1 Gy for X-Omat V films and in the order of 0.8 Gy for EDR-2 films.

Figure 5.2 (a) *The influence of field size variation on the normalized sensitometric curve for X-Omat V films. The symbols represent measured data for various energies and field sizes of 5×5 cm² and 20×20 cm², respectively. The solid lines represent the normalized sensitometric curve for a field size of 10×10 cm². All measurements are performed at 5 cm depth.* **(b)** *The influence of field size variation on the normalized sensitometric curve for EDR-2 films. The symbols represent measured data for various energies and field sizes of 5×5 cm² and 20×20 cm², respectively. The solid lines represent the normalized sensitometric curve for a field size of 10×10 cm². All measurements are performed at 5 cm depth.*

(a) *Influence of Depth on Normalized Sensitometric Curve - Kodak X-Omat V*

Legend:
- □ D10-X6
- ◇ D10-X10
- ○ D10-X25
- + D15-X6
- × D15-X10
- ✳ D15-X25
- — NSC-XV

(b) *Influence of Depth on Normalized Sensitometric Curve - Kodak EDR-2*

Legend:
- □ D10-X6
- ◇ D10-X10
- ○ D10-X25
- + D15-X6
- × D15-X10
- ✳ D15-X25
- — NSC-EDR-2
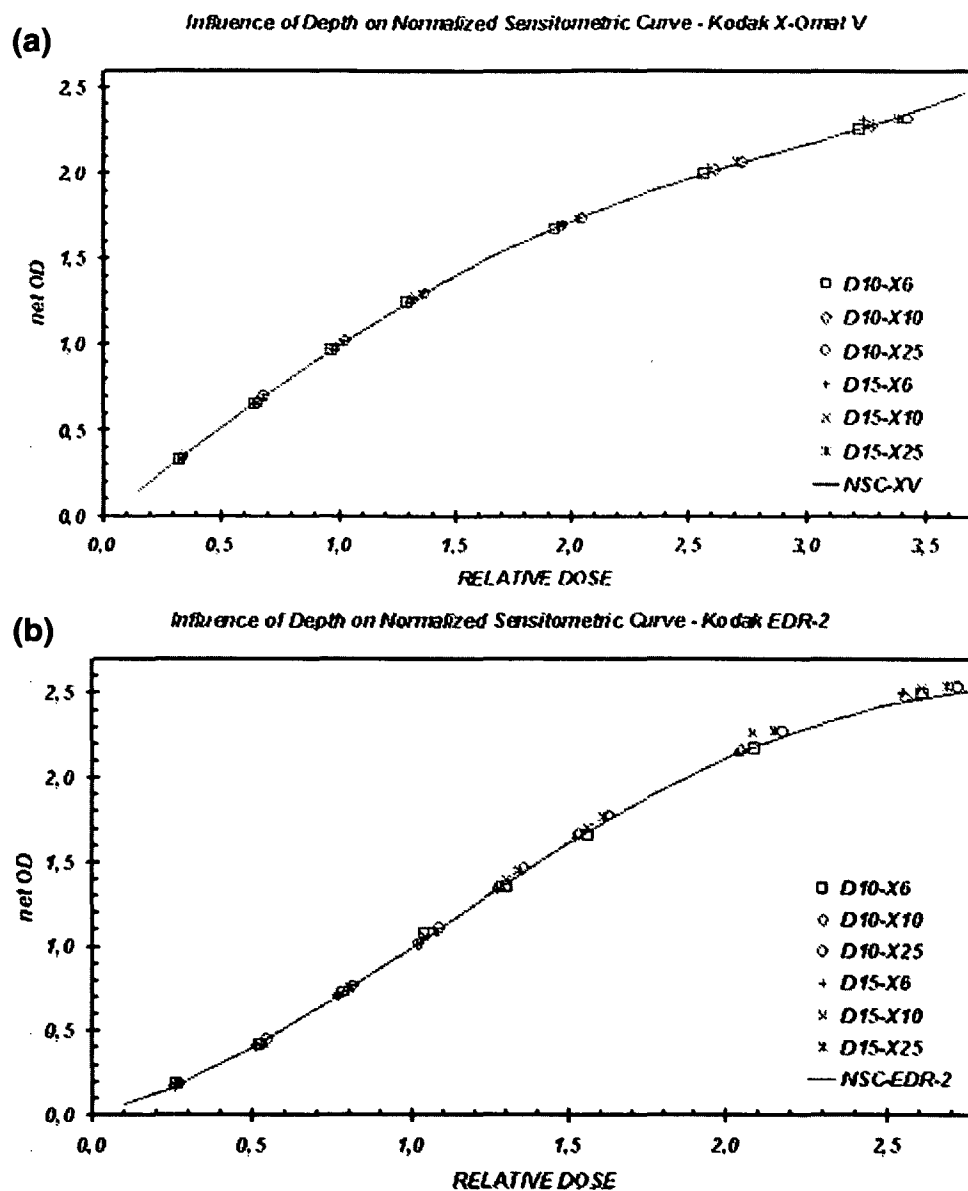
Figure 5.3 (a) *The influence of depth on the normalized sensitometric curve for X-Omat V films. The symbols represent measured data for various energies and a depth of 10 cm and 15 cm, respectively. The solid lines represent the normalized sensitometric curve determined at 5 cm depth. All measurements are performed for a field size of 10×10 cm². **(b)** The influence of depth on the normalized sensitometric curve for EDR-2 films. The symbols represent measured data for various energies and depth of 10 cm and 15 cm, respectively. The solid lines represent the normalized sensitometric curve determined at 5 cm depth. All measurements are performed for a field size of 10×10 cm².*

(a) *Influence of Parallel Incidence on Normalized Sensitometric Curve - Kodak X-Omat V*

(b) *Influence of Parallel Incidence on Normalized Sensitometric Curve - Kodak EDR-2*
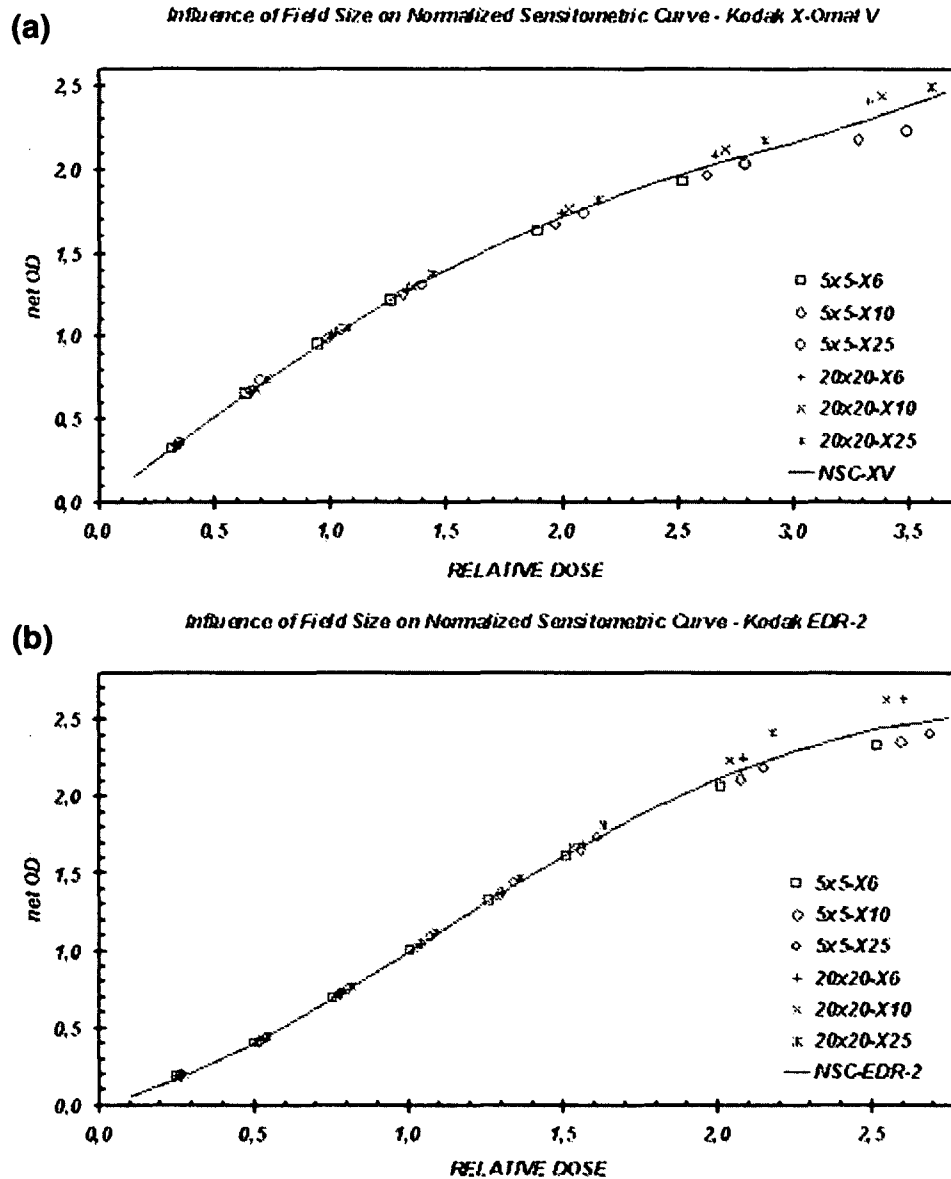
Figure 5.4 (a) *The influence of parallel beam incidence on the normalized sensitometric curve for X-Omat V films. The symbols represent measured data for various energies and depth of 5 cm and 15 cm for parallel geometry. The solid lines represent the normalized sensitometric curve determined for perpendicular beam incidence for a field size of 10×10 cm² at 5 cm depth.* **(b)** *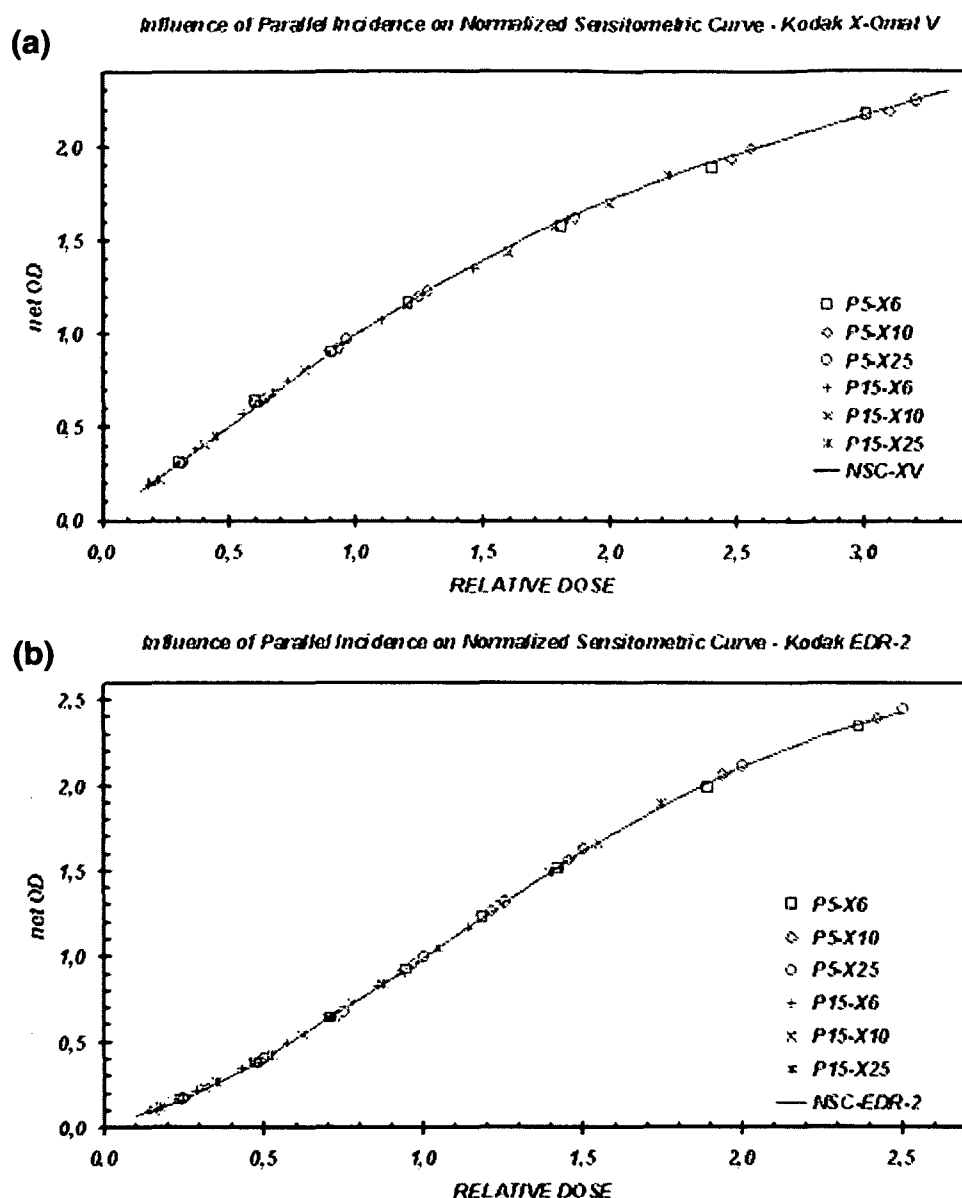The influence of parallel beam incidence on the normalized sensitometric curve for EDR-2 films. The symbols represent measured data for various energies and of 5 cm and 15 cm for parallel geometry. The solid lines represent the normalized sensitometric curve determined for the perpendicular beam incidence for a field size of 10×10 cm² at 5 cm depth.*

All relative dose values given previously refer to deviations ≤3% between measured net OD for the respective geometry and calculated net OD using the reference sensitometric curve. However, if relative doses are within the given threshold values these differences are much smaller. Table 5.2 summarizes the deviations between measured net OD for the respective geometry and net OD calculated from the reference sensitometric curve. For calculating mean deviation and standard deviation between calculated and measured values only measurement points are included with deviations ≤3%, i.e., measurements within the dose range recommended above. The last column of Table 5.2 indicates the number of measurements contributing to average deviation and standard deviation.

film type	parameter	mean dev.	std. dev.	meas. number
X-Omat V	field size	1.1%	0.8%	34/42
	depth	0.7%	0.7%	41/41
	parallel incidence	1.0%	0.8%	34/40
EDR-2	field size	1.0%	1.0%	33/48
	depth	1.1%	0.8%	42/48
	parallel incidence	1.0%	1.0%	39/48

Table 5.2 *Mean deviation and standard deviation between calculated values using the normalized reference sensitometric curve and measured values as a function of geometry. Note that only points in the recommended dose range (deviation ≤3%) are taken into account. The last column indicates the number of measurements being within this range.*

5.3.3 Batch and processor sensitivity

In order to test the stability of the normalized sensitometric curve another set of curves is determined for either type of film after 9 months. During this time period different film batches are used and all chemicals of the film processor have been replaced as well. Deviations between measured data points and the fit function derived from initial measurements are mostly less than 1% and do not exceed 1.5% for single points.

Finally, the influence of the film processing machine on the shape of the normalized sensitometric curve is investigated. Another set of films is irradiated at a depth of 5 cm in isocentric conditions with a 10×10 cm² field size and a normalized sensitometric curve is constructed. Figure 5.5 illustrates the influence of different film processing devices on normalized sensitometric curve.

Influence of Film Processor on Normalized Sensitometric Curve
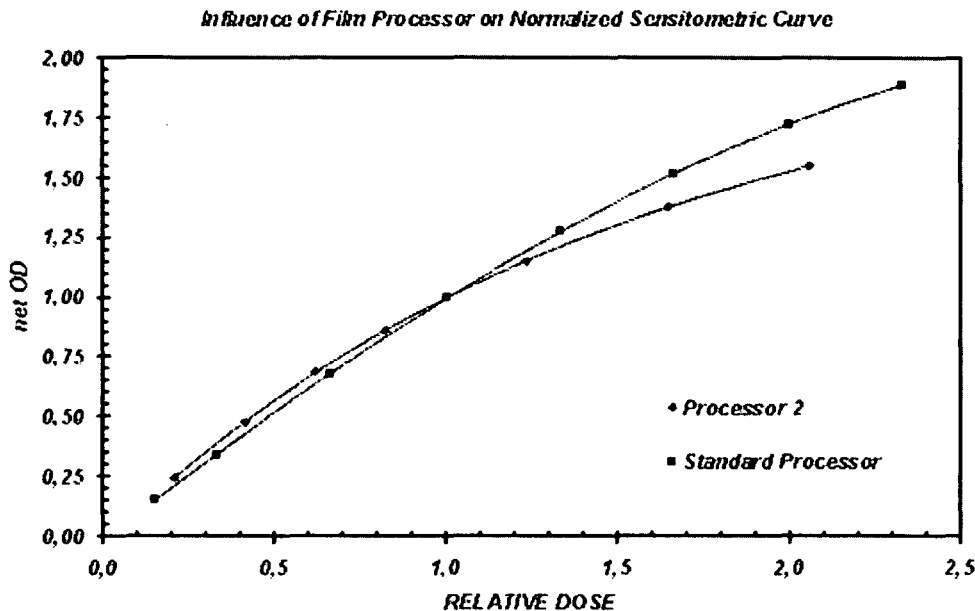
Figure 5.5 *The influence of film processor on normalized sensitometric curves for X-Omat V films.*

5.4 DISCUSSION

The introduction of new treatment techniques requires great caution and special attention has to be paid to the verification of dose distributions prior to patient treatments, especially when highly conformal dose distributions are to be delivered. In IMRT one treatment field is generated by the superposition of MLC shaped segments or by dynamic techniques where mechanical components are moving during irradiation. Thus, the resulting dose distribution depends critically on mechanical components as well as on the dose calculation accuracy of the local treatment planning system. IMRT implies that the dose may be correct at some points in the field but can be wrong at other points. Therefore it has been generally accepted that the dose should be verified in many points. In contrast to static fields with uniform fluence distributions the use of scanning point detectors is very time consuming as for the verification of treatment techniques with time variable dose

89

patterns a whole field (or treatment plan) has to be applied completely for each measurement point.

To overcome this time consuming and cumbersome verification, two- or three-dimensional dosimetric techniques are applied, e.g., films, detector arrays or gels [Cadman et al 2002, Curtin-Savard and Podgorsak 1999, Van Esch et al 2001, Low et al 1998a, Depuydt et al 2002]. Gels provide three-dimensional information but many radiotherapy departments have no or only limited access to magnetic resonance scanners which are needed for gel dosimetry. Detector arrays can be hardly used in anthropomorphic phantoms and have often limited spatial resolutions. On the contrary, films have high spatial resolution, but they do not provide an on-line evaluation and show critical dependence on various factors [Martens et al 2002b, Zhu et al 2002, Danciu et al 2001]. Nevertheless, films have become an important tool for IMRT verifications.

One critical parameter in film dosimetry is the dependence of the sensitometric curve on beam energy. As displayed in Figure 5.1 (a) this dependence can amount up to several percent and cannot be neglected. When applying different beam qualities for a treatment plan it is not straightforward to verify such a composite plan. Using films one option is to verify each beam individually and use an energy specific sensitometric curve. Another option is to construct normalized sensitometric curves and to verify composite treatment plans with multiple beam energies in a relative manner. As shown in Figure 5.1 (b) for relative dosimetry, only one sensitometric curve is needed for different photon beam qualities in order to convert optical densities into relative dose values. The verification of hybrid IMRT plans with films in terms of relative dose distributions is not critical because the absolute dose in the normalization point can be easily measured in a phantom if an appropriate insert (e.g., for a chamber or TLD) is available. Moreover, such a two step process in QA of IMRT is widely applied [Cadman et al 2002, Low et al 1998a, Chuang et al 2002, Olch 2002, Georg and Kroupa 2002].

The variation of sensitometric curves with depth is not critical for both Kodak EDR-2 and X-Omat V films, which is in agreement with published results on X-Omat V films and EDR-2 films [Esthappan et al 2002, Danciu et al 2001]. The most critical parameters in our investigation are energy and field size. In our study the energy dependence of EDR-2 films is larger than the one for X-Omat V films, which is opposite to the findings of Dogan et al (2002).

90

For doses smaller than 0.8 Gy for X-Omat V and doses smaller than 3 Gy for EDR-2 films the field size variation of normalized sensitometric curves is much smaller than 3% for fields up to 20x20 cm^2 (see Table 5.2). Hence the normalization introduced decreases the field size dependence of sensitometric curves. Depending on film type, depth of measurement and energy, unnormalized or uncorrected sensitometric curves can vary largely (~10%) in the FS range considered in the present study [Esthappan et al 2002, Danciu et al 2001, Dogan et al 2002, Suchowerska et al 1999]. By introducing a depth correction, Dogan et al (2002) reported a substantial reduction of the field size dependence of sensitometric curves for the same film types as used in our study.

The dependence of film orientation on the normalized sensitometric curve is found to be not critical. However, literature data on the influence of beam orientation is controversial. Suchowerska et al (2001) and Danciu et al (2001) suggested to tilt the beam with respect to the film by 2° in order to minimize the over-response of films when measuring in parallel geometry. Another proposed method for correcting the film over-response in parallel geometry is to use lead filters placed in the phantom [Ju et al 2002]. In our investigation we simply used some weight on the phantom in order to minimize the possible influence of air gaps. When using anthropomorphic slab phantoms a similar effect can be obtained for films in axial planes by using large screws or a pair of tongs. From our results we conclude that the most crucial impact on films in parallel geometry is the one of air gaps. The influence of air gaps on the film dosimetry of electron beams has been described in detail already in 1969 [Dutreix and Dutreix 1969].

The largest deviations between measured and calculated net OD are observed either at very high or at very low net OD. At high OD the accuracy of a 12 bit deep reading device is limited by noise. Thus a 16 bit scanner would probably help to overcome the limitations at the high dose end. Larger variations between measured and calculated net OD at the low dose end are basically due to the small OD values, as a small absolute difference can become a very large relative deviation.

Although the stability of normalized sensitometric curves with time and different film batches is very good for the limited time period considered, it is important to check the shape of the sensitometric curve at regular intervals as part of the QA program, especially when new film batches or chemicals are used. Sensitometric curves are most critically influenced by processing conditions (see

Figure 5.5). Depending on the film processor, the difference in sensitometric curves for the same batch of films can amount up to 20%, which is in the same order of magnitude as the inter-institutional variation in film processing described by Bos *et al* (2002). They have introduced another normalization method in order to obtain relative OD as a function of the absolute dose. By doing so they could reduce variations of sensitometric curves with batch composition, irradiation conditions, film processing, and film scanning. However, they used a fixed field size of 5×5 cm^2 and a fixed depth of 1.6 cm throughout their study.

In a recent publication Zhu *et al* (2002) concluded that the double hit process is the dominant mechanism that renders the grains on EDR-2 films developable. According to this theory, sensitometric curves for EDR-2 films can be fitted using following equation:

$$OD = OD_1\left(1 - e^{-\alpha_1 D}\right) + OD_2\left(1 - e^{-\alpha_2 D}\left(1 + \alpha_2 D\right)\right) \tag{5.1}$$

where *OD* is the optical density, OD_1 and OD_2 are the maximum optical density by single hit and double hit processes, respectively, and α_1 and α_2 describe the film sensitivity for single and double hit processes, respectively. *D* is the absolute or relative dose. As for X-Omat V films only the single hit is involved, (5.1) can be reduced to

$$OD = OD_1\left(1 - e^{\alpha_1 D}\right) \tag{5.2}$$

In our study, for normalized sensitometric curves in reference conditions (FS = 10×10 cm^2, SSD = 95 cm, d = 5 cm) the following fitting parameters are obtained for EDR-2 films after an iteration to minimize the quadratic deviation between measured and calculated values: OD_1 = 0.1106, OD_2 = 3.2984, α_1 = 5.3165, and α_2 = 1.0177. For X-Omat V films the respective fitting parameters are OD_1 = 3.329 and α_1 = 0.359. It is noteworthy that the convergence of such a fitting procedure depends largely on starting parameters as there are several local minima. In our study the original data set of Zhu *et al* (2002) is used as starting values for the iteration.

5.5 CONCLUSION

EDR-2 films have become available recently and have been subject to a few investigations and dosimetric comparisons [Zhu *et al* 2002, Esthappan *et al* 2002, Olch 2002, Dogan *et al* 2002]. It is generally agreed that the main advantage of this film type is its extended dose range which allows us to deliver IMRT hybrid plans at dose levels where the linac output is stable. However, this film type presents similar characteristics and limitations as other film types, such as the dependence of sensitometric curves on energy, field size, depth, and orientation.

All these influences can be minimized when normalizing sensitometric curves to the dose value necessary to obtain a net OD = 1 for that respective geometry and energy. By doing so the large energy dependence of sensitometric curves can be almost eliminated which becomes especially important for the verification of hybrid IMRT plans with multiple energies. Such a normalization is generally applicable to both Kodak X-Omat V and EDR-2 films. In order to achieve the highest accuracy level an upper dose limit of 0.8 Gy for X-Omat V films and 3 Gy for EDR-2 films should be taken into account. However, these dose limits may vary with film reading instrument and film processor.

For irradiation in parallel geometry it is concluded that air gaps play the most important role. Their influence can be largely eliminated by puncturing holes in film envelopes together with additional weight or large screws when using slab phantoms.

CHAPTER 6

DEVELOPMENT OF A PATIENT SPECIFIC VERIFICATION PROCEDURE FOR IMRT TREATMENT PLANS

The commissioning of the intensity modulated radiotherapy system available at the Medical University of Vienna has been completed successfully. Its major components, the treatment planning system Helax-TMS (Nucletron) and the linear accelerator PRECISE (Elekta), have been investigated extensively, as described in CHAPTER 3 and CHAPTER 4. By identifying the system's limitations it has turned out to be well-suited for the delivery of segmental MLC based IMRT. However, due to the complex nature of IMRT treatment planning and application processes, a pre-treatment dosimetric verification for each patient is strongly recommended [Low *et al* 1998c, Essers *et al* 2001]. In the TPS, certain inaccuracies do not significantly affect the calculations of conventional treatment plans but possibly sum up to critical errors in IMRT deliveries, due to the superposition of multiple segments [Azcona *et al* 2002]. Thus, the establishment of a dosimetric QA protocol is essential to provide correct IMRT treatments. In the following sections, the development of a patient specific verification procedure at the Medical University of Vienna will be reported. It is based on a combination of single point ionization chamber measurements to verify the number of MU and subsequent film measurements to acquire relative 2D dose distributions, using the normalized sensitometric curve described in CHAPTER 5. Within various slab phantoms, the procedure can either be done for each individual beam or the composite hybrid IMRT plan. Both ways have been tested and will be explained. Finally, the development of dedicated phantoms and a quantitative method to compare measured and calculated dose distributions will be illustrated.

6.1 PHASE 1: SINGLE BEAM VERIFICATION

The first approach for the establishment of a patient specific QA programme was the method to verify each individual beam of an IMRT treatment plan. In the planning system a $30 \times 30 \times 20$ cm^3 cuboid phantom with a density of 1 g/cm^3 was

available, on which a medically approved IMRT treatment plan could be copied from the patient's CT set by DICOM transfer. In the phantom plan the gantry angles were changed to 0°, with the isocenter set to a depth of 10 cm. The MU were renormalized in order to deliver 2 Gy to the isocenter by each beam, while the relative segment fluence patterns taken from the original patient plan were left unmodified. Finally, the recalculated plan was transferred to the Linac, where the phantom was rebuilt of piled up Solid Water slabs (Gammex/RMI, Middleton, US) of various thickness allowing film measurements at any depth required, as well as ionization chamber measurements by special inserts.

For the single beam verification of IMRT treatment plans the ion chamber was positioned at the isocenter. After the point dose measurements, the chamber insert was replaced by films to measure 2D dose distributions perpendicular to beam incidence at a phantom depth of 10 cm, i.e. through the isocenter. Figure 6.1 illustrates the measurement geometry.
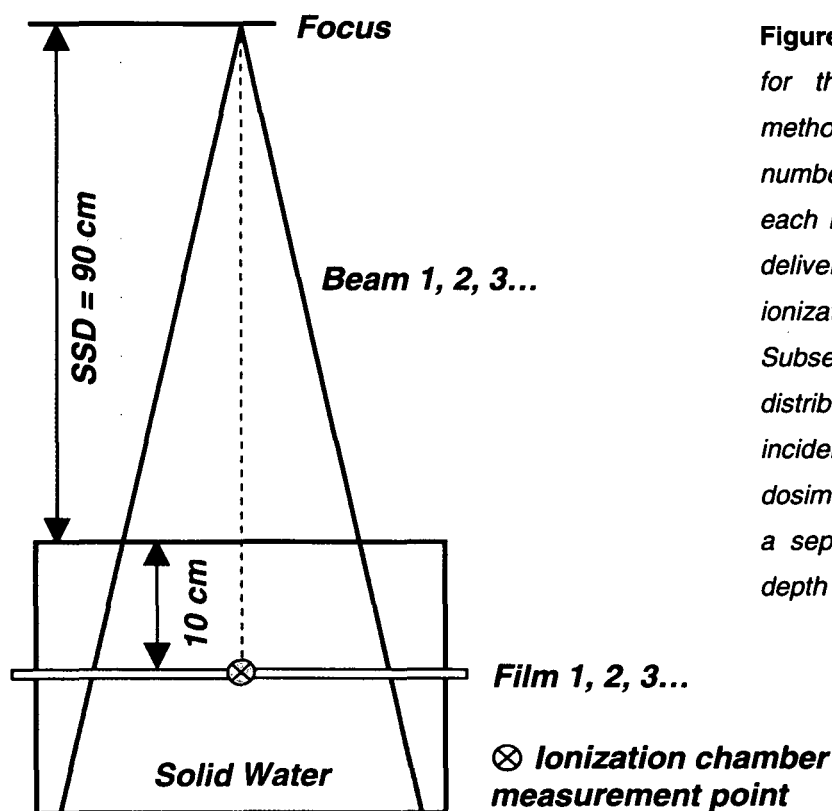
Figure 6.1 *Measurement geometry for the single beam verification method. In a first step, the absolute number of MU was checked for each beam by measuring the dose delivered to isocenter, where the ionization chamber was positioned. Subsequently, 2D relative dose distributions perpendicular to beam incidence were measured by film dosimetry, whereas for each beam a separate film was inserted at a depth of 10 cm (figure not to scale).*

For each beam, the dose delivered to isocenter was measured with a PTW 31002 ionization chamber having a sensitive volume of 0.125 cm^3, connected to a PTW UNIDOS electrometer. Its reference point was positioned on the central beam axis at a depth of 10 cm with the phantom at 90 cm SSD. This corresponds to the Linac calibration geometry, where the accelerator is tuned to give 2 Gy per 200 MU for each beam quality, at the centre of a square field of 10 cm length. Thus, for each IMRT beam the dose delivered to isocenter was determined indirectly by relating the collected charge to the calibration field of the respective energy, with the quotient ideally resulting in unity. The indirect measurement method is advantageous for three reasons. As the ratio of collected charges is calculated, corrections for air temperature and air pressure are not necessary, since they can be regarded as constant throughout the measurements (<20 min). Additionally, energy dependent chamber calibration factors cancel out when defining the quotient. Finally, inevitable daily variations of the Linac output do not affect the indirect measurement results. This is desirable since the verification procedure only aims at inspections of the calculation and delivery accuracy of IMRT segments, while other quality assurance aspects of the linear accelerator are covered by the routine maintenance programme.

For the relative dose measurements, Kodak EDR2 films were placed at 10 cm depth through the isocenter. For each single beam a separate film was used to measure 2D dose distributions perpendicular to beam incidence. After processing and scanning, the films were evaluated by the normalized sensitometric curve which has been developed in-house (CHAPTER 5). By doing so, relative isodose lines could be generated and printed on transparencies. In the virtual TPS phantom, the dose distribution was calculated in a perpendicular slice for each beam, corresponding to the film measurement plane. By overlaying the transparencies on the printouts from the planning system, the measured dose distribution could be optically compared to the calculated one.

The described single beam verification method revealed some major difficulties and disadvantages. Unlike in conventional radiotherapy, where open beams show flat profiles with steep dose gradients only at the field edges, IMRT treatment fields are characterized by inhomogeneous dose distributions within the beam cross-sections. Thus, cross-section profiles of single beams generally show variable dose gradients, as exemplarily displayed in Figure 6.2. It illustrates relative dose profiles (a) in gun-target direction (G-T) and (b) in perpendicular direction (A-B),

calculated at 10 cm phantom depth through the isocenter where the dose was normalized to 100%. The example is taken from the verification plan of the right-anterior beam in the prostate case that is described as case study 1 in section 7.1 (cf. Figure 7.1).
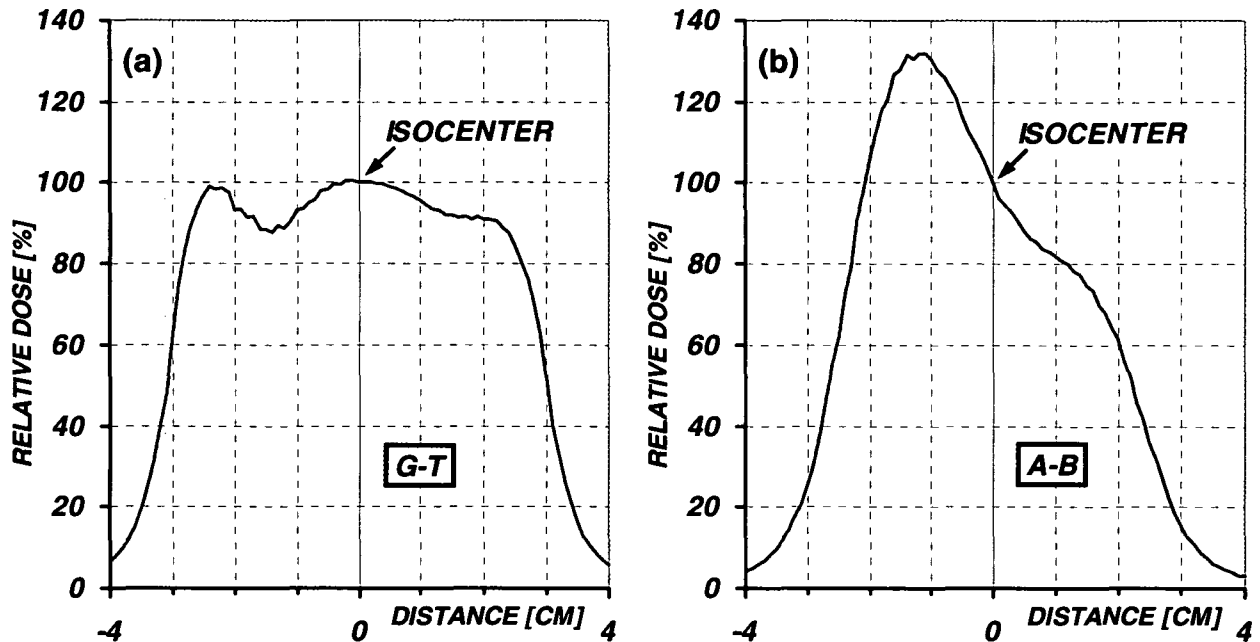
Figure 6.2 *Cross-section dose profiles of a typical IMRT treatment beam, plotted* **(a)** *in gun-target direction (G-T) and* **(b)** *in perpendicular (A-B). The data were calculated by the TPS at a phantom depth of 10 cm through the isocenter, where the dose was normalized to unity. Note the steep gradient in A-B direction, leading to large uncertainties in point dose measurements at the isocenter.*

At the isocenter, the dose gradient of the profile in G-T direction is negligible, while it rises up to more than 4% per mm in A-B. Hence, in such cases even a small misalignment of the phantom produces significant errors in the measured dose per beam delivered to isocenter. Additionally, the differences may be increased by inevitable mechanical margins of the MLC and certain inaccuracies of the penumbra modelling in the TPS. For the five treatment beams in case study 1, deviations of 1–9% from the calculated dose per beam (2 Gy) were found. However, measuring the total dose of the five IMRT beams (10 Gy) resulted in only 2.6% overall error. This is due to the fact that the composite treatment plan generates a quite homogeneous dose distribution around the isocenter, thus reducing the uncertainties mentioned above.

The relative dose verification of single IMRT beams by film dosimetry is affected analogously. For the application of the normalized sensitometric curve in order to convert optical density to relative dose values, a normalization point on the film has to be defined, where at the corresponding position in the TPS phantom the calculated dose is set to 100%. When using the isocenter as normalization point, steep dose gradients as depicted in Figure 6.2 (b) may lead to large differences between corresponding isodose lines, caused by geometrical inaccuracies in the normalization procedure. Defining the maxima of the calculated and measured dose distributions as normalization points does not solve the problem, since in IMRT the maxima are frequently sharp dose peaks, with values depending on the calculation grid size in the TPS as well as on the scanning resolution and filtering process during the film evaluation. Hence, in order to get a satisfying solution it is necessary to define appropriate normalization points in preferably homogenous regions for each individual beam, which can emerge as a very tedious procedure, particularly in more complex cases.

In addition to the severe normalization difficulties, the single beam verification method has turned out to be time-consuming and expensive, since for each beam a film has to be irradiated, processed, scanned, and evaluated. This counts especially for cases with a larger number of incidence directions.

Due to the mentioned drawbacks of the single beam verifications is was decided to omit this procedure. Instead, a method to verify the composite IMRT treatment plan has been developed that is described in the next section.

6.2 PHASE 2: HYBRID PLAN VERIFICATION

Like the single beam verification procedure, the hybrid plan verification method is based on a combination of a single point ionization chamber measurement and film measurements to obtain relative dose distributions. In a similar way, after the medical approval of an IMRT treatment plan, it is copied to the Solid Water slab phantom described in section 6.1. However, not only the segment fluence patterns are left unmodified as it has been done in the single beam method, but also the complete patient plan geometry, i.e. gantry, collimator, and couch angles. Additionally, the original relative beam weights are preserved as well. Thus, an exact clone of the

patient treatment plan is generated, a so-called "Hybrid" IMRT plan. In order to deliver a certain dose to isocenter the MU have to be recalculated, accounting for the different phantom shape compared to the patient outline.

Usually, the isocenter of the hybrid plan was positioned at the centre of the phantom, i.e. at a depth of 10 cm. Only in special cases with the isocenter being located in a region of noticeable dose gradients, it was moved in such a way that a homogenous dose region was established around the phantom centre, where the ionization chamber was positioned. After the point dose measurement, the chamber was removed and three coronal films were inserted instead, one at 10 cm depth through the isocenter, the others 2 cm above and 2 cm below, respectively. In Figure 6.3 the typical phantom setup for the verification of a five-field hybrid plan is shown.
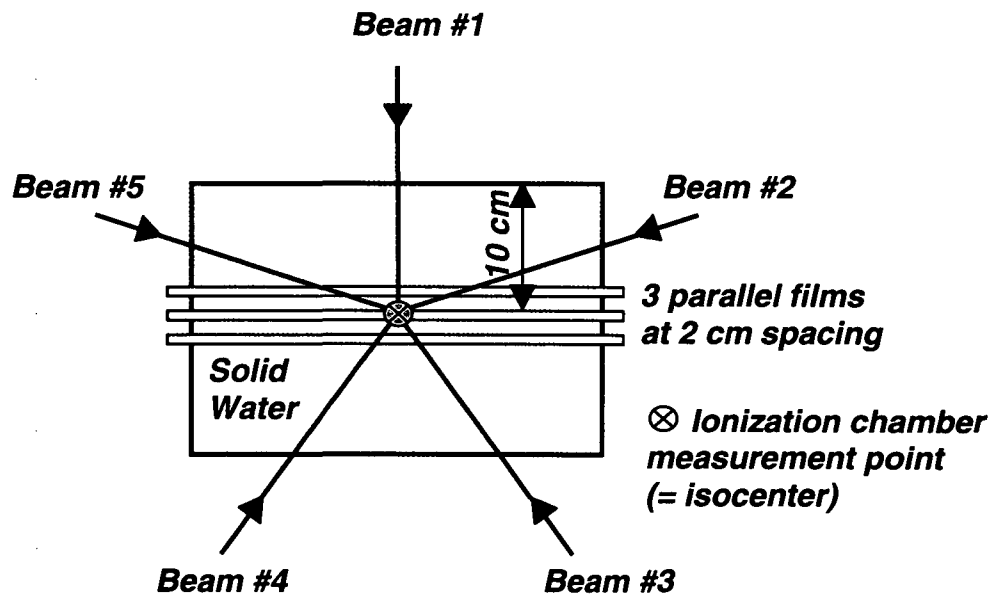
Figure 6.3 *Measurement geometry of the hybrid plan verification method in a typical 5-field configuration. In a first step, the absolute number of MU was checked for the entire treatment plan by measuring the cumulative dose delivered to isocenter, where the ionization chamber was positioned. Subsequently, the complete hybrid plan was investigated by film dosimetry in order to get 2D relative dose distributions. Films were inserted in three coronal planes at 2 cm spacing, with the central one positioned at 10 cm depth through the isocenter (figure not to scale).*

To determine the dose delivered to the isocenter, the hybrid IMRT plan was irradiated onto the phantom with the ionization chamber positioned at the phantom centre, i.e. at a depth of 10 cm and 90 cm SSD in vertical direction. The collected charges delivered by each beam were summed up and compared to a reference field

of the respective energy (see section 6.1). As already mentioned, the chamber was positioned in a homogeneous dose region to prevent artefacts due to steep dose gradients.

For the measurement of relative dose distributions, the entire hybrid plan was irradiated again, but with three films inserted in the phantom. They were evaluated by the normalized sensitometric curve, with the relative dose to the phantom centre set to 100%. In the TPS, relative dose distributions in the corresponding coronal planes were calculated and printed to be qualitatively comparable to the measurement results. As an example, a verification slice of the paraspinal case described as case study 2 in CHAPTER 7 is illustrated in Figure 6.4. It depicts a coronal slice 2 cm below the isocenter. The black isodose lines represent the measured distribution, while the calculated one is characterized by the coloured lines. To emphasize the high dose region, the measured 90%- isodose level is highlighted as thick line. With small exceptions, it is found to be located between the calculated 87% and 93%, as 3% dose difference have been defined as acceptance criteria. Two high dose regions can be identified, with the spinal cord in between being spared by 20–30% (cf. also Figure 7.9 (b)).

The hybrid plan verification method was found to be advantageous for the following reasons. The phantom irradiation exactly resembles the patient treatment, except for different absolute MU values due to the geometrical differences between phantom and patient. Additionally, the composite IMRT treatment plan provides quite homogeneous dose distributions around the isocenter (or in another well-defined region), where the film dosimetry results may be normalized, without being affected by steep dose gradients. The point dose measurements by ionization chamber are representative only if performed in a rather uniform dose region. Furthermore, the hybrid verification method is less time-consuming and cheaper since only three films are needed and irradiated at once, independent of the number of beams. Finally, it has to be mentioned that the measurement of relative dose distributions by film dosimetry in the hybrid plan verification method is possible only because the normalized sensitometric curve in use does not significantly depend on the direction of beam incidence (cf. Figure 6.3).
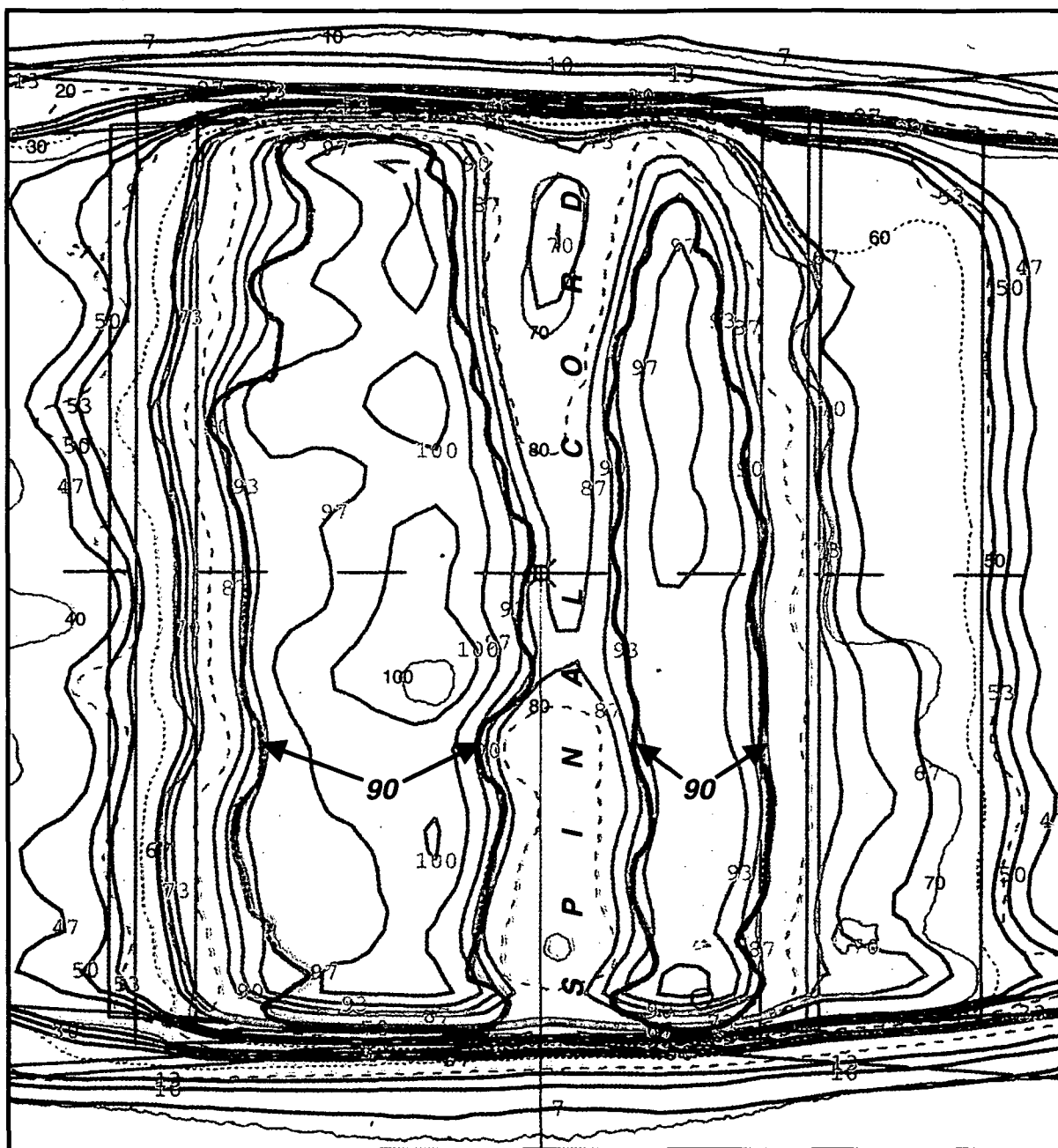
Figure 6.4 *Comparison of measured and calculated dose distributions for a paraspinal case, extracted from the central part of a coronal verification plane 2 cm below the isocenter, where both data sets were normalized to 100%. The measurement results are presented by black isodose lines (alternately solid, dotted, and dashed), showing values between 100% and 10%, with steps of 10%. To emphasize the high dose region, the measured 90%- isodose level is highlighted as thick blue line. The calculated distribution is characterized by coloured lines with values of 100% (green), 90 and 70% (light blue), as well as 50, 30, and 10% (dark blue), where at each dose level the respective isodose lines for a ±3% deviation are added, which correspond to the required accuracy interval (e.g. 87–93%).*

6.3 PHASE 3: QUANTITATIVE EVALUATIONS IN DEDICATED PHANTOMS

To optimize the hybrid plan verification method, two dedicated phantoms were constructed, improving its efficiency and handling. Additionally, a method was developed to compare measured to calculated dose distributions in a quantitative way, in order to replace the optical assessment with its qualitative information.

6.3.1 Construction of IMRT verification phantoms

Two different slab phantoms were designed in order to resemble body regions frequently indicated for IMRT treatments: one pelvic phantom which is mostly used for prostate cases, but also is appropriate for tumours in the thorax or abdomen region, and a smaller one for head-and-neck cases. They are shown in Figure 6.5. Both are assembled by octogonally shaped plates of 3 cm thickness, made of black polystyrene with a homogeneous density of 1.04 g/cm^3. The slabs are positioned vertically and fixed by large laterally mounted screws. The pelvic phantom is 35 cm wide and 25 cm in height and consists of eight plates, while the six plates of the head-and-neck phantom show diameters of 20 cm in either direction. A special ionization chamber insert is available for both types of verification phantoms. It is adapted to house the cylindrical Farmer type chamber NE 2611A (Nuclear Enterprise Technology Ltd), connected to a NE 2620 electrometer. This chamber has a sensitive volume of 0.325 cm^3 and has been chosen in agreement with Leybovich et al (2003). According to their study, even chamber volumes of 0.6 cm^3 represent IMRT dose deliveries correctly, as long as the chamber is positioned in a quite homogeneous dose region. Although the temporal electron fluence through the chamber may not be uniform during the measurement, the cumulative fluence distribution becomes uniform at the chamber location when the IMRT treatment is delivered completely. Additionally, small chambers (≤ 0.125 cm^3) need to be corrected for leakage to present correct results following Leybovich et al (2003), which is a second indication to use a larger chamber volume. To confirm the report, the leakage of the NE 2611A chamber used at the Medical University of Vienna was investigated

separately. It was found to be ≤0.2% of the measurement signal, when delivering 2 Gy within 20 minutes.

(a)

(b)
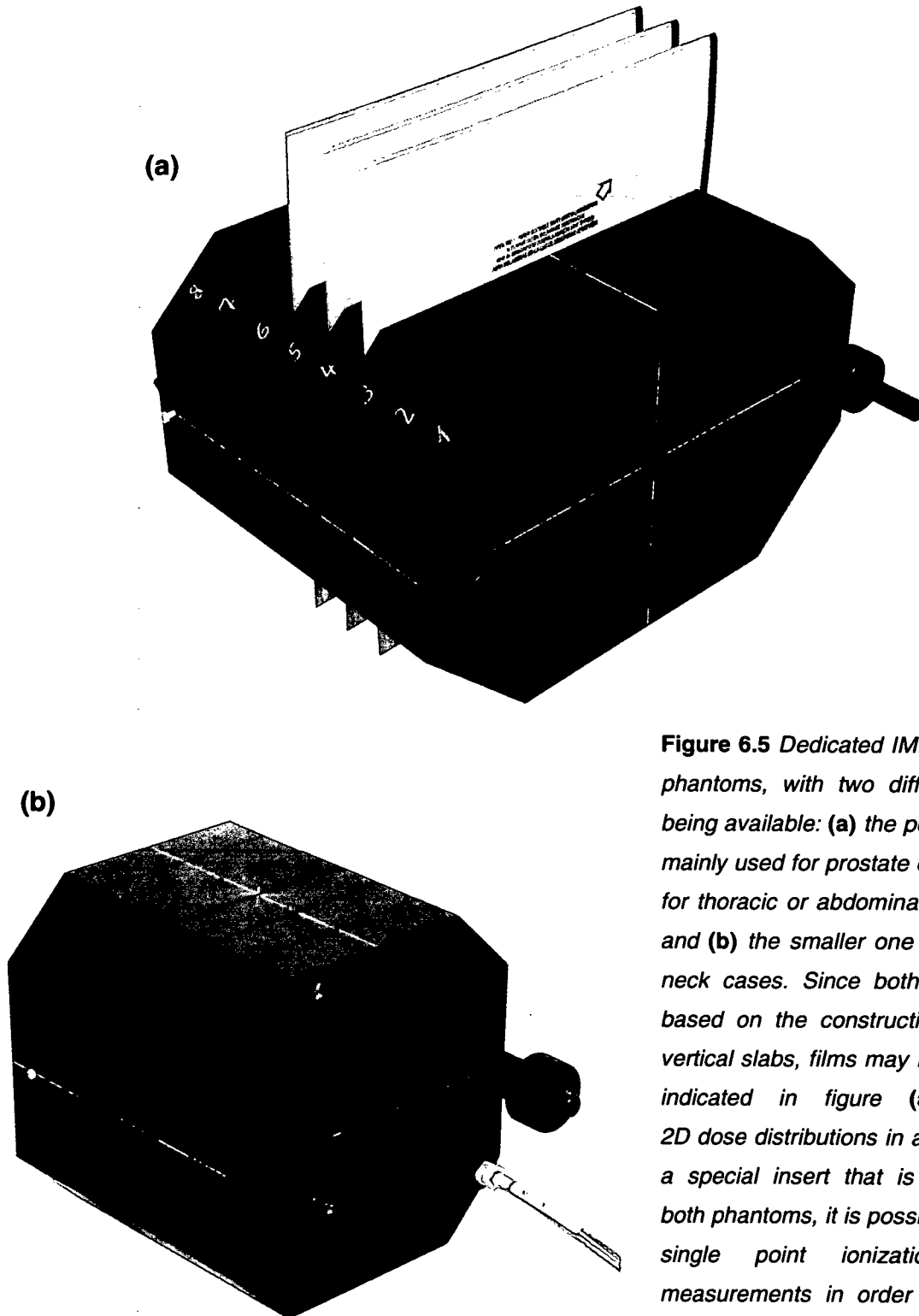
Figure 6.5 *Dedicated IMRT verification phantoms, with two different designs being available:* **(a)** *the pelvic phantom, mainly used for prostate cases but also for thoracic or abdominal IMRT cases, and* **(b)** *the smaller one for head-and-neck cases. Since both versions are based on the construction of several vertical slabs, films may be inserted as indicated in figure* **(a)***, providing 2D dose distributions in axial slices. By a special insert that is applicable in both phantoms, it is possible to perform single point ionization chamber measurements in order to check the absolute number of MU, which is illustrated in figure* **(b)***.*

With the chamber inserted in the head-and-neck phantom, the chamber reference point is exactly positioned at the phantom centre, i.e. at 10 cm depth and 90 cm SSD in vertical direction. Thus, as explained in section 6.1, these parameters resemble the geometry used for the Linac calibration procedure, allowing measurements of the delivered dose by relating the collected charge of the IMRT hybrid plan and the reference field of the respective energy. To enable this method in the pelvic phantom as well, the chamber is positioned at 10 cm depth at half distance between the two screws.

In contrast to the previous Solid Water phantom, it is possible to measure 2D dose distributions in axial planes with the dedicated verification phantoms. For that purpose, the chamber insert is replaced by pure polystyrene parts, before EDR2 films are sandwiched between the vertical plates. In order to remove any air gaps in the film paper envelopes, the phantom is squeezed by the lateral screws as far as mechanically possible. Simultaneously, the major axes are marked on the films by needles fixed on three adjoining slabs. The markings are needed to geometrically relate the measured and calculated dose distributions, whereas in the previous Solid Water phantom the pinning has been done manually.

In the TPS, the phantoms have been rebuilt virtually according to their exact geometrical dimensions. Additionally, the density of 1.04 g/cm^3 has been entered, which is considered in the hybrid plan calculations as well as in the reference fields used for the point dose measurements.

The principal verification procedure is very similar as described in section 6.2. The approved patient plan is copied to one of the dedicated phantoms without any changes. Only the MU are recalculated to deliver the required fractional dose, considering the phantom geometry. After transferring the hybrid plan parameters to the Linac, the plan is irradiated the first time, with the chamber being inserted to verify the absolute number of MU. Then the chamber is replaced by three films and the irradiation of the hybrid plan is restarted. Generally, one film is positioned in the isocenter plane, the others 3 cm cranial and caudal, respectively. However, if in the TPS the dose gradient around the isocenter is found to be significant, the isocenter is moved in order to obtain a homogenous dose region at the chamber position. In case a cranio-caudal translation is sufficient to reach a uniform dose region, simply the normalization point and the film planes are moved since the axial phantom cross-sections do not vary. Finally, the films are processed, scanned, and translated to

relative dose values by the normalized sensitometric curve. However, for the comparison between the measured and calculated distributions a quantitative method has been developed which is described in the next section.

6.3.2 The γ-index concept

In traditional concepts for comparing 2D dose distributions in a quantitative way, the area of interest is separated into regions of steep or flat dose gradients, for which various acceptance and tolerance criteria are applied [Van Dyk *et al* 1993, Venselaar *et al* 2001]. While in areas of flat gradients the difference between calculated and measured dose is investigated, the distance to agreement (DTA) is determined in steep dose gradients. This is the geometrical distance from the point of measurement to the nearest calculation point with the same dose value. Since in IMRT different gradient regions can alternate, such simple area classifications are hardly possible, thus making the traditional acceptance concepts not applicable for the verification of IMRT treatments.

The γ-evaluation method represents a combination of dose difference criteria and DTA criteria [Low *et al* 1998b]. In fact, it is a generalization of the traditional concepts, where Figure 6.6 gives a graphical overview of the geometrical basics.
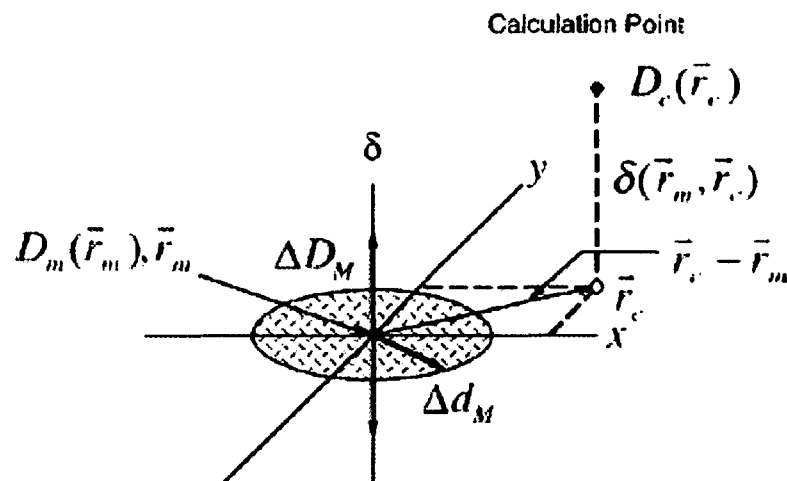

Figure 6.6 *Graphical explanation of the geometrical terminology used in the* γ *-evaluation method, which is based on a combination of DTA criteria in the (x,y)-plane and dose difference criteria, plotted in the third dimension (δ).*

By the axes x and y, the spatial coordinates of the measurement point ($\vec{r}_m$) under investigation and one of the calculation points ($\vec{r}_c$) are defined. The third dimension δ represents the dose difference $\delta(\vec{r}_m, \vec{r}_c)$ between the measured dose $D_m(\vec{r}_m)$ and the calculated one $D_c(\vec{r}_c)$. The labelling ΔD_M describes the dose difference criterion, while the DTA criterion is illustrated as circular area with the radius Δd_M. Usual criteria values are 3 mm for the DTA and 3% (of the dose to normalization point) for the dose difference.

Based on this terminology, the γ-index is calculated as follows:

$$\gamma(\vec{r}_m) = \min\{\Gamma(\vec{r}_m, \vec{r}_c)\} \forall \{\vec{r}_c\} \tag{6.1}$$

$$\Gamma(\vec{r}_m, \vec{r}_c) = \sqrt{\frac{r^2(\vec{r}_m, \vec{r}_c)}{\Delta d_M^2} + \frac{\delta^2(\vec{r}_m, \vec{r}_c)}{\Delta D_M^2}} \tag{6.2}$$

$$r(\vec{r}_m, \vec{r}_c) = |\vec{r}_c - \vec{r}_m| \tag{6.3}$$

$$\delta(\vec{r}_m, \vec{r}_c) = D(\vec{r}_c) - D(\vec{r}_m) \tag{6.4}$$

The minimum distance between the measurement point under investigation and all points of the calculated distribution is called γ-index, as depicted in Figure 6.7.
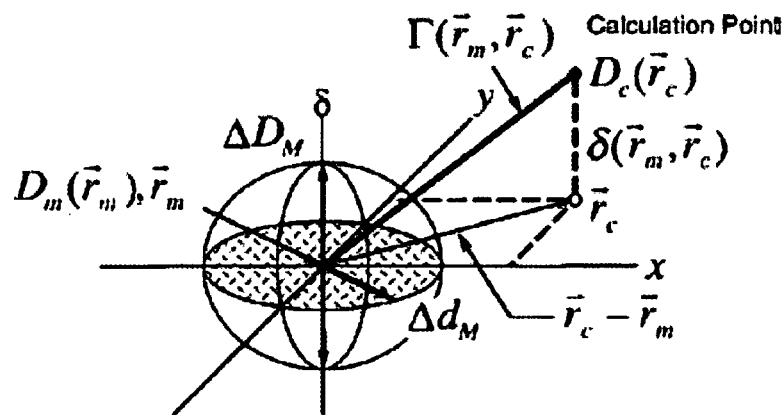
Figure 6.7 The γ -index is defined as the minimum distance between the measurement point under investigation and the entire set of calculation points. The combined acceptance criteria, geometrically describing the shape of an ellipsoid, are violated if the index is larger than unity.

The ellipsoid represents the surface of the combined acceptance criteria. Thus, if the $D_c(\vec{r}_c)$ surface intersects with the ellipsoid, the criteria for the point $\vec{r}_m$ are fulfilled, which is mathematically expressed:

$$\gamma(\vec{r}_m) \leq 1 \qquad (6.5)$$

In other words, for regions with γ-values larger than unity the criteria are violated. Due to the mathematical concept of the γ-evaluation it is possible to determine the degree of deviation for each measurement point. Furthermore, the angle between the δ-axis and the γ-vector indicates which of the acceptance criteria is predominant, as shown in Figure 6.8. If the angle θ is 0°, only the dose difference criterion is deciding at the measurement point, while for an angle of 90° the DTA criterion is dominating.
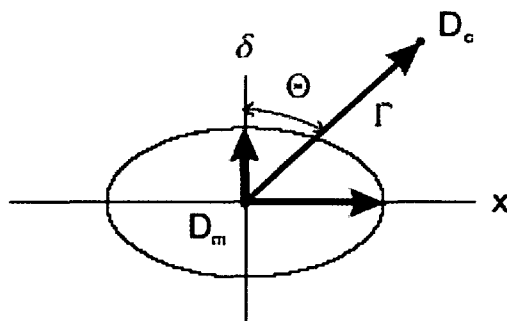
Figure 6.8 *The angle between the δ-axis and the γ-vector gives information about the relative weight of DTA and dose difference criteria at the measurement point.*

For a comfortable evaluation, it is preferable to graphically display the γ-index distribution as well as the γ-angle distribution. In addition, it is possible to statistically evaluate the γ-values by means of histograms. Both features are implemented in the program described in the following section.

6.3.3 The "DosVer" program

The software package "DosVer" (Dosis Verifikation) provides a fast generation of γ-index distributions due to an optimized calculation algorithm. The program and its mathematical functionalities are described in detail in the diploma thesis of Stock (2003), who has developed the software at the Medical University of Vienna. Here, only the main features and highlights of the program shall be presented. As an example, the verification procedure of the head-and-neck case described as case study 3 in section 7.3 is outlined, which has been performed in the dedicated IMRT head-and-neck phantom.

First of all, the software needs the measured and calculated dose distributions as input data. After application of the normalized sensitometric curve in the RIT 113 software, the relative dose values are exported as text-files which can directly be imported into the DosVer program. However, the calculated dose distributions in the corresponding axial slices are stored as DICOM-RT files when being exported from the Helax-TMS planning system. Thus, the data have to be converted to be readable by the DosVer software.

In a second step, the following parameters have to be entered by the user. The positions of isocenter and normalization point in both distributions are essential in order to connect them geometrically. Furthermore, the absolute dose delivered to norm point (100%) and the pixel resolutions of the input data are needed. Equal pixel spacing in both distributions is necessary to run the program. The most crucial part is the definition of appropriate acceptance criteria. Usually, 3% dose difference and 3 mm DTA are permitted. According to Low and Dempsey (2003), the ratio of pixel resolution to DTA criterion shall be 1:3 or smaller to prevent artefacts in the γ-index calculation. Thus, dose matrices of 1 mm pixel size are used by default. Finally, a region of interest (ROI) can be defined to exclude the pin marks on the films used as geometrical references. They appear as small dots of seemingly high dose and would influence the γ-evaluation.

Figure 6.9 illustrates the main screen of the DosVer software after the input of data and parameters for the isocenter plane of the head and neck case (cf. also Figure 7.11). In the upper left chart, the dose distribution imported from the TPS is presented, with the white lines marking the major axes. Correspondingly, on the right

side the measured dose distribution is shown, in which the yellow rectangle indicates the ROI. In the lower left area a simple dose difference map between the measured and calculated distributions is depicted, which primarily helps to detect geometrical misalignment between the two data sets. As expected, the highest dose differences are found along the steep dose gradients at the field edges.
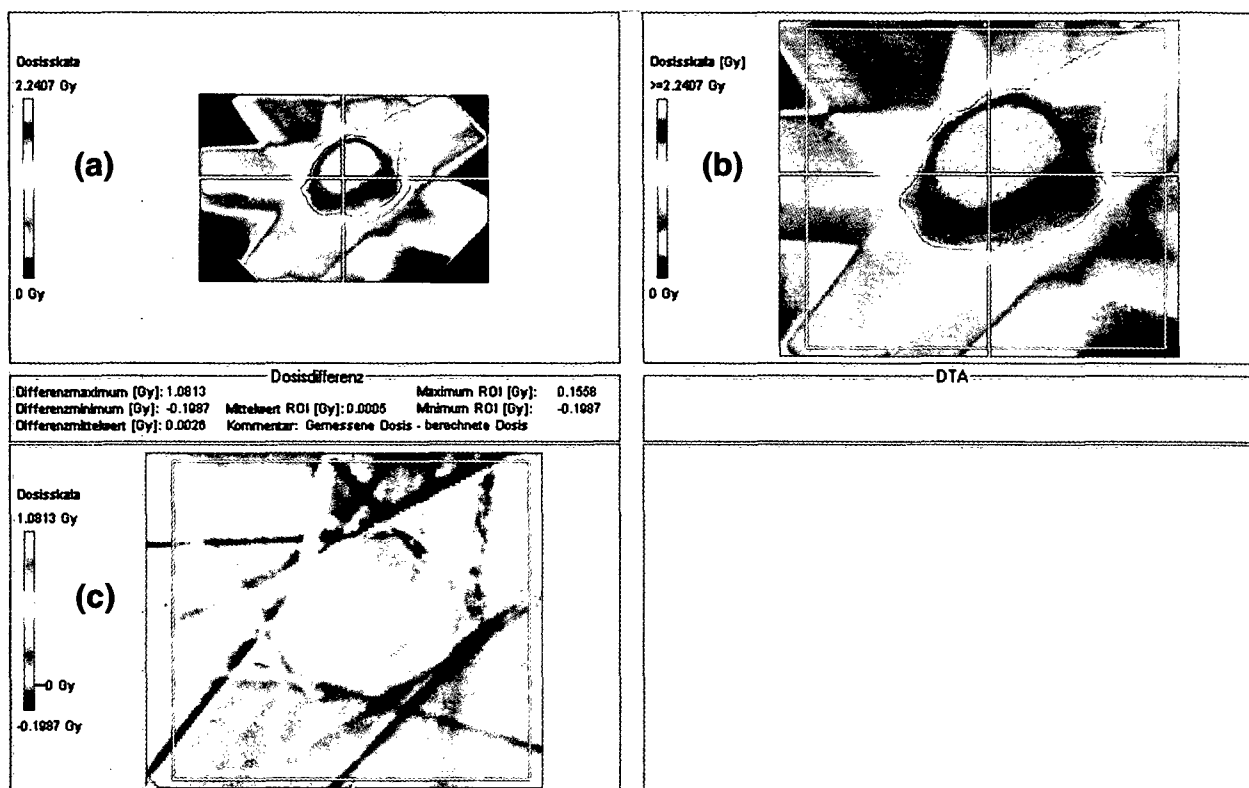
Figure 6.9 *Central part of the DosVer main screen as it appears after the input of data and parameters.* **(a)** *Calculated dose distribution, with the white lines indicating the major axes.* **(b)** *Measured dose distribution, imported from the film converting software. The ROI necessary to exclude the pin marks is marked by the yellow rectangle.* **(c)** *Dose difference map (measured minus calculated).*

Before calculating the actual γ-index values, the program offers the possibility to check row and column profiles (see Figure 6.10) through the dose distributions. The red lines indicate the measured values, while the green lines represent the calculated ones. This is another tool to test for geometrical misalignment and helps to investigate the deviations more precisely than just by looking at the dose difference map. The two exemplarily chosen profiles show good agreement without any significant displacements.
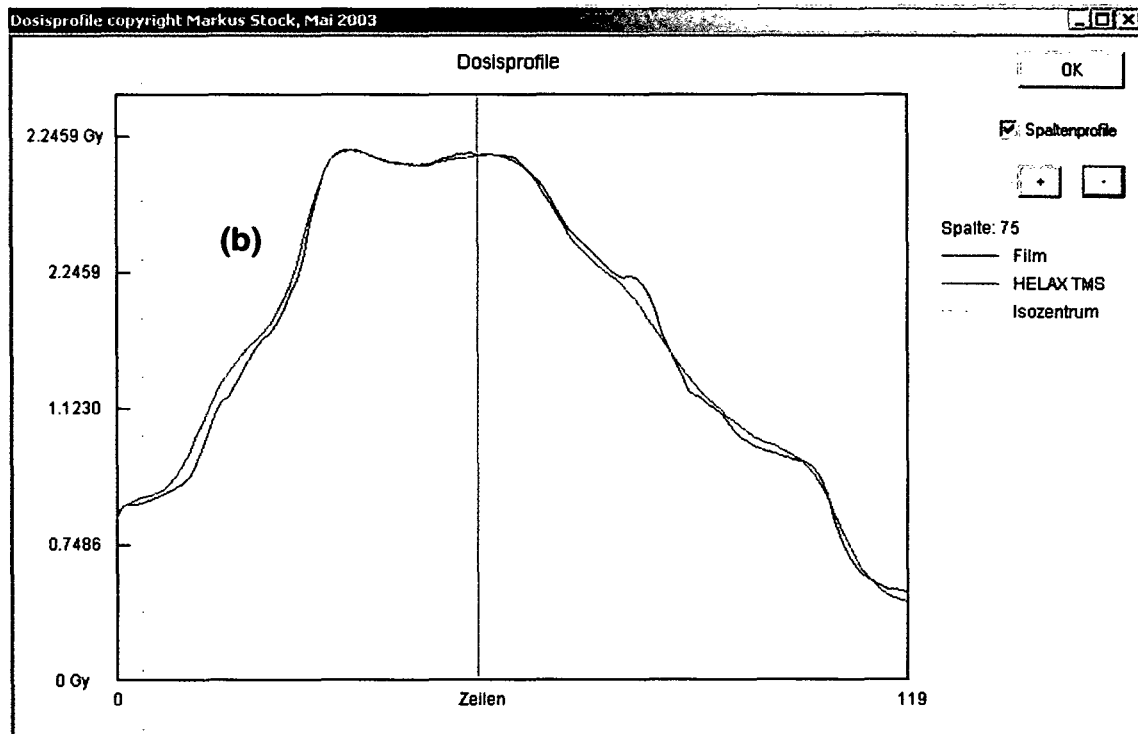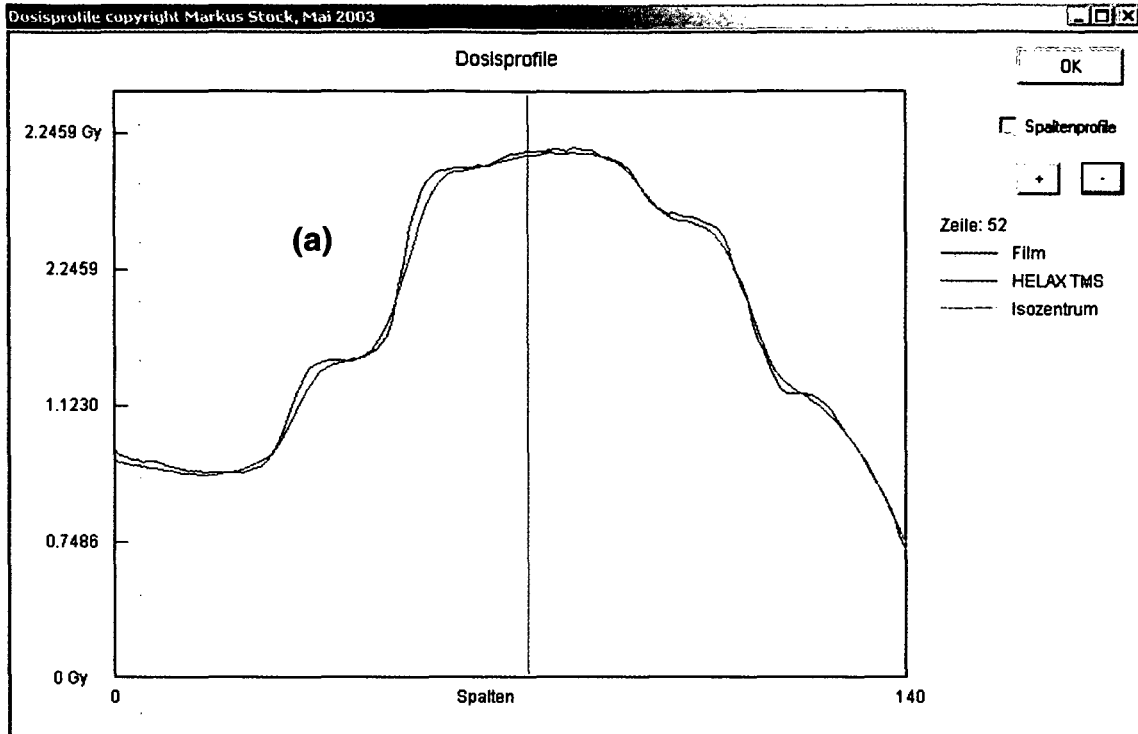
Figure 6.10 (a) *Row dose profile and* **(b)** *column dose profile. The measured and calculated values are illustrated as red and green lines, respectively. This tool helps to detect geometrical misalignment, which may be corrected by changing the isocenter coordinates of the measured distribution.*

By clicking the button "Gamma opt." the optimized γ-index calculation algorithm is activated. The procedure takes only some seconds for a 15×20 cm² large film at 1 mm pixel resolution. The results are shown in Figure 6.11.
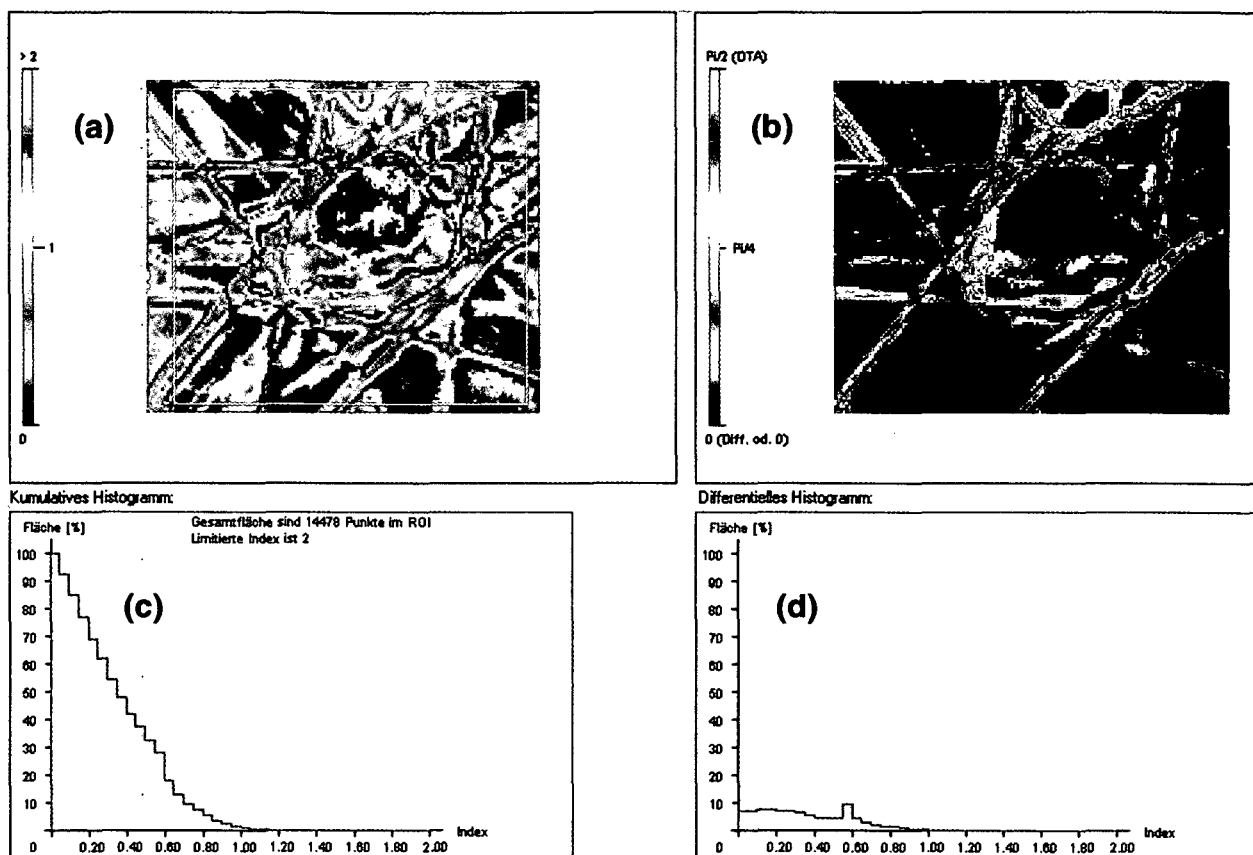
Figure 6.11 *Central part of the DosVer main screen, presenting the results of the optimized γ -index calculation algorithm. (a) γ -index distribution, with the yellow rectangle indicating the previously defined ROI. (b) γ -angle distribution. (c) Cumulative and (d) differential γ -area-histograms, based on the results within the ROI only. The data may be exported to spread-sheet programs in order to determine the amount of acceptance criteria violation (i.e. the area with γ > 1).*

In the upper left chart, the γ-index values are graphically displayed. While the blue and green areas indicate agreement between the dose distributions within the requested acceptance criteria (3% and 3 mm), the yellow and red regions represent points of violation. Again, the yellow rectangle delineates the ROI, for which the mean γ-value is calculated. In the upper right part the γ-angle distribution is illustrated. The red areas indicate the DTA criterion to be predominant, coinciding with the steep dose gradients at the field edges. In the lower part of Figure 6.11,

cumulative (left) and differential (right) γ-area-histograms are shown. The software allows exporting the histograms to further process the data, e.g. by a spreadsheet program. By doing so, the number of points exceeding the acceptance criteria (i.e. with γ >1) may be determined. For the example presented, 1.5% of the ROI was found to violate the combined criteria of 3% dose difference and 3 mm DTA.

6.3.4 Patient statistics and evaluation filter

From the verification protocols of the first 35 IMRT patient treatments at the Medical University of Vienna, the average deviation in the single point ionization chamber measurements performed to check the absolute number of MU is found to be (-1.6±1.3)%. For 34 patients, the difference between calculated and measured dose was within the requested interval of ±3%, while for one patient a deviation of -6.6% was detected. Since this value was reproducible when repeating the measurement with a different chamber, the calculated MU were manually increased by 5% in order to deliver the prescribed dose.

For a statistical analysis of the γ-evaluation method, the data of 20 hybrid plan verifications are available. As in each measurement three films were used, the values in Table 6.1 are calculated from 60 planes. The mean values ± one standard deviation are displayed, where the γ_{MAX} parameter is defined as the value which can be found in 1% of the ROI area, derived from the cumulative histogram. This definition helps to exclude irrelevant maxima caused by film or scanner artefacts.

parameter	mean value	standard deviation
γ_{MAX} in ROI	1.49	±0.44
γ_{MEAN} in ROI	0.46	±0.09
area with γ >1	6.99%	±5.13%

Table 6.1 *Statistical analysis of the results obtained by the γ -evaluation method. The values are based on the data of 60 verification planes in 20 IMRT plans.*

Finally, at the Medical University of Vienna an evaluation filter for the hybrid IMRT plan verification has been established [Stock *et al* 2005], which is summarized in Table 6.2.

parameter	range	appraisal and approach
γ_{MAX}	0–1.5	acceptable
	1.5–2	acceptable, but other verification tools like angle distribution, dose difference map and profiles needed for further evaluation
	>2	measurement has to be repeated - if violation remains, treatment plan has to be re-optimized
γ_{MEAN}	0–0.5	acceptable
	0.5–0.6	acceptable, but other verification tools like angle distribution, dose difference map and profiles needed for further evaluation
	>0.6	measurement has to be repeated - if violation remains, treatment plan has to be re-optimized
area with $\gamma>1$	0–5%	acceptable
	5–10%	acceptable, but other verification tools like angle distribution, dose difference map and profiles needed for further evaluation
	>10%	measurement has to be repeated - if violation remains, treatment plan has to be re-optimized

Table 6.2 *Evaluation filter and measures for the hybrid IMRT plan verification, based on the use of dedicated phantoms and the application of the DosVer Software to calculate γ-index distributions.*

This evaluation cascade has been introduced in 2004, and since then it has been applied to 20 IMRT treatment plans. It facilitates the decision process in the very complex field of IMRT verifications and helps to standardize the procedures. However, it is also recommended to test conformal uniform intensity beams in order to check the evaluation filter for its feasibility.

CHAPTER 7

CLINICAL IMRT CASE STUDIES

To highlight the advantages and advanced possibilities of intensity modulated radiotherapy, treatment plans for three different tumour entities are presented, namely for prostate cancer, paraspinal tumours in the torso region and for head and neck cancer. For each of the tumour sites, patients treated by typical IMRT plans have been selected and will be described as demonstrative examples. IMRT treatments for other tumour entities like breast cancer [e.g. Landau *et al* 2001] are not included since they are not (yet) performed at the Medical University of Vienna. The description of the case studies is focussed on physical aspects of IMRT planning and delivery and is not supposed to give comprehensive medical information.

7.1 CASE STUDY 1: PROSTATE TUMOUR

In radiotherapy of prostate cancer, IMRT has found large acceptance and has been propagated worldwide, aiming at a substantial reduction of side effects in organs at risk, especially in the rectal wall [Zelefsky *et al* 2000], and at dose escalation for high risk patients [Pollack *et al* 2003]. The patient described in this section was the very first one treated by IMRT at the Medical University of Vienna. Primarily, the PTV was generated from the CTV with an isotropic margin of 10 mm. It was irradiated by 3D conformal radiotherapy in a 4-field-box technique up to 60 Gy with daily fractions of 2 Gy. Subsequently, the PTV was modified by reducing the margin in the dorsal direction (i.e. towards the rectum) to 5 mm and was treated by IMRT for another 14 Gy to an overall dose of 74 Gy, as a kind of boost therapy.

For the treatment planning process a configuration of five equiangular incidence directions was chosen, with beam qualities of 25 MV, consistently. To start the IMRT optimization procedure, the following dose-volume-constraints were defined. For the PTV, dose values between 95% and 105% were requested, with the mean dose to the CTV normalized to 100%. For the rectal wall a maximum dose of 105% was permitted, while the volumes encompassed by the 70% and 50% isodose

surfaces were requested to be smaller than 25% and 50% of the delineated rectal wall volume, respectively. The dose-volume-constraints were deduced from findings of Wachter *et al* (2001).

The optimization algorithm generated a sequence of overall 38 segments, of which the resulting dose distribution is illustrated in Figure 7.1. It presents the CT slice at the isocenter position, with isodose lines of 95%, 90%, 70%, 50%, and 30% being displayed. The orange arrows indicate the beam incidence directions, while the dotted lines present the PTV (orange), CTV (yellow) and rectal wall (brown). Furthermore, the air-filled balloon catheter inserted in the rectum may be identified, which is a simple method to immobilize the prostate and to consequently reduce the safety margins [Wachter *et al* 2002]. Without this rectal balloon it would not be possible to use margins of only 5 mm. Additionally, it helps to increase the distance between prostate and posterior rectal wall, enabling an improved protection of the latter [Gerstner *et al* 1999]. The use of rectal balloons in combination with IMRT treatments has been investigated extensively by Teh *et al* (2001, 2002a, 2002b) and has been proven as a useful tool for prostate immobilization.
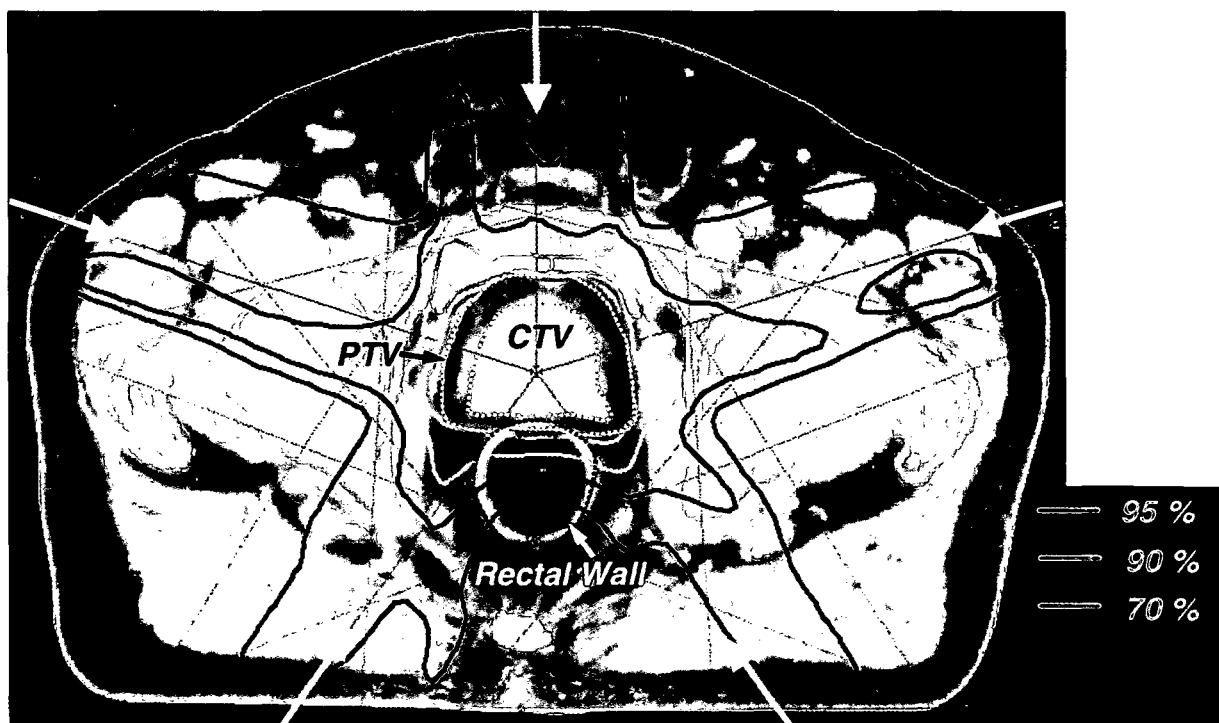

Figure 7.1 *Dose distribution in the isocenter slice of an IMRT prostate case, resulting from overall 38 segments in five beam incidence directions (orange arrows). Beside the target volumes CTV and PTV, the rectal wall is delineated as organ at risk which is immobilized by an air-filled balloon catheter.*

To point out the advantages of the IMRT treatment plan, a 3D conformal plan using the 4-field-box technique has been made for comparison, which is shown in Figure 7.2. As both plans are conformed to the same PTV with 5 mm margin towards the rectum, Figure 7.2 (b) does not correspond to the actually treated 4-field-box by which the patient was given 60 Gy, since that one was conformed to the larger PTV with 10 mm margin in the direction of the rectum (not displayed here).
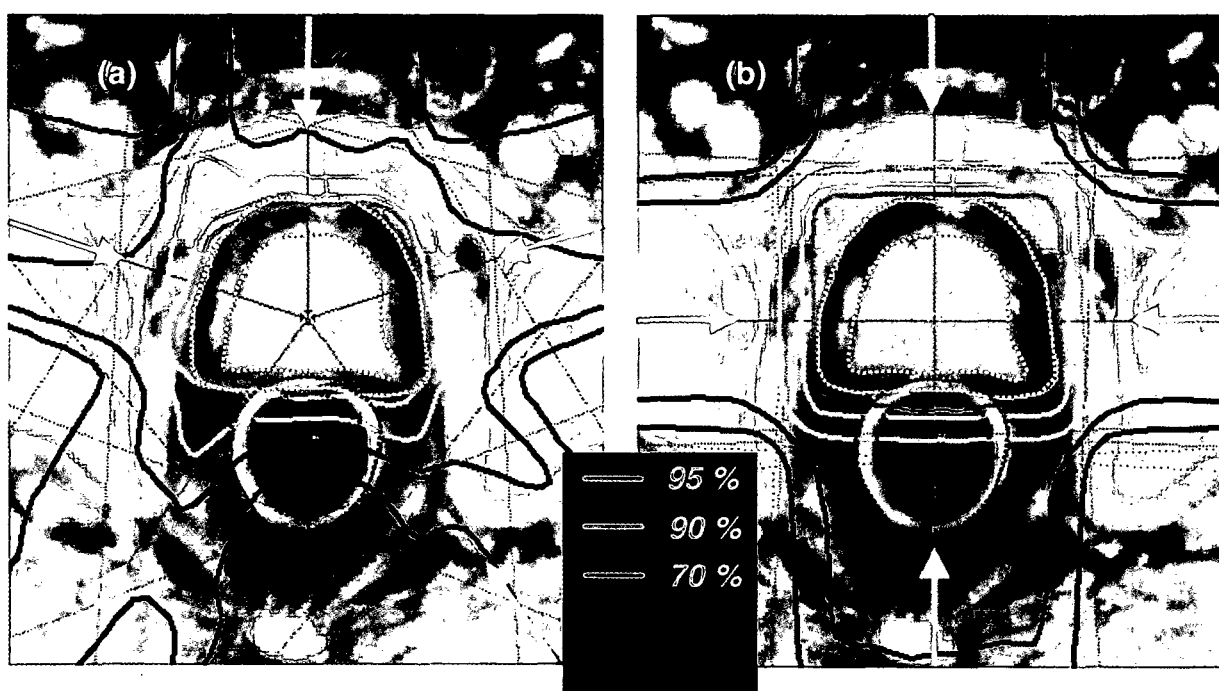
Figure 7.2 *Comparison between* **(a)** *the IMRT treatment plan and* **(b)** *a conventional 4-field-box technique, both conformed to the same PTV. Note the concavely shaped dose distribution around the rectal region in the IMRT solution as well as the improved conformity of the high dose region in the anterior part of the prostate.*

In Figure 7.2, there are two items which are obvious on first sight. First, the conformity of the high dose region (90% and 95% isodose lines) surrounding the PTV could be improved by using the IMRT technique. Second and even more important, it was possible to generate a concave dose distribution around the rectum, significantly reducing the exposure to the rectal wall. In Figure 7.2 (b) the whole rectum is encompassed by the 50% isodose line, while in Figure 7.2 (a) roughly only half of the rectal wall gets doses higher than 50%. This fact is also demonstrated in Figure 7.3, where the plan comparison is illustrated in sagittal reconstructions through the isocenter.
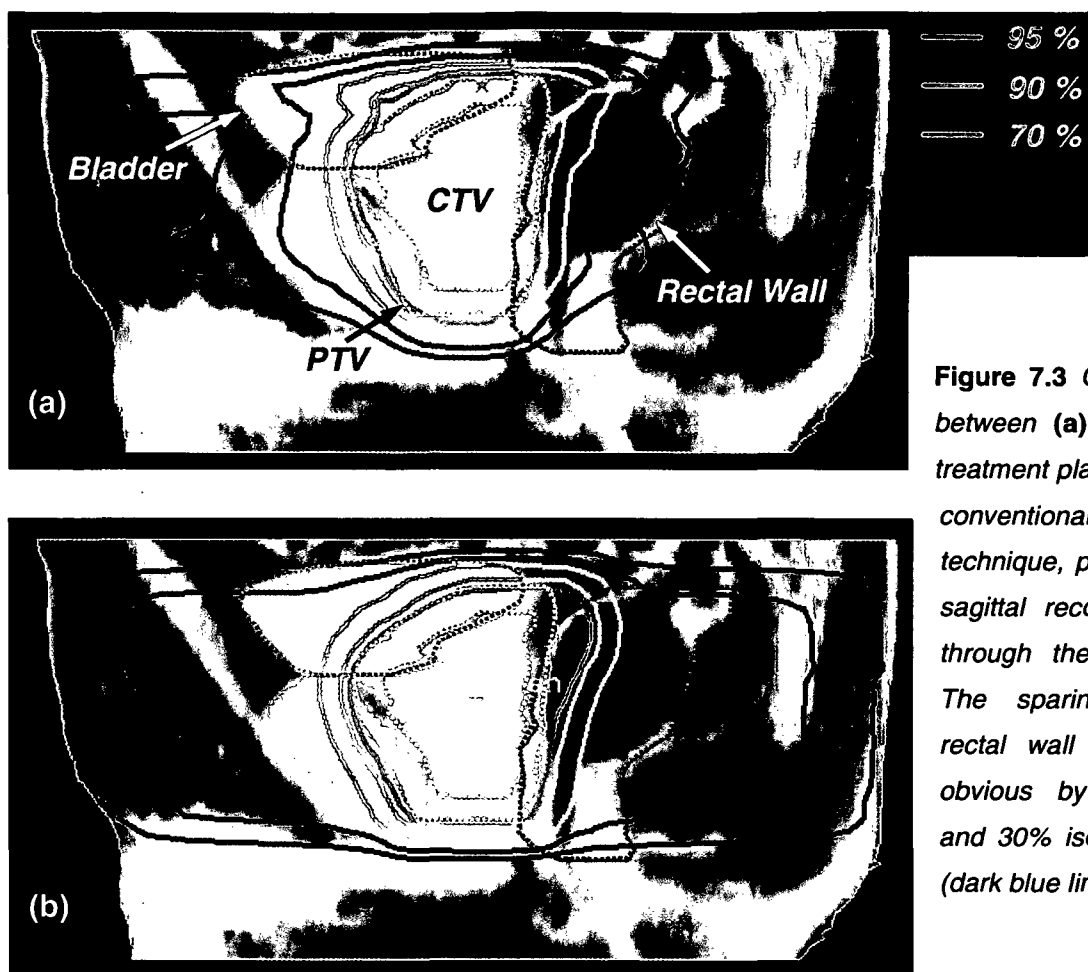
Figure 7.3 *Comparison between* **(a)** *the IMRT treatment plan and* **(b)** *a conventional 4-field-box technique, presented in sagittal reconstructions through the isocenter. The sparing of the rectal wall gets most obvious by the 50% and 30% isodose lines (dark blue lines).*

By calculating dose-volume-histograms, the above findings may be confirmed in a quantitative way. Figure 7.4 (a) shows the DVH for the rectal wall, where the greatest benefit of IMRT appears around the 50% dose level. With the conformal 4-field-box technique, 92% of the rectal wall volume is covered by the 50% isodose, while the volume decreases to 53% in case of IMRT. Thus, the lower dose-volume-constraint for the rectal wall was nearly fulfilled, whereas the constraint for the 70% dose level was violated by 9% in volume. Nevertheless, in the high dose region a sparing of roughly 10% in volume could be achieved by the IMRT solution as compared to the 4-field-box version. Also the mean dose to the rectal wall was reduced from 69.3% to 56.4%.

When inspecting the DVH of PTV (see Figure 7.4 (b)), the larger dose inhomogeneity of the IMRT plan is quite obvious. With the 3D conformal technique, the dose to PTV is found to be in a range of 95% to 101%. By the use of IMRT, the PTV is treated within a dose level of 90% to 113%, exceeding the level requested in the dose-volume-constraints. However, the 95% isodose covers 97% of the target

volume (i.e. V$_{95}$ = 97%) and only 9% gets higher doses than 105%. The increased dose inhomogeneity in the target is typical for IMRT treatment plans and somehow necessary to achieve satisfying sparing of organs at risk, which has to be balanced in a medical decision process (cf. section 2.6).
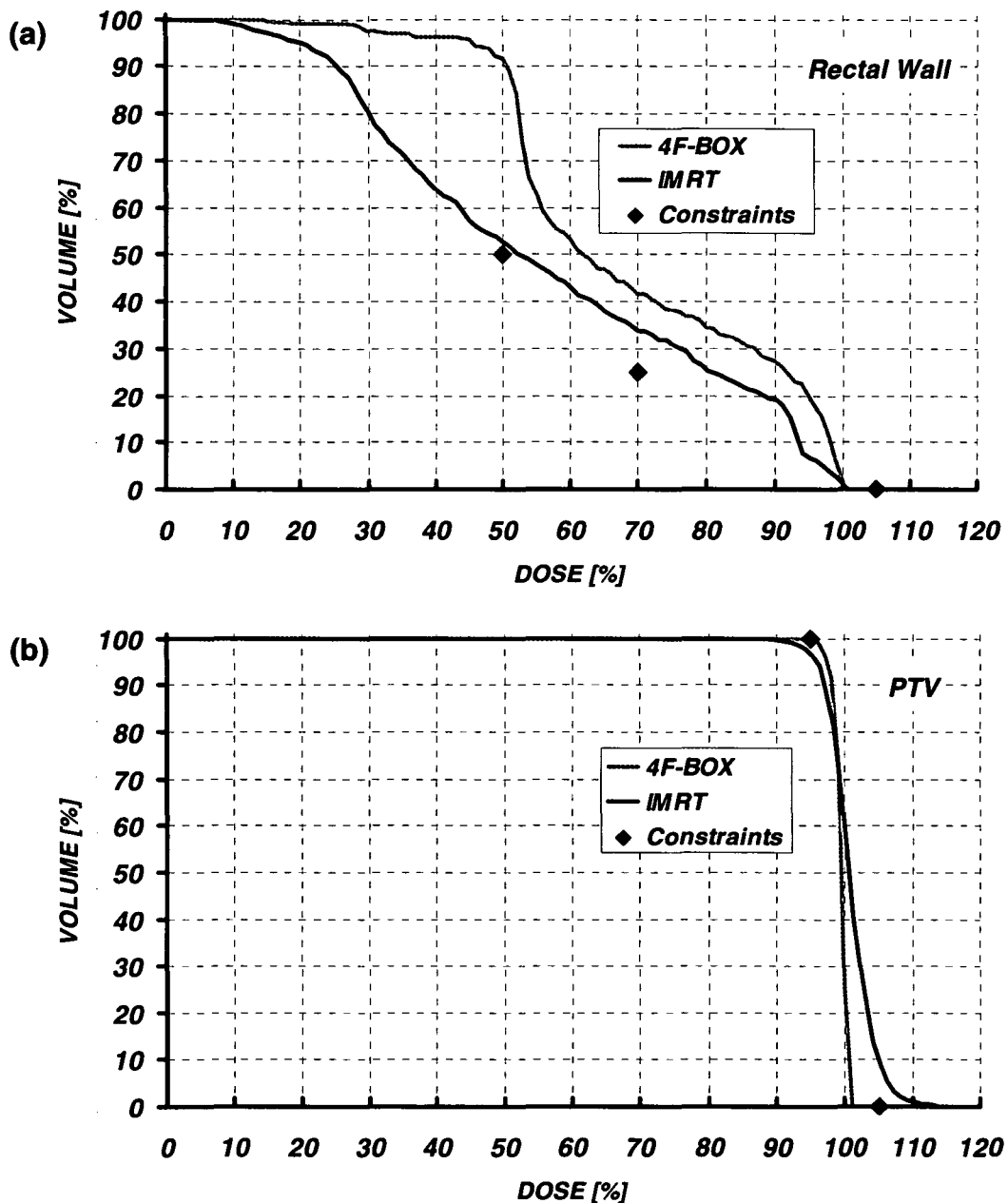
Figure 7.4 *Cumulative dose-volume-histograms, obtained by the IMRT solution (dark blue line) and the corresponding 4-field-box technique (light blue line) for* **(a)** *the rectal wall and* **(b)** *the PTV. Additionally, the dose-volume constraints used in the optimization procedure are indicated as dark blue markers, defining the desired PTV dose level (minimum and maximum) and three upper constraints for the dose to the rectal wall.*

The above described comparison does not definitely prove the superiority of intensity modulation since it is based on different beam geometries (five fields vs. four fields). In order to clarify this matter, another 3D conformal plan has been made that is configured in exactly the same geometry as the IMRT plan, i.e. with five equiangular fields conformed to the same PTV, as shown in Figure 7.5. In fact, by doing so the conformity in the anterior part of the prostate becomes similar to the IMRT version. However, towards the rectum the dose distribution is affected unfavourably as the high dose region is enlarged, increasing the exposure to the rectal wall. This comparison impressively emphasises the influence of intensity modulation within equal beam geometries.
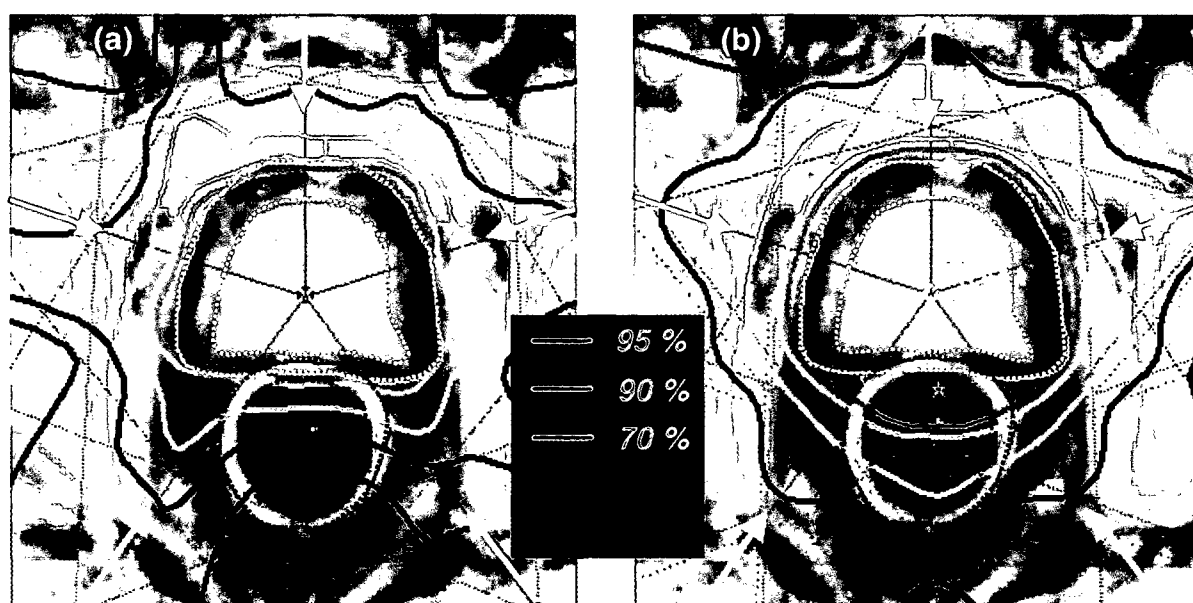
Figure 7.5 *Comparison between* **(a)** *the IMRT treatment plan and* **(b)** *a conventional 5-field technique, conformed to the same PTV and based on identical beam incidence directions. Thus, the difference is only caused by the influence of intensity modulation applied in the left case. Note the unfavourable dose distribution around the rectum in the conventional treatment plan.*

7.2 CASE STUDY 2: PARASPINAL TUMOUR

Paraspinal tumours, partially or totally encompassing the spinal canal, generally pose a special challenge in the radiotherapy treatment planning process. To prevent the patient from any kind of myelopathy, the dose to the spinal cord has

to be kept below 46 Gy. However, in many cases higher doses are needed to control the tumour. Therefore, the generation of concave dose distributions or even with "islands" of low dose (intentional cold spots) are needed. This calls for the application of intensity modulated treatment plans, as it has been reported in literature [e.g. Bilsky *et al* 2004].

The patient reported in this case study suffered from a tumour in the region of the ninth thoracic vertebral body. Before radiotherapy, the tumour was resected and the affected bony structure was reconstructed by a special implant [Plathow *et al* 2001], which is shown in Figure 7.6.
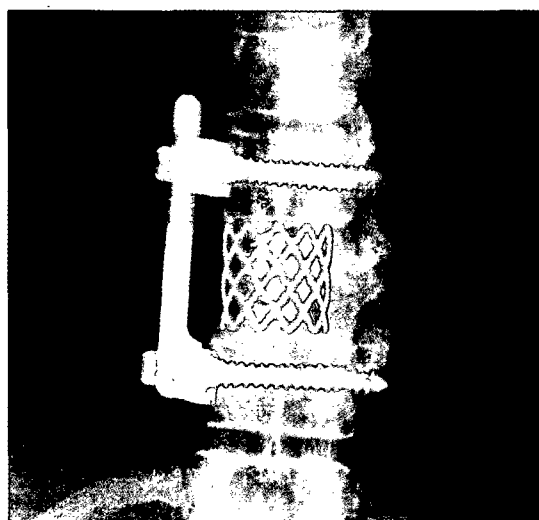
Figure 7.6 *Radiography of an implant that was inserted after tumour resection in order to reconstruct the affected bony structure of the ninth thoracic vertebral body.*

Figure 7.7 illustrates a CT slice through the centre of the tumour bed with the delineated volumes of interest (VOI) used in the IMRT optimization procedure. The CTV (red area) contains the thoracic vertebral body and the onset of the ninth rib to the right side of the patient. To create the PTV (yellow outline) margins of 7 mm were used, while towards the spinal canal the safety margin was reduced to 3 mm. This was only possible because the patient was positioned in a body frame, as visible in Figure 7.8. The tool guarantees reproducible patient positioning and is widely used in high precision radiotherapy, such as stereotactic or IMRT treatments. The accuracy of this immobilization device was found to be better than 2 mm [Yenice *et al* 2003]. For the myelon as the only organ at risk in that case, an "anatomical" safety margin was applied by drawing the cross sections of the entire spinal canal (black dotted line in Figure 7.7) rather than just the spinal cord. This has also been suggested for IMRT by McKenzie *et al* (2002) and corresponds to the philosophy of ICRU report 62

[International Commission on Radiation Units and Measurements 1999]. While CTV and spinal canal are just adjacent, there is an overlap between PTV and spinal canal. Such voxels belonging to target and organ at risk at the same time are likely to influence the Helax-TMS optimization algorithm in a negative way. Thus, a subset of the spinal canal was delineated, only adjoining to PTV rather than intersecting with. It was called "spinal canal ex PTV" and is depicted as blue area in Figure 7.7 (a). Furthermore, an artificial help structure (green area in Figure 7.7 (b)) was defined, completely filling the concavity formed by the PTV. Its meaning will be explained later on and illustrated in Figure 7.10.
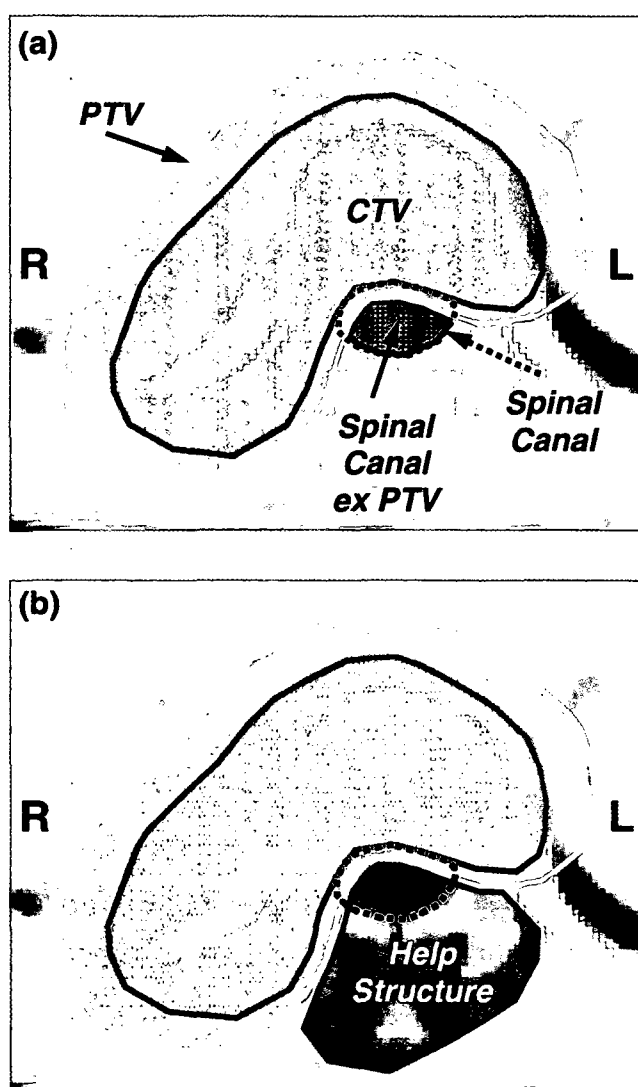
Figure 7.7 *CT slice through the centre of a paraspinal tumour to be treated by IMRT.* **(a)** *Beside the target volumes CTV and PTV, the spinal canal (black dotted line) is contoured as organ at risk, partly overlapping with the PTV (yellow outline). In order to prevent ambiguities in the optimization algorithm, a separate structure called "spinal canal ex PTV" (blue area) is defined by excluding the intersection region.* **(b)** *Additionally, the entire concavity shaped by the PTV is delineated as an artificial help structure (green area), including the spinal canal ex PTV. Its utility is illustrated in* **Figure 7.10.**

The isocenter was set to the centre of the affected vertebral body. Due to the position of the tumour bed, six fields with beam qualities of 6 MV were arranged,

121

predominately incident from posterior to minimize the beam entrance depths and the exposure to normal tissue in the anterior part of the torso. The medical goal was to treat the tumour bed up to 54 Gy, while the maximum dose to the spinal cord should not exceed 45 Gy. Hence, the following dose-volume-constraints were defined for use in the optimization algorithm. The dose to the CTV was prescribed between 95% and 105%, with the mean dose normalized to 100% (54 Gy). For the PTV a dose level within 90%–105% was required. A maximum dose of 83% (45 Gy) was prescribed to spinal canal ex PTV, while the dose to the help structure was limited to 90%.
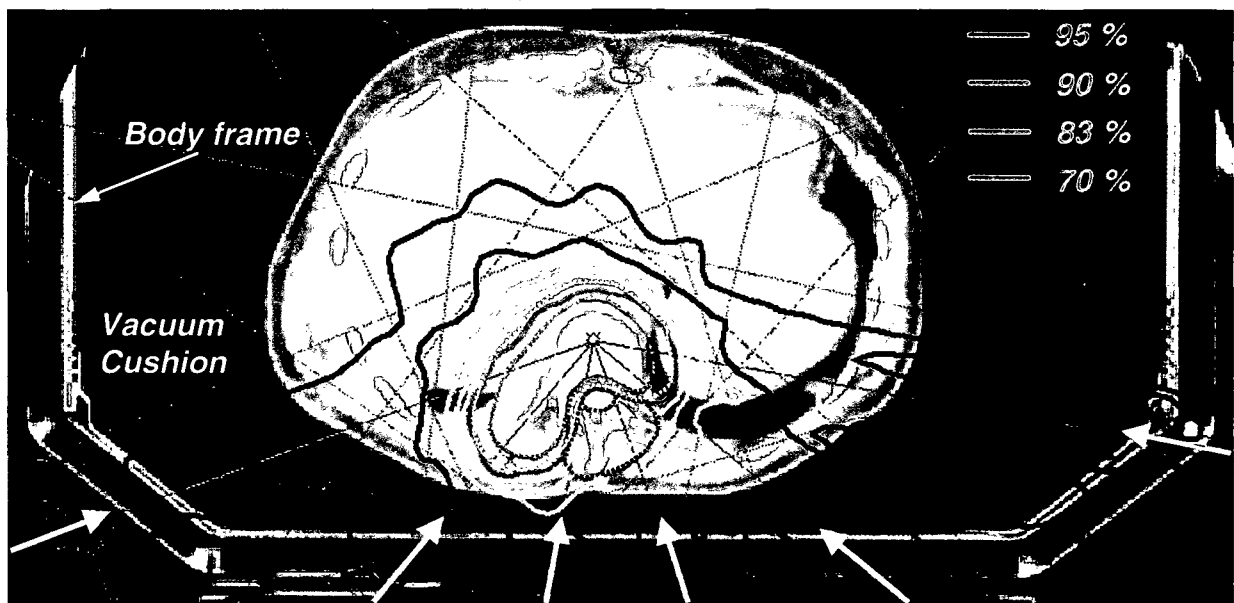
Figure 7.8 *Dose distribution in an axial CT slice, resulting from overall 69 segments in six beam incidence directions (orange arrows). In order to allow reduced safety margins, the patient was positioned in a body frame and immobilized by a vacuum mattress, adapted to the patient's outline.*

The results of the optimization process are illustrated in Figure 7.8, which also shows the body frame, serving for patient positioning and definition of stereotactic coordinates. Beside the beam incidence directions marked by orange arrows, isodose lines of 95%, 90%, 83%, 70%, 50%, and 30% are displayed. Overall 69 segments were generated, producing a highly conformal dose distribution with steep dose gradients surrounding the PTV. The concavity containing the spinal canal is excluded from the high dose region very precisely, as requested by the dose-volume-constraints. To highlight this fact, a perpendicular plane has been reconstructed that

intersects the concavity following the black dotted line in Figure 7.9 (a). The plane is shown in Figure 7.9 (b), where both parts of the tumour bed are found to be surrounded by the 95% and 90% isodose lines, while the spinal canal in between is spared. In some regions the dose to the myelon is even lower than 70%.
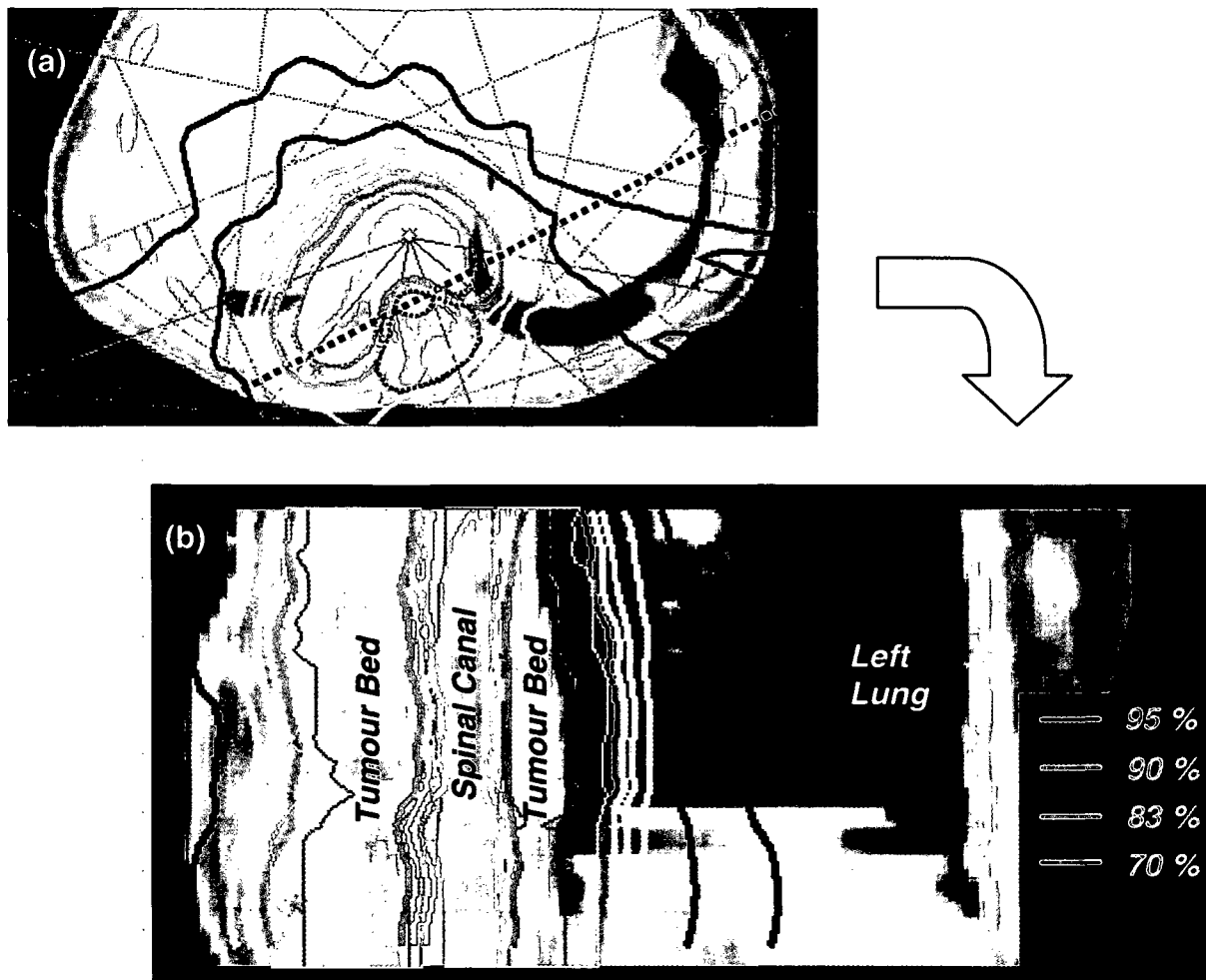
Figure 7.9 (a) *Definition of a perpendicular plane that intersects the concavity following the black dotted line.* **(b)** *Resulting dose distribution in the reconstructed slice, with the high dose region encompassing both parts of the tumour bed, while the spinal canal is spared in between.*

The significance of the artificial help structure is explained in Figure 7.10. While the left image (a) recalls the IMRT solution the patient actually was treated with, the right image (b) depicts the optimization result for exactly the same beam configuration and the same dose-volume-constraints for CTV, PTV and spinal canal ex PTV, but without any dose prescription to the help structure (therefore it is not displayed). In this case, the conformity of the high dose region is decreased, especially in the vicinity of the spinous process. The dose distribution tends to form a

low dose island instead of a low dose concavity although there is no target volume delineated on the opposite side of the spinal canal. When analyzing the treatment plans quantitatively, the same target coverage of 98% is found for both versions, which is well acceptable. However, the maximum dose to spinal canal ex PTV amounts to 86% without help structure, whereas it decreases to 84% if the help structure is taken into account in the calculation process. This seems to be quite surprising, as one would expect worse results with more structures being considered in the optimization process. Though, obviously the delineated help structure does not only help to improve the conformity, but also supports the sparing effect of the spinal canal. A reason for this behaviour may be found in the fact that the latter is incorporated in the help structure, as illustrated in Figure 7.7 (b), leading to a double consideration of the respective voxels in the optimization algorithm.
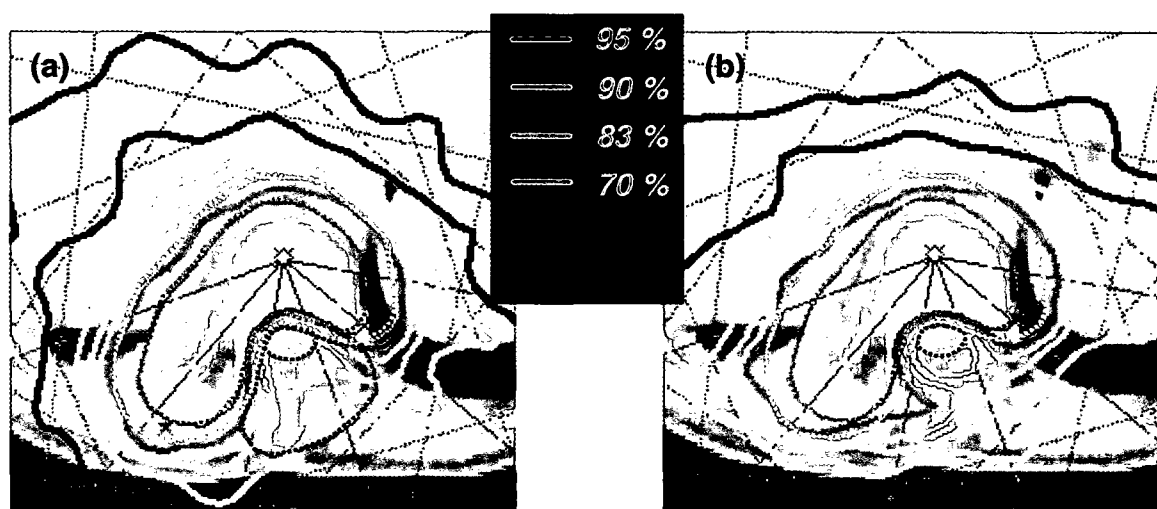
Figure 7.10 *Utility of the help structure.* **(a)** *IMRT treatment solution that actually was applied to the patient, with the help structure taken into account (dark green dotted line).* **(b)** *Alternative version with identical beam setup and constraints for CTV, PTV, and spinal canal ex PTV, but without any consideration of the help structure. Note the reduced conformity of the high dose region in the concavity, which would lead to larger exposures of normal tissue and consequently would make the patient more prone to geometric uncertainties.*

7.3 CASE STUDY 3: HEAD AND NECK TUMOUR

Radiotherapy in the head and neck region needs particular attention due to the numerous organs at risk involved in the treatments, for example the spinal cord,

brainstem, larynx, salivary glands or structures of the optical organ system. Consequently, it has been of special interest for the application of intensity modulated techniques to prevent or to minimize radiation induced side effects [Eisbruch et al 1998, Cozzi et al 2004]. The possibility to escalate the prescription dose in order to effectively treat aggressive tumours has also become a matter of investigations [Zhou et al 2003]. One of the main goals of IMRT in the head and neck region is the sparing of salivary glands, especially of the parotid glands, to save the patient from xerostomia [Eisbruch et al 2001]. A sufficient capacity of the salivary glands is not only significant for the patient's quality of life but also for a healthy ambience in the oral cavity. Even tumours in the parotid glands themselves [Nutting et al 2001a, Bragg et al 2002] or in the thyroid gland [Nutting et al 2001b] have been described as being suited for IMRT treatments, since a substantial sparing of various organs at risk has been observed.

For this case study a patient was selected who was diagnosed with cancer of the base of tongue. The tumour mainly affected the right side of the base of tongue, with involvement of the right tonsillar region. It was decided to perform a primary radiotherapy treatment, i.e. without any additional surgery or chemotherapy. Thus, two different types of targets were identified on the CT slices, as illustrated in Figure 7.11. First of all, the tumour itself (1) was contoured (CTV-tumour, red line) and expanded to PTV-tumour (yellow line) with isotropic margins of 5 mm. Additionally, the cervical lymph node regions right (2) and left (3) were delineated (bright brown lines), with analogously generated PTVs (dark brown lines). By a single IMRT treatment plan only, two different dose levels should be applied to the targets. While the cervical lymph node regions on both sides of the neck were to be treated up to 50 Gy, the dose to the primary tumour was prescribed to 60 Gy. This method is called simultaneous integrated boost (SIB) [Fogliata et al 2003], which is superior to the application of sequential IMRT plans, concerning both the conformity of the high dose region as well as the sparing of critical structures [Dogan et al 2003]. However, the SIB technique implies different fractional doses to the respective target volumes, consequently affecting the radiobiological effectiveness [Mohan et al 2000, Wu et al 2000]. For the patient described in this section, a minimum dose of 1.8 Gy per fraction was specified for the cervical lymph node regions. Thus, 28 daily irradiations were necessary to give the prescribed dose, leading to a fractional dose of 2.16 Gy in the primary tumour volume.

Due to the vicinity of the target volumes to the patient's surface only 6 MV beams could be used in the treatment planning process. Six fields were set up, where the isocenter was positioned outside the PTVs, as visible in Figure 7.11. This was necessary to be able to circumscribe the targets by symmetric fields, representing an advantageous starting configuration in the Helax-TMS optimization algorithm. The beam incidence directions are indicated by orange arrows.

Target 60 Gy	CTV-tumour	minimum dose = 57 Gy maximum dose = 63 Gy
	PTV-tumour	minimum dose = 54 Gy maximum dose = 63 Gy
Targets 50 Gy	right and left CTV lymph nodes	minimum dose = 47.5 Gy 54 Gy isodose <5% volume
	right and left PTV lymph nodes	minimum dose = 45 Gy 54 Gy isodose <5% volume
Organs at risk	left parotid gland	45 Gy isodose <20% volume 30 Gy isodose <40% volume 15 Gy isodose <60% volume
	myelon/brainstem	maximum dose = 45 Gy

Table 7.1 *Dose-volume-constraints of the head and neck case for targets and organs of risk used in the optimization algorithm. To prevent ambiguities due to the different target dose levels absolute dose values are described. However, in the TPS relative dose values were entered with the mean dose to CTV-tumour normalized to 100% = 60 Gy. For further explanations see text.*

In Table 7.1 the dose-volume-constraints used in the optimization algorithm are listed. The minimum target dose requirements correspond to the 95% and 90% values of the respective prescription doses, while the maximum constraint for the 54 Gy isodose in the lymph node regions were intended to improve the conformity of the high dose region (~60 Gy) surrounding the primary tumour and to prevent overdosage in the lymph node regions. For the myelon/brainstem (pink line in Figure 7.11 to Figure 7.13) a maximum dose of 45 Gy was prescribed, whereas for the left parotid gland (black dotted line in Figure 7.12) three dose-volume-constraints were required in order to get a mean dose of less than 24 Gy [Eisbruch *et al* 1999], a generally accepted tolerance dose for parotid gland recovery.

The results of the optimization process are illustrated in Figure 7.11 to Figure 7.13, where the first one shows the CT slice at the isocenter position. The

primary tumour (1) is surrounded by the 57 Gy and 54 Gy isodose lines, while the lymph node regions right (2) and left (3) are encompassed by the 47.5 Gy and 45 Gy dose levels, with only small overdosed areas close to the primary tumour. The maximum dose constraint for the myelon is clearly fulfilled.
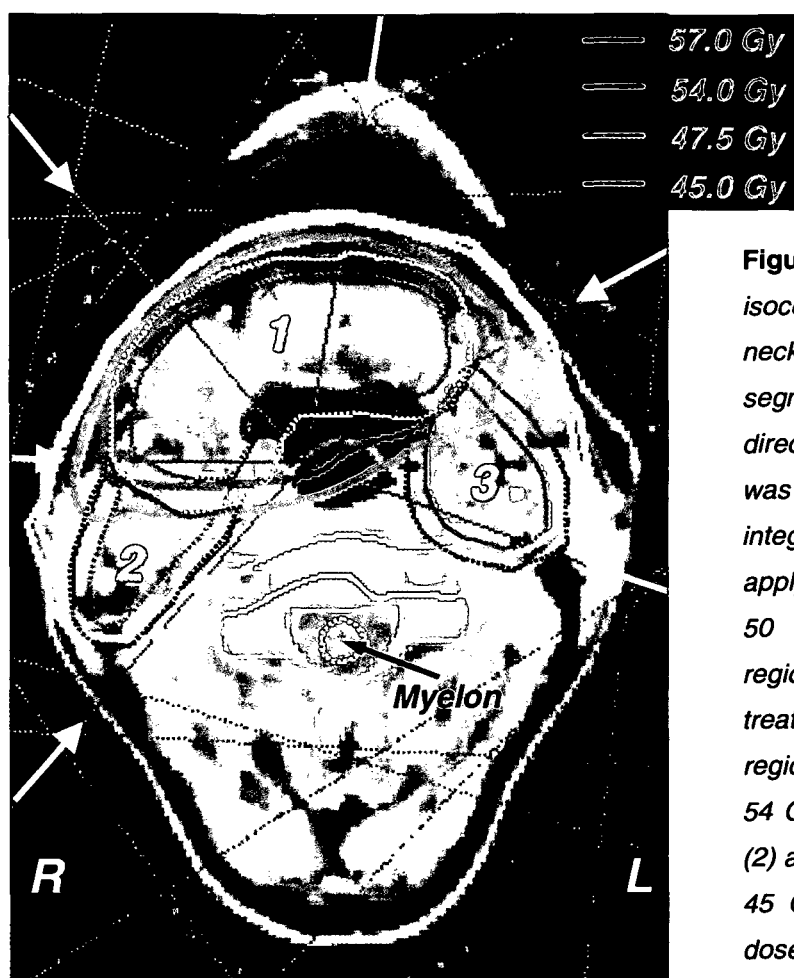
Figure 7.11 *Dose distribution in the isocenter slice of an IMRT head-and-neck case, resulting from overall 56 segments in six beam incidence directions (orange arrows). The patient was treated by a simultaneous integrated boost (SIB) technique, applying 60 Gy to the tumour (1) and 50 Gy to the cervical lymph node regions right (2) and left (3) by a single treatment plan only. Correspondingly, region (1) is surrounded by the 57 and 54 Gy isodose lines, while the volumes (2) and (3) are enclosed by the 47.5 and 45 Gy levels. The tolerated maximum dose to myelon was set to 45 Gy.*

Figure 7.12 depicts the CT slice 5 cm above the isocenter plane. In this region there are no lymph nodes to be treated, but the primary tumour CTV (red line) and PTV (yellow line) that are surrounded by the 57 Gy and 54 Gy isodose lines, respectively. In addition, the 47.5 Gy and 45 Gy dose levels are displayed to demonstrate the proper sparing of the brainstem (pink line). The compliance of the mean dose constraint defined for the left parotid gland (black dotted line) can only be evaluated by calculating the corresponding DVH, which is displayed in Figure 7.14 (b) and described in the last paragraph of this chapter.

Before CT-scanning, the patient was positioned in a head-and-neck mask, with an integrated bite block to minimize the movements of mandible and tongue.

The mask was fixed to a head-and-neck immobilization system (Brainlab AG, Heimstetten, Germany), equipped with a localizer frame to generate stereotactic coordinates of the isocenter. Figure 7.12 illustrates the bite block inserted in the oral cavity and the localizer box surrounding the patient.
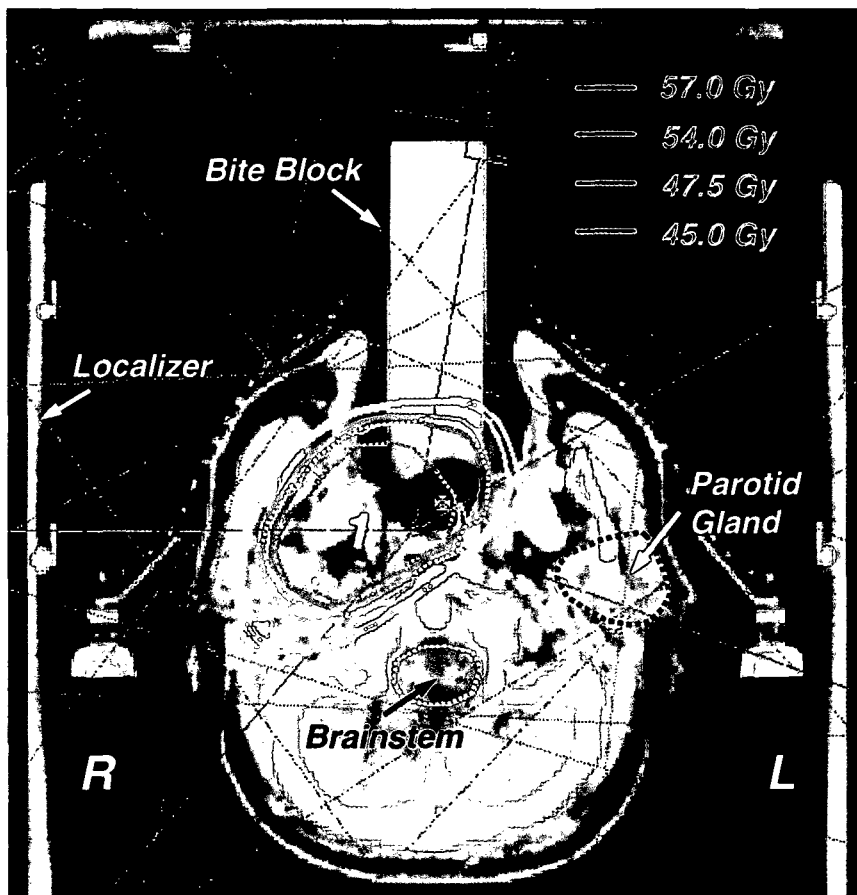
Figure 7.12 *CT slice 5 cm above the isocenter. Beside the tumour (1) as single target volume, brainstem and left parotid gland are delineated as organs at risk. The patient was positioned in a head-and-neck fixation mask system with an integrated localizer box providing stereotactic isocenter coordinates. To immobilize tongue and mandible, a bite block was inserted in the oral cavity and fixed to the mask.*

Finally, the CT slice 3 cm below the isocenter plane is shown in Figure 7.13, representing a section beyond the primary tumour volume. It only contains the cervical lymph node regions on both sides of the neck to be treated, appropriately surrounded by the 47.5 Gy and 45 Gy isodose lines.
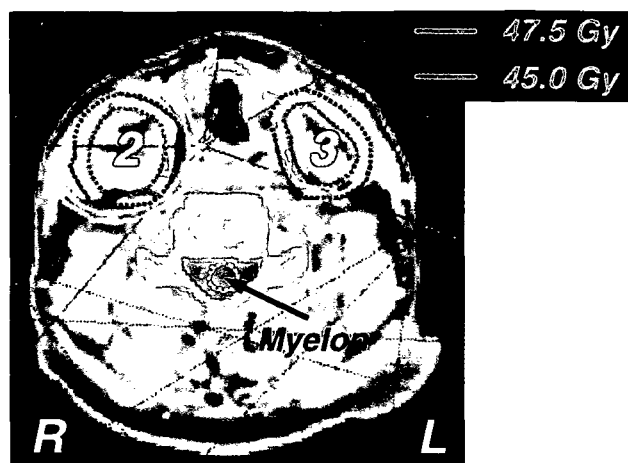
Figure 7.13 *CT slice 3 cm below the isocenter plane, with the cervical lymph node regions right (2) and left (3) defined as target volumes to be treated up to 50 Gy.*

128
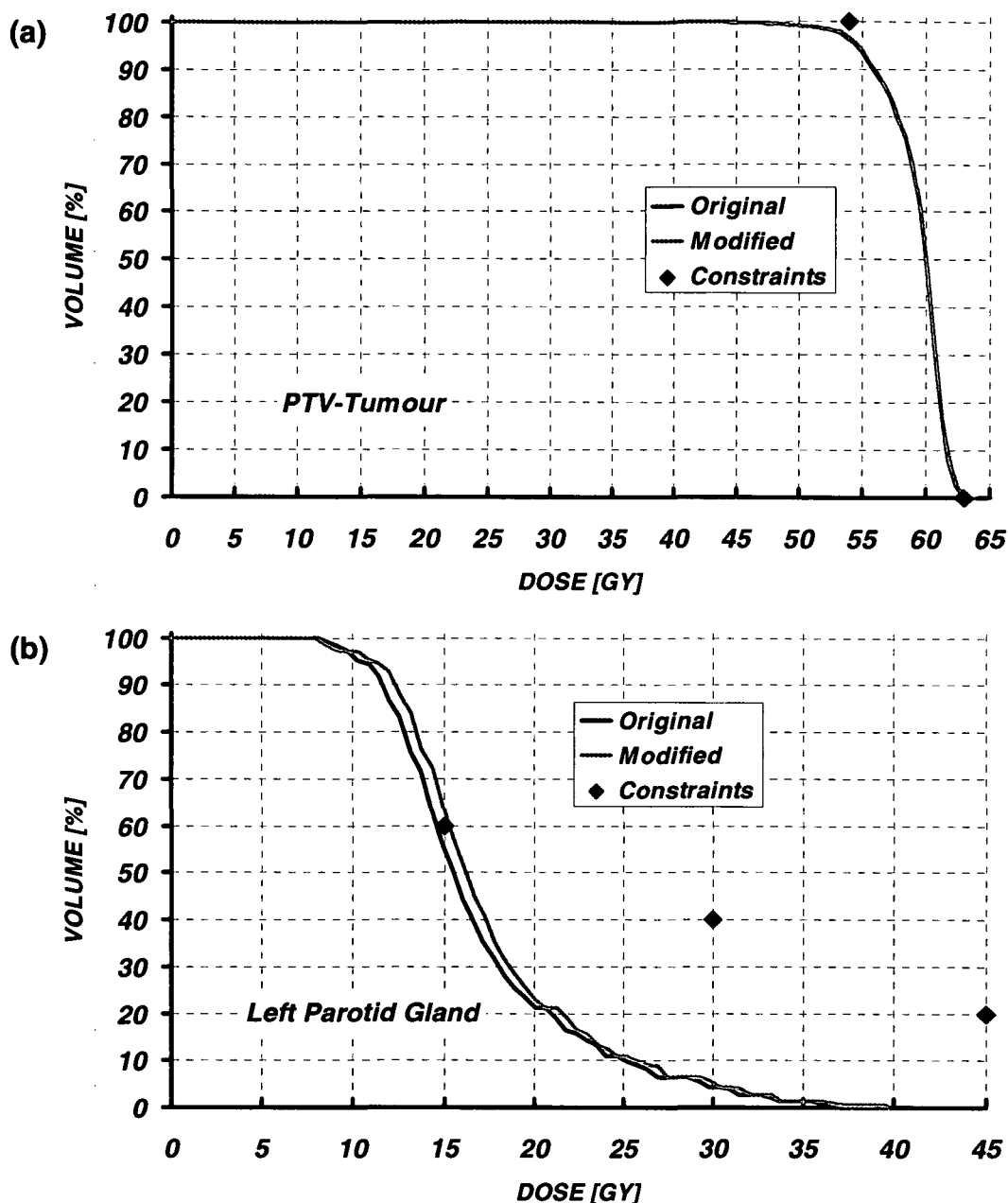
Figure 7.14 *Cumulative dose-volume-histograms, comparing the originally optimized IMRT solution (dark blue line) to the manually modified version without segments smaller than 2 MU (light blue line) for (a) the PTV-tumour and (b) the left parotid gland. Additionally, the dose-volume constraints used in the optimization procedure are indicated as dark blue markers, defining the desired PTV dose level (minimum and maximum) and three upper limits for the exposure to the parotid gland.*

The DVHs for PTV-tumour and left parotid gland are shown in Figure 7.14 (a) and (b), respectively. As it has been mentioned in section 4.2.3, the planning system in use does not offer a possibility to define a minimum number of MU per segment. Thus, very small segments have to be erased manually after the optimization process has finished. Since the patient presented here was treated before the Linac

upgrade, i.e. with the original magnetron, segments with less than 2 MU had to be deleted to provide optimal dosimetric performance, following the results of the study described in section 4.2. In Figure 7.14 (a) and (b) the dark blue curves represent the originally optimized treatment plan, while the light blue lines correspond to the manually modified plan without segments smaller than 2 MU. The mean dose to CTV-tumour is equal for both versions.

In Figure 7.14 (a) no significant difference is detectable, as the curves are nearly congruent. The manual modification did not affect the target coverage that was calculated to 97% in both cases, considering the minimum prescription dose of 54 Gy. Additionally, the dose inhomogeneity within the PTV was not altered in any direction by deleting segments with less than 2 MU.

In contrast, a small difference introduced by the manual segment editing was found in the DVH of the left parotid gland, displayed in Figure 7.14 (b). In fact, it was the only histogram within this case study showing a visible variation. Nevertheless, the deviation is still clinically well acceptable, since the mean dose to the parotid gland has changed from 17.5 Gy in the originally optimized plan to 18.0 Gy in the modified one, which is far below the requested dose level of 24 Gy.

7.4 PATIENT STATISTICS

In Table 7.2 relevant treatment planning parameters are presented as mean values ± one standard deviation, derived from the first 35 patients treated by IMRT at the Medical University of Vienna. As shown in the first column, more than ¾ of the patients suffered from tumours in the head and neck region. While for treatments of the prostate almost six beams were used on average, seven beams were necessary to produce satisfying plans in the head and neck region, with the paraspinal tumours in between. No significant difference between the tumour entities was found in the mean overall number of segments per treatment plan, which was in the order of magnitude of 60–70. With less than ten segments per beam, nearly the same averaged value was obtained for prostate as well as for head and neck cases. However, the IMRT optimization algorithm generated more than 11 segments per beam to fulfil the requirements in the treatment of paraspinal tumours. This reflects the complexity of such cases, as within a relatively small volume a strongly curved

concavity has to be encompassed with a steep dose gradient. The mean number of MU related to a fraction dose of 2 Gy was found to be within 350–400 with quite large standard deviations. Again, no significant dependence on tumour site could be identified.

For the patient described as case study 1 (section 7.1), 341.9 MU were calculated to give 2 Gy by IMRT, while the corresponding 3D conformal 4-field-box technique (see Figure 7.2 (b)) would have needed 240.9 MU per fraction. Hence, the number of MU was increased by 42% as compared to the conventional treatment, which is due to the smaller and more irregularly shaped segments in the IMRT delivery. Consequently, the beam-on time and thus the leakage radiation the patient was exposed to were enlarged by the same amount. However, this seems to be a tolerable trade-off when considering the improved conformity and the significant sparing of the rectal wall.

Tumour Entity	Number of Beams	Number of Segments	Segments per Beam	MU per 2 Gy
Prostate 5 Patients (14%)	5.8±1.0	58.2±25.6	9.6±2.6	377.8±42.9
Head and Neck 28 Patients (80%)	6.9±0.9	66.1±22.2	9.4±2.3	376.6±78.5
Paraspinal 2 Patients (6%)	6.5±0.5	73.5±4.5	11.3±0.2	382.2±46.5

Table 7.2 *Relevant treatment planning parameters derived from the first 35 patients treated by IMRT at the Medical University of Vienna. The mean values ± one standard deviations are presented.*

SUMMARY

Intensity modulated radiotherapy (IMRT) is currently one of the most complex options in the treatment of cancer by ionizing radiation. It uses megavoltage photon beams of time-variable intensity patterns to further increase the conformity of three-dimensional conformal radiotherapy. This is especially helpful in case of concavely shaped tumour volumes with sensitive structures in their direct vicinity, since IMRT offers the possibility to "paint" the high dose region following the target outline. Correspondingly, the exposure of organs at risk (OAR) and normal tissue may be reduced without loosing tumour control. In the segmental multileaf collimation approach (SMLC), intensity modulated beams are generated by superimposing several sub-fields or segments, individually shaped by a conventional multileaf collimator (MLC). Due to the vast number of degrees of freedom, in general computerized optimization algorithms are applied to find the optimal intensity distribution (inverse planning).

Within the scope of a pre-clinical test phase, the plausibility of the computational model and the influence of user-defined parameters on the optimization outcome were investigated for the integrated Helax-TMS IMRT module (V 6.0). Single beam phantom tests were performed in order to compare the "target primary feasibility" and the "weighted feasibility" algorithm, where only the latter allows the user to specify weights for structures. In the absence of organs at risk, both optimization algorithms were found to assign the highest priority to low dose constraints for targets. Furthermore, tests resembling clinical relevant configurations were carried out with multiple beam arrangements, where the limitation of segment number and segment size did not largely compromise treatment plans. On the other hand, these restrictions are important for delivery efficiency and dosimetry. The system's default number of iterations and voxels per volume of interest were found to be sufficient. Additionally, it was demonstrated that precautions must be taken to precisely define treatment goals when using computerized treatment optimization.

The dosimetric performance during the beam start-up phase and the precision of the mechanical components of an ELEKTA Precise Linac were checked pre-clinically, since the segments applied in a typical SMLC-IMRT treatment are often irregularly shaped and likely to be small in terms of field dimensions and number of monitor units (MU). The dose per MU linearity, beam symmetry and flatness (IEC 60976 standard) were investigated for three photon beam qualities (6 MV, 10 MV, 25 MV) at three different dose rate settings (100 MU/min, 200 MU/min, 400 MU/min). The requested stability in terms of dose linearity ($\pm 1\%$), beam flatness ($\leq 3\%$), and beam symmetry ($\leq 103\%$) was achievable for all beam qualities at a dose rate of 400 MU/min, when delivering segments with 2 MU or more. After the installation of a fast-tuning magnetron to reduce the treatment times of SMLC-IMRT delivery, even segments with only 1 MU turned out to completely fulfil the dosimetric acceptance criteria. For nominal square field sizes of 3 cm and 5 cm, deviations of ± 1 mm resulted in output variations of $\leq 1\%$ for all beam qualities, while the error increased to 2% for 25 MV beams at a field size of 2 cm.

It was therefore decided to set the minimum segment size to an area of 9 cm^2 with at least three leaf pairs opened. To investigate the mechanical accuracy of the integrated MLC, gaps of 2 cm nominal width at three different off-axis positions were irradiated, where for each leaf pair the full width at half maximum (FWHM) of the profile was measured by film. Additionally, the correct abutment of adjoining gaps was verified by inspecting the composed field. Three leaf pairs had to be re-calibrated to meet the required precision of better than 0.5 mm for each leaf.

Due to the complex nature of IMRT planning and delivery, it is necessary to verify each treatment plan before its first application onto the patient. In general, hybrid plans are created, i.e., the patient plan is transferred to a phantom and recalculated with unmodified fluence patterns. To check the calculated number of MU, single point ionization chamber measurements are appropriate, while relative 2D dose distributions are verified preferably by film dosimetry. For that purpose, a sensitometric curve to convert the optical density to dose is needed, which should not depend critically on beam energy, field size and depth, or film orientation. Thus, a normalization of sensitometric curves for 6 MV, 10 MV, and 25 MV to the dose value necessary to obtain a net OD = 1 for the respective energy was performed. By doing so one unique sensitometric curve can be used for the three beam qualities, which is true for Kodak X-Omat V films and EDR-2 films. The normalized curve is widely independent of field size, depth, and film orientation (deviations ≤3%). However, differences up to 20% can result when using different film processors.

A patient-specific quality assurance (QA) procedure was developed, including the specification of clinical acceptance criteria. While the verification of single beams turned out to be critical due to the typically steep dose gradients within IMRT fields, the hybrid plan verification method was found to be practical and reliable. Dedicated phantoms were designed to further ease the handling. Within an in-house developed software package, the mathematical concept of γ-index distributions was introduced to quantitatively evaluate 2D dose distributions. The concept combines criteria for dose difference and distance to agreement (DTA), which are violated if the γ-index is larger than unity. Typical values are 3% and 3 mm for the dose difference and DTA criteria, respectively. An IMRT treatment plan is accepted if the following conditions are fulfilled: absolute deviation of number of MU ≤3%, less than 10% of measurement area with γ-values larger than unity, mean γ-value ≤0.6, and maximum γ-value ≤2. Otherwise, the verification is repeated or the plan has to be re-optimized.

Finally, typical patient cases for three different tumour entities (prostate, paraspinal tumour, and head-and-neck) are presented and elaborately discussed. The examples are taken from actual IMRT treatments and clearly illustrate their advantages and possibilities: concavely shaped high dose regions, sparing of organs at risk located close to the target or even (partially) surrounded by the tumour, sparing of normal tissue, tumour dose escalation, and application of simultaneous integrated boost techniques. Presently, studies are performed in several institutions around the world to demonstrate the clinical benefit of IMRT.

REFERENCES

Adams EJ, Convery DJ, Cosgrove VP, McNair HA, Staffurth JN, Vaarkamp J, Nutting CM, Warrington AP, Webb S, Balyckyi J, Dearnaley DP 2004 Clinical implementation of dynamic and step-and-shoot IMRT to treat prostate cancer with high risk of pelvic lymph node involvement *Radiother Oncol.* **70**(1) 1-10

Ahnesjo A 1989 Collapsed cone convolution of radiant energy for photon dose calculation in heterogeneous media *Med Phys.* **16**(4) 577-92

Ahnesjo A, Aspradakis MM 1999 Dose calculations for external photon beams in radiotherapy *Phys Med Biol.* **44**(11) R99-155

Alber M, Paulsen F, Eschmann SM, Machulla HJ 2003 On biologically conformal boost dose optimization *Phys Med Biol.* **48**(2) N31-5

Azcona JD, Siochi RA, Azinovic I 2002 Quality assurance in IMRT: importance of the transmission through the jaws for an accurate calculation of absolute doses and relative distributions *Med Phys.* **29**(3) 269-74

Bar W, Alber M, Nusslin F 2001 A variable fluence step clustering and segmentation algorithm for step and shoot IMRT *Phys Med Biol.* **46**(7) 1997-2007

Basran PS, Ansbacher W, Field GC, Murray BR 1998 Evaluation of optimized compensators on a 3D planning system *Med Phys.* **25**(10) 1837-44

Bilsky MH, Yamada Y, Yenice KM, Lovelock M, Hunt M, Gutin PH, Leibel SA 2004 Intensity-modulated stereotactic radiotherapy of paraspinal tumors: a preliminary report *Neurosurgery* **54**(4) 823-30

Bortfeld T, Burkelbach J, Boesecke R, Schlegel W 1990 Methods of image reconstruction from projections applied to conformation radiotherapy *Phys Med Biol.* **35**(10) 1423-34

Bortfeld T, Schlegel W 1993 Optimization of beam orientations in radiation therapy: some theoretical considerations *Phys Med Biol.* **38**(2) 291-304

Bortfeld T, Boyer AL, Schlegel W, Kahler DL, Waldron TJ 1994a Realization and verification of three-dimensional conformal radiotherapy with modulated fields *Int J Radiat Oncol Biol Phys.* **30**(4) 899-908

Bortfeld TR, Kahler DL, Waldron TJ, Boyer AL 1994b X-ray field compensation with multileaf collimators *Int J Radiat Oncol Biol Phys.* **28**(3) 723-30

Bortfeld T 1999 Optimized planning using physical objectives and constraints *Semin Radiat Oncol.* **9**(1) 20-34

Bos LJ, Danciu C, Cheng CW, Brugmans MJ, van der Horst A, Minken A, Mijnheer BJ 2002 Interinstitutional variations of sensitometric curves of radiographic dosimetric films *Med Phys.* **29**(8) 1772-80

Bragg CM, Conway J, Robinson MH 2002 The role of intensity-modulated radiotherapy in the treatment of parotid tumors *Int J Radiat Oncol Biol Phys.* **52**(3) 729-38

Brahme A 1987 Design principles and clinical possibilities with a new generation of radiation therapy equipment. A review *Acta Oncol.* **26**(6) 403-12

Bridier A, Nystrom H, Ferreira I, Gomola I, Huyskens D 2000 A comparative description of three multipurpose phantoms (MPP) for external audits of photon beams in radiotherapy: the water MPP, the Umea MPP and the EC MPP *Radiother Oncol.* **55**(3) 285-93

Buchgeister M, Nusslin F 1998 Startup performance of the traveling wave versus standing wave linear accelerator *Med Phys.* **25**(4) 493-5

Budgell GJ, Martens C, Claus F 2001 Improved delivery efficiency for step and shoot intensity modulated radiotherapy using a fast-tuning magnetron *Phys Med Biol.* **46**(11) N253-61

Byrd RH, Lu P, Nocedal J, Zhu C 1995 A limited memory algorithm for bound constrained optimization *SIAM Journal on Scientific Computing* **16** 1190-1208

Cadman P, Bassalow R, Sidhu NP, Ibbott G, Nelson A 2002 Dosimetric considerations for validation of a sequential IMRT process with a commercial treatment planning system *Phys Med Biol.* **47**(16) 3001-10

Cheng CW, Das IJ 2002 Comparison of beam characteristics in intensity modulated radiation therapy (IMRT) and those under normal treatment condition *Med Phys.* **29**(2) 226-30

Chuang CF, Verhey LJ, Xia P 2002 Investigation of the use of MOSFET for clinical IMRT dosimetric verification *Med Phys.* **29**(6) 1109-15

Chui CS, LoSasso T, Spirou S 1994 Dose calculation for photon beams with intensity modulation generated by dynamic jaw or multileaf collimations *Med Phys.* **21**(8) 1237-44

Chui CS, Spirou S, LoSasso T 1996 Testing of dynamic multileaf collimation *Med Phys.* **23**(5) 635-41

Convery DJ, Rosenbloom ME 1995 Treatment delivery accuracy in intensity-modulated conformal radiotherapy *Phys Med Biol.* **40**(6) 979-99

Cormack AM 1987 A problem in rotation therapy with X rays *Int J Radiat Oncol Biol Phys.* **13**(4) 623-30

Cozzi L, Fogliata A, Bolsi A, Nicolini G, Bernier J 2004 Three-dimensional conformal vs. intensity-modulated radiotherapy in head-and-neck cancer patients: comparative analysis of dosimetric and technical parameters *Int J Radiat Oncol Biol* Phys. **58**(2) 617-24

Curtin-Savard AJ, Podgorsak EB 1999 Verification of segmented beam delivery using a commercial electronic portal imaging device *Med Phys.* **26**(5) 737-42

Danciu C, Proimos BS, Rosenwald JC, Mijnheer BJ 2001 Variation of sensitometric curves of radiographic films in high energy photon beams *Med Phys.* **28**(6) 966-74

De Gersem W, Claus F, De Wagter C, De Neve W 2001 An anatomy-based beam segmentation tool for intensity-modulated radiation therapy and its application to head-and-neck cancer *Int J Radiat Oncol Biol Phys.* **51**(3) 849-59

De Neve W, De Gersem W, Derycke S, De Meerleer G, Moerman M, Bate MT, Van Duyse B, Vakaet L, De Deene Y, Mersseman B, De Wagter C 1999 Clinical delivery of intensity modulated conformal radiotherapy for relapsed or second-primary head and neck cancer using a multileaf collimator with dynamic control *Radiother Oncol.* **50**(3) 301-14 Erratum in: 1999 *Radiother Oncol* **52**(1) 89

De Wagter C, Colle CO, Fortan LG, Van Duyse BB, Van den Berge DL, De Neve WJ 1998 3D conformal intensity-modulated radiotherapy planning: interactive optimization by constrained matrix inversion *Radiother Oncol.* **47**(1) 69-76

Deasy JO 1997 Multiple local minima in radiotherapy optimization problems with dose-volume constraints *Med Phys.* **24**(7) 1157-61

Deng J, Pawlicki T, Chen Y, Li J, Jiang SB, Ma CM 2001 The MLC tongue-and-groove effect on IMRT dose distributions *Phys Med Biol.* **46**(4) 1039-60

Depuydt T, Van Esch A, Huyskens DP 2002 A quantitative evaluation of IMRT dose distributions: refinement and clinical assessment of the gamma evaluation *Radiother Oncol.* **62**(3) 309-19

Dirkx ML, Heijmen BJ, van Santvoort JP 1998 Leaf trajectory calculation for dynamic multileaf collimation to realize optimized fluence profiles *Phys Med Biol.* **43**(5) 1171-84

Dogan N, Leybovich LB, Sethi A, Krasin M, Emami B 2000 A modified method of planning and delivery for dynamic multileaf collimator intensity-modulated radiation therapy *Int J Radiat Oncol Biol Phys.* **47**(1) 241-5

Dogan N, Leybovich LB, Sethi A 2002 Comparative evaluation of Kodak EDR2 and XV2 films for verification of intensity modulated radiation therapy *Phys Med Biol.* **47**(22) 4121-30

Dogan N, King S, Emami B, Mohideen N, Mirkovic N, Leybovich LB, Sethi A 2003 Assessment of different IMRT boost delivery methods on target coverage and normal-tissue sparing *Int J Radiat Oncol Biol Phys.* **57**(5) 1480-91

Dutreix J, Dutreix A 1969 Film dosimetry of high-energy electrons *Ann N Y Acad Sci.* **161**(1) 33-43

Eisbruch A, Marsh LH, Martel MK, Ship JA, Ten Haken R, Pu AT, Fraass BA, Lichter AS 1998 Comprehensive irradiation of head and neck cancer using conformal multisegmental fields: assessment of target coverage and noninvolved tissue sparing *Int J Radiat Oncol Biol Phys.* **41**(3) 559-68

Eisbruch A, Ten Haken RK, Kim HM, Marsh LH, Ship JA 1999 Dose, volume, and function relationships in parotid salivary glands following conformal and intensity-modulated irradiation of head and neck cancer *Int J Radiat Oncol Biol Phys.* **45**(3) 577-87

138

Eisbruch A, Kim HM, Terrell JE, Marsh LH, Dawson LA, Ship JA 2001 Xerostomia and its predictors following parotid-sparing irradiation of head-and-neck cancer *Int J Radiat Oncol Biol Phys.* **50**(3) 695-704

Elekta Oncology Systems Ltd. 2002 Precise Treatment System – Clinical Mode Operators Manual UK

Essers M, de Langen M, Dirkx ML, Heijmen BJ 2001 Commissioning of a commercially available system for intensity-modulated radiotherapy dose delivery with dynamic multileaf collimation *Radiother Oncol.* **60**(2) 215-24

Esthappan J, Mutic S, Harms WB, Dempsey JF, Low DA 2002 Dosimetry of therapeutic photon beams using an extended dose range film *Med Phys.* **29**(10) 2438-45

Ezzell GA 1996 Genetic and geometric optimization of three-dimensional radiation therapy treatment planning *Med Phys.* **23**(3) 293-305

Ezzell GA, Galvin JM, Low D, Palta JR, Rosen I, Sharpe MB, Xia P, Xiao Y, Xing L, Yu CX; IMRT subcommitte; AAPM Radiation Therapy committee 2003 Guidance document on delivery, treatment planning, and clinical implementation of IMRT: report of the IMRT Subcommittee of the AAPM Radiation Therapy Committee *Med Phys.* **30**(8) 2089-115

Fogliata A, Bolsi A, Cozzi L, Bernier J 2003 Comparative dosimetric evaluation of the simultaneous integrated boost with photon intensity modulation in head and neck cancer patients *Radiother Oncol.* **69**(3) 267-75

Followill D, Geis P, Boyer A 1997 Estimates of whole-body dose equivalent produced by beam intensity modulated conformal therapy *Int J Radiat Oncol Biol Phys.* **38**(3) 667-72 Erratum in: 1997 *Int J Radiat Oncol Biol Phys.* **39**(3) 783

Fowler JF, Welsh JS, Howard SP 2004 Loss of biological effect in prolonged fraction delivery *Int J Radiat Oncol Biol Phys.* **59**(1) 242-9

Fraass B, Doppke K, Hunt M, Kutcher G, Starkschall G, Stern R, Van Dyke J 1998 Report of the American Association of Physicists in Medicine Radiation Therapy Committee Task Group 53: quality assurance for clinical radiotherapy treatment planning *Med Phys.* **25**(10) 1773-829

Frenzel T 2000 Einsatz Intensitätsmodulierter Photonenfelder in der Strahlentherapie *Berichte aus der Physik, Shaker Aachen*

Galvin JM, Chen XG, Smith RM 1993 Combining multileaf fields to modulate fluence distributions *Int J Radiat Oncol Biol Phys.* **27**(3) 697-705

Georg D 1997a The Mini-Phantom Concept applied to a new type of Multileaf Collimator *Doctoral Thesis* Vienna, Vienna University of Technology

Georg D, Julia F, Briot E, Huyskens D, Wolff U, Dutreix A 1997b Dosimetric comparison of an integrated multileaf-collimator versus a conventional collimator *Phys Med Biol.* **42**(11) 2285-303

Georg D, Kroupa B 2002 Pre-clinical evaluation of an inverse planning module for segmental MLC based IMRT delivery *Phys Med Biol.* **47**(24) N303-14

Georg D 2003 Physikalische Grundlagen der Strahlentherapie *Lecture script* Vienna, Medical University of Vienna

Gerstner N, Wachter S, Dorner D, Goldner G, Colotto A, Pötter R 1999 Significance of a rectal balloon as internal immobilization device in conformal radiotherapy of prostatic carcinoma *Strahlenther Onkol.* **175**(5) 232-8

Granke RC, Wright KA, Evans WW, Nelson JE, Trump JG 1954 The film method of tissue dose studies with 2.0 mev. roentgen rays *Am J Roentgenol Radium Ther Nucl Med.* **72**(2) 302-7

Gregoire V, Daisne JF, Geets X, Levendag P 2003a Selection and delineation of target volumes in head and neck tumors: beyond ICRU definition *Rays.* **28**(3) 217-24

Gregoire V, Levendag P, Ang KK, Bernier J, Braaksma M, Budach V, Chao C, Coche E, Cooper JS, Cosnard G, Eisbruch A, El-Sayed S, Emami B, Grau C, Hamoir M, Lee N, Maingon P, Muller K, Reychler H 2003b CT-based delineation of lymph node levels and related CTVs in the node-negative neck: DAHANCA, EORTC, GORTEC, NCIC,RTOG consensus guidelines *Radiother Oncol.* **69**(3) 227-36

Gregoire V, Maingon P 2004 Intensity-modulated radiation therapy in head and neck squamous cell carcinoma: an adaptation of 2-dimensional concepts or a reconsideration of current clinical practice *Semin Radiat Oncol.* **14**(2) 110-20

Gustafsson A 1994a Development of a Versatile Algorithm for Optimization of Radiation Therapy *Doctoral Thesis* Stockholm, Universitet Stockholm

Gustafsson A, Lind BK, Brahme A 1994b A generalized pencil beam algorithm for optimization of radiation therapy *Med Phys.* **21**(3) 343-56

Gustafsson A, Lind BK, Svensson R, Brahme A 1995 Simultaneous optimization of dynamic multileaf collimation and scanning patterns or compensation filters using a generalized pencil beam algorithm *Med Phys.* **22**(7) 1141-56

Hansen VN, Evans PM, Budgell GJ, Mott JH, Williams PC, Brugmans MJ, Wittkamper FW, Mijnheer BJ, Brown K 1998 Quality assurance of the dose delivered by small radiation segments *Phys Med Biol.* **43**(9) 2665-75

Helax AB 2000 Helax-TMS Optimization Algorithm *TM-000-DPU-GB_IMRT-OptAv1* Sweden

Hettinger G, Svensson H 1967 Photographic film for determination of isodose curves from betatron electron radiation *Acta Radiol Ther Phys Biol.* **6**(1) 74-80

Hristov DH, Fallone BG 1998 A continuous penalty function method for inverse treatment planning *Med Phys.* **25**(2) 208-23

Intensity Modulated Radiation Therapy Collaborative Working Group 2001 Intensity-modulated radiotherapy: current status and issues of interest *Int J Radiat Oncol Biol Phys.* **51**(4) 880-914

International Commission on Radiation Units and Measurements 1993 Prescribing, recording and reporting photon beam therapy, Bethesda, MD: ICRU Report 50

International Commission on Radiation Units and Measurements 1999 Prescribing, recording and reporting photon beam therapy (supplement to ICRU Report 50), Bethesda, MD: ICRU Report 62

International Electrotechnical Commission 1989 Medical electrical equipment - Medical electron accelerators - Functional performance characteristics IEC 60976

Jeraj R, Keall PJ, Siebers JV 2002 The effect of dose calculation accuracy on inverse treatment planning *Phys Med Biol.* **47**(3) 391-407

Jiang SB, Ayyangar KM 1998 On compensator design for photon beam intensity-modulated conformal therapy *Med Phys.* **25**(5) 668-75

Ju SG, Ahn YC, Huh SJ, Yeo IJ 2002 Film dosimetry for intensity modulated radiation therapy: dosimetric evaluation *Med Phys.* **29**(3) 351-5

Kallman P, Lind BK, Brahme A 1992 An algorithm for maximizing the probability of complication-free tumour control in radiation therapy *Phys Med Biol.* **37**(4) 871-90

142

Karlsson MG, Karlsson M, Zackrisson B 1998 Intensity modulation with electrons: calculations, measurements and clinical applications *Phys Med Biol.* **43**(5) 1159-69

Kung JH, Chen GT, Kuchnir FK 2000 A monitor unit verification calculation in intensity modulated radiotherapy as a dosimetry quality assurance *Med Phys.* **27**(10) 2226-30

Landau D, Adams EJ, Webb S, Ross G 2001 Cardiac avoidance in breast radiotherapy: a comparison of simple shielding techniques with intensity-modulated radiotherapy *Radiother Oncol.* **60**(3) 247-55

Langer M, Thai V, Papiez L 2001 Improved leaf sequencing reduces segments or monitor units needed to deliver IMRT using multileaf collimators *Med Phys.* **28**(12) 2450-8

Laub WU, Bakai A, Nusslin F 2001 Intensity modulated irradiation of a thorax phantom: comparisons between measurements, Monte Carlo calculations and pencil beam calculations *Phys Med Biol.* **46**(6) 1695-706

Leybovich LB, Sethi A, Dogan N 2003 Comparison of ionization chambers of various volumes for IMRT absolute dose verification *Med Phys.* **30**(2) 119-23

Llacer J. 1997 Inverse radiation treatment planning using the Dynamically Penalized Likelihood method *Med Phys.* **24**(11) 1751-64

Llacer J, Solberg TD, Promberger C 2001 Comparative behaviour of the dynamically penalized likelihood algorithm in inverse radiation therapy planning *Phys Med Biol.* **46**(10) 2637-63

LoSasso T, Chui CS, Ling CC 1998 Physical and dosimetric aspects of a multileaf collimation system used in the dynamic mode for implementing intensity modulated radiotherapy *Med Phys.* **25**(10) 1919-27

Low DA, Gerber RL, Mutic S, Purdy JA 1998a Phantoms for IMRT dose distribution measurement and treatment verification *Int J Radiat Oncol Biol Phys.* **40**(5) 1231-5

Low DA, Harms WB, Mutic S, Purdy JA 1998b A technique for the quantitative evaluation of dose distributions *Med Phys.* **25**(5) 656-61

Low DA, Mutic S, Dempsey JF, Gerber RL, Bosch WR, Perez CA, Purdy JA 1998c Quantitative dosimetric verification of an IMRT planning and delivery system *Radiother Oncol.* **49**(3) 305-16

Low DA, Dempsey JF 2003 Evaluation of the gamma dose distribution comparison method *Med Phys.* **30**(9) 2455-64

Lutz W, Winston KR, Maleki N 1988 A system for stereotactic radiosurgery with a linear accelerator *Int J Radiat Oncol Biol Phys.* **14**(2) 373-81

Mackie TR, Holmes T, Swerdloff S, Reckwerdt P, Deasy JO, Yang J, Paliwal B, Kinsella T 1993 Tomotherapy: a new concept for the delivery of dynamic conformal radiotherapy *Med Phys.* **20**(6) 1709-19

Mageras GS, Mohan R 1993 Application of fast simulated annealing to optimization of conformal radiation treatments *Med Phys.* **20**(3) 639-47

Martens C, De Wagter C, De Neve W 2000 The value of the PinPoint ion chamber for characterization of small field segments used in intensity-modulated radiotherapy *Phys Med Biol.* **45**(9) 2519-30

Martens C, De Gersem W, De Neve W, De Wagter C 2001a Combining the advantages of step-and-shoot and dynamic delivery of intensity-modulated radiotherapy by interrupted dynamic sequences *Int J Radiat Oncol Biol Phys.* **50**(2) 541-50

Martens C, De Wagter C, De Neve W 2001b The value of the LA48 linear ion chamber array for characterization of intensity-modulated beams *Phys Med Biol.* **46**(4) 1131-48

Martens C, Reynaert N, De Wagter C, Nilsson P, Coghe M, Palmans H, Thierens H, De Neve W 2002a Underdosage of the upper-airway mucosa for small fields as used in intensity-modulated radiation therapy: a comparison between radiochromic film measurements, Monte Carlo simulations, and collapsed cone convolution calculations *Med Phys.* **29**(7) 1528-35

Martens C, Claeys I, De Wagter C, De Neve W 2002b The value of radiographic film for the characterization of intensity-modulated beams *Phys Med Biol.* **47**(13) 2221-34

McKenzie A, van Herk M, Mijnheer B 2002 Margins for geometric uncertainty around organs at risk in radiotherapy *Radiother Oncol.* **62**(3) 299-307

MDS Nordion 2001 Helax-TMS – Measurement and Verification of Radiation Data *TM-000-MPU-GB_TMS-MVv1* Sweden

Mohan R, Wu Q, Manning M, Schmidt-Ullrich R 2000 Radiobiological considerations in the design of fractionation strategies for intensity-modulated radiation therapy of head and neck cancers *Int J Radiat Oncol Biol Phys.* **46**(3) 619-30

Morrill SM, Lane RG, Jacobson G, Rosen II 1991 Treatment planning optimization using constrained simulated annealing *Phys Med Biol.* **36**(10) 1341-61

Mutic S, Low DA, Klein EE, Dempsey JF, Purdy JA 2001 Room shielding for intensity-modulated radiation therapy treatment facilities *Int J Radiat Oncol Biol Phys.* **50**(1) 239-46

Niemierko A, Goitein M 1990 Random sampling for evaluating treatment plans *Med Phys.* **17**(5) 753-62

Niemierko A 1992 Random search algorithm (RONSC) for optimization of radiation therapy with both physical and biological end points and *constraints Int J Radiat Oncol Biol Phys.* **23**(1) 89-98

Niemierko A, Urie M, Goitein M 1992 Optimization of 3D radiation therapy with both physical and biological end points and constraints *Int J Radiat Oncol Biol Phys.* **23**(1) 99-108

Novotny J, Gomola I, Izewska J, Huyskens D, Dutreix A 1997 External audit of photon beams by mailed film dosimetry: feasibility study *Phys Med Biol.* **42**(7) 1277-88

Nutting CM, Rowbottom CG, Cosgrove VP, Henk JM, Dearnaley DP, Robinson MH, Conway J, Webb S 2001a Optimisation of radiotherapy for carcinoma of the parotid gland: a comparison of conventional, three-dimensional conformal, and intensity-modulated techniques *Radiother Oncol.* **60**(2) 163-72

Nutting CM, Convery DJ, Cosgrove VP, Rowbottom C, Vini L, Harmer C, Dearnaley DP, Webb S 2001b Improvements in target coverage and reduced spinal cord irradiation using intensity-modulated radiotherapy (IMRT) in patients with carcinoma of the thyroid gland *Radiother Oncol.* **60**(2) 173-80

Olch AJ 2002 Dosimetric performance of an enhanced dose range radiographic film for intensity-modulated radiation therapy quality assurance *Med Phys.* **29**(9) 2159-68

Palta JR and Mackie TR (Editors) 2003 Intensity-Modulated Radiation Therapy: The State of The Art *Medical Physics Monograph No. 29, Medical Physics Publishing Madison Wisconsin*

Plathow C, Thilmann C, Delorme S, Stippich C, Wannenmacher M, Debus J 2001 Radiotherapy planning for paraspinal tumors with CT-myelography *Strahlenther Onkol.* **177**(6) 307-12

Pollack A, Hanlon A, Horwitz EM, Feigenberg S, Uzzo RG, Price RA 2003 Radiation therapy dose escalation for prostate cancer: a rationale for IMRT *World J Urol.* **21**(4) 200-8

Potter LD, Chang SX, Cullip TJ, Siochi AC 2002 A quality and efficiency analysis of the IMFAST segmentation algorithm in head and neck "step & shoot" IMRT treatments *Med Phys.* **29**(3) 275-83

Press WH, Teukolsky SA 1989 Quasi- (that is, sub-) random numbers *Computers in Physics* **3** 76-79

Radiological Imaging Technology 2001 RIT 113, Version 3.11, User's Manual and Guide USA

Rosen II, Lane RG, Morrill SM, Belli JA 1991 Treatment plan optimization using linear programming *Med Phys.* **18**(2) 141-52

Ruchala KJ, Olivera GH, Schloesser EA, Mackie TR 1999 Megavoltage CT on a tomotherapy system *Phys Med Biol.* **44**(10) 2597-621

Scholz C, Nill S, Oelfke U 2003 Comparison of IMRT optimization based on a pencil beam and a superposition algorithm *Med Phys.* **30**(7) 1909-13

Seco J, Evans PM, Webb S 2001 Analysis of the effects of the delivery technique on an IMRT plan: comparison for multiple static field, dynamic and NOMOS MIMiC collimation *Phys Med Biol.* **46**(12) 3073-87

Sharpe MB, Miller BM, Yan D, Wong JW 2000 Monitor unit settings for intensity modulated beams delivered using a step-and-shoot approach *Med Phys.* **27**(12) 2719-25

Siebers JV, Lauterbach M, Tong S, Wu Q, Mohan R 2002 Reducing dose calculation time for accurate iterative IMRT planning *Med Phys.* **29**(2) 231-7

Spirou SV, Chui CS 1994 Generation of arbitrary intensity profiles by dynamic jaws or multileaf collimators *Med Phys.* **21**(7) 1031-41

Spirou SV, Chui CS 1998 A gradient inverse planning algorithm with dose-volume constraints *Med Phys.* **25**(3) 321-33

Stavrev P, Hristov D, Warkentin B, Sham E, Stavreva N, Fallone BG 2003 Inverse treatment planning by physically constrained minimization of a biological objective function *Med Phys.* **30**(11) 2948-58

Stein J, Mohan R, Wang XH, Bortfeld T, Wu Q, Preiser K, Ling CC, Schlegel W 1997 Number and orientations of beams in intensity-modulated radiation treatments *Med Phys.* **24**(2) 149-60

Stock M 2003 Implementierung eines Güteparameters zur Beurteilung von Bestrahlungsplänen in der IMRT *Diploma Thesis* Vienna, Vienna University of Technology

Stock M, Kroupa B, Georg D 2005 Interpretation and evaluation of the gamma index and the gamma index angle for the verification of IMRT hybrid plans *Phys Med Biol.* **50**(3) 399-41

Suchowerska N, Hoban P, Davison A, Metcalfe P 1999 Perturbation of radiotherapy beams by radiographic film: measurements and Monte Carlo simulations *Phys Med Biol.* **44**(7) 1755-65

Suchowerska N, Hoban P, Butson M, Davison A, Metcalfe P 2001 Directional dependence in film dosimetry: radiographic and radiochromic film *Phys Med Biol.* **46**(5) 1391-7

Teh BS, Mai WY, Uhl BM, Augspurger ME, Grant WH 3rd, Lu HH, Woo SY, Carpenter LS, Chiu JK, Butler EB 2001 Intensity-modulated radiation therapy (IMRT) for prostate cancer with the use of a rectal balloon for prostate immobilization: acute toxicity and dose-volume analysis *Int J Radiat Oncol Biol Phys.* **49**(3) 705-12

Teh BS, Woo SY, Mai WY, Mcgary JE, Carpenter LS, Lu HH, Chiu JK, Vlachaki MT, Grant WH 3rd, Butler EB 2002a Clinical experience with intensity-modulated radiation therapy (IMRT) for prostate cancer with the use of rectal balloon for prostate immobilization *Med Dosim.* **27**(2) 105-13

Teh BS, McGary JE, Dong L, Mai WY, Carpenter LS, Lu HH, Chiu JK, Woo SY, Grant WH, Butler EB 2002b The use of rectal balloon during the delivery of intensity modulated radiotherapy (IMRT) for prostate cancer: more than just a prostate gland immobilization device? *Cancer J.* **8**(6) 476-83

Vaarkamp J, Krasin M 2001 Reduction of target dose inhomogeneity in IMRT treatment planning using biologic objective functions *Int J Radiat Oncol Biol Phys.* **49**(5) 1518-20

Van Dyk J, Barnett RB, Cygler JE, Shragge PC 1993 Commissioning and quality assurance of treatment planning computers *Int J Radiat Oncol Biol Phys.* **26**(2) 261-73

Van Esch A, Vanstraelen B, Verstraete J, Kutcher G, Huyskens D 2001 Pre-treatment dosimetric verification by means of a liquid-filled electronic portal imaging device during dynamic delivery of intensity modulated treatment fields *Radiother Oncol.* **60**(2) 181-90

Venselaar J, Welleweerd H, Mijnheer B 2001 Tolerances for the accuracy of photon beam dose calculations of treatment planning systems *Radiother Oncol.* **60**(2) 191-201

Wachter S, Gerstner N, Goldner G, Potzi R, Wambersie A, Pötter R 2001 Rectal sequelae after conformal radiotherapy of prostate cancer: dose-volume histograms as predictive factors *Radiother Oncol.* **59**(1) 65-70

Wachter S, Gerstner N, Dorner D, Goldner G, Colotto A, Wambersie A, Pötter R 2002 The influence of a rectal balloon tube as internal immobilization device on variations of volumes and dose-volume histograms during treatment course of conformal radiotherapy for prostate cancer *Int J Radiat Oncol Biol Phys.* **52**(1) 91-100

Webb S 1991 Optimization by simulated annealing of three-dimensional conformal treatment planning for radiation fields defined by a multileaf collimator *Phys Med Biol.* **36**(9) 1201-26

Webb S 1999 Conformal intensity-modulated radiotherapy (IMRT) delivered by robotic linac--testing IMRT to the limit? *Phys Med Biol.* **44**(7) 1639-54

Webb S 2000 Conformal intensity-modulated radiotherapy (IMRT) delivered by robotic linac--conformality versus efficiency of dose delivery *Phys Med Biol.* **45**(7) 1715-30

Webb S 2001 Intensity-Modulated Radiation Therapy *Series in Medical Physics - Institute of Physics Publishing Bristol and Philadelphia*

Wu Q, Manning M, Schmidt-Ullrich R, Mohan R 2000 The potential for sparing of parotids and escalation of biologically effective dose with intensity-modulated radiation treatments of head and neck cancers: a treatment design study *Int J Radiat Oncol Biol Phys.* **46**(1) 195-205

Wu X, Zhu Y 2001 A maximum-entropy method for the planning of conformal radiotherapy *Med Phys.* **28**(11) 2241-6

Xing L, Chen GT 1996 Iterative methods for inverse treatment planning *Phys Med Biol.* **41**(10) 2107-23

Xing L, Curran B, Hill R, Holmes T, Ma L, Forster KM, Boyer AL 1999 Dosimetric verification of a commercial inverse treatment planning system *Phys Med Biol.* **44**(2) 463-78

Xing L, Chen Y, Luxton G, Li JG, Boyer AL 2000 Monitor unit calculation for an intensity modulated photon field by a simple scatter-summation algorithm *Phys Med Biol.* **45**(3) N1-7

Yenice KM, Lovelock DM, Hunt MA, Lutz WR, Fournier-Bidoz N, Hua CH, Yamada J, Bilsky M, Lee H, Pfaff K, Spirou SV, Amols HI 2003 CT image-guided intensity-modulated therapy for paraspinal tumors using stereotactic immobilization *Int J Radiat Oncol Biol Phys.* **55**(3) 583-93

Yu CX, Symons MJ, Du MN, Martinez AA, Wong JW 1995a A method for implementing dynamic photon beam intensity modulation using independent jaws and a multileaf collimator *Phys Med Biol.* **40**(5) 769-87

Yu CX 1995b Intensity-modulated arc therapy with dynamic multileaf collimation: an alternative to tomotherapy *Phys Med Biol.* **40**(9) 1435-49

Zelefsky MJ, Fuks Z, Happersett L, Lee HJ, Ling CC, Burman CM, Hunt M, Wolfe T, Venkatraman ES, Jackson A, Skwarchuk M, Leibel SA 2000 Clinical experience with intensity modulated radiation therapy (IMRT) in prostate cancer *Radiother Oncol.* **55**(3) 241-9

Zhou J, Fei D, Wu Q 2003 Potential of intensity-modulated radiotherapy to escalate doses to head-and-neck cancers: what is the maximal dose? *Int J Radiat Oncol Biol Phys.* **57**(3) 673-82

Zhu XR, Jursinic PA, Grimm DF, Lopez F, Rownd JJ, Gillin MT 2002 Evaluation of Kodak EDR2 film for dose verification of intensity modulated radiation therapy delivered by a static multileaf collimator *Med Phys.* **29**(8) 1687-92

ANNEX

ABBREVIATIONS

A-B .... Cross-plane direction (orthogonal to Gun-Target)

CRT .... Conformal Radiotherapy

CT .... Computer Tomography

CTV .... Clinical Target Volume

DMLC .... Dynamic Multileaf Collimation

DTA .... Distance-To-Agreement

DVH .... Dose Volume Histogram

EDR .... Extended Dose Range

ESTRO .... European Society for Therapeutic Radiology and Oncology

FS .... Field Size

FTM .... Fast Tuning Magnetron

FWHM .... Full Width at Half Maximum

G-T .... In-plane direction (Gun-Target)

ICRU .... International Commission on Radiation Units and Measurements

IM .... Intensity Modulation

IMAT .... Intensity Modulated Arc Therapy

IMRT .... Intensity Modulated Radiotherapy

Linac .... Linear Accelerator

MIMiC .... Multileaf Intensity Modulating Collimator

MLC .... Multileaf Collimator

MPP .... Multi-Purpose Phantom

MRI .... Magnetic Resonance Imaging

MU .... Monitor Unit(s)

NSC .... Normalized Sensitometric Curve

OAR .... Organ At Risk

OD .... Optical Density

PB .... Pencil Beam

PET .... Positron Emission Tomography

CURRICULUM VITAE

Name: Bernhard KROUPA

Date of birth: 20. 06. 1974

Place of birth: Vienna

Nationality: Austria

Degree: Dipl.-Ing. in Physics

EDUCATION

Sept. 1984 – June 1992   Secondary School
Bundesgymnasium Wien 13, Fichtnergasse 15

Oct. 1992 – June 1998   Physics Study, University of Technology Vienna
Thesis: *"Dreidimensionale Dosimetrie in der Strahlen-therapie"*
Experimental performance: University of Vienna, Medical School, Department of Radiotherapy and Radiobiology

Since October 1998   Doctoral Study, University of Technology Vienna
Doctoral Thesis: *"Clinical Implementation of Intensity Modulated Radiotherapy based on Segmental Multileaf Modulation"*
Experimental performance: Medical University of Vienna, Department of Radiotherapy and Radiobiology

SCIENTIFIC WORK

Publications

Georg D, **Kroupa B** 2002 Pre-clinical evaluation of an inverse planning module for segmental MLC based IMRT delivery *Phys Med Biol.* **47**(24) N303-14

Georg D, **Kroupa B**, Winkler P, Pötter R 2003 Normalized sensitometric curves for the verification of hybrid IMRT treatment plans with multiple energies *Med Phys.* **30**(6) 1142-50

Stock M, **Kroupa B**, Georg D 2005 Interpretation and evaluation of the gamma index and the gamma index angle for the verification of IMRT hybrid plans *Phys Med Biol.* **50**(3) 399-411

Dvorak P, Georg D, Bogner J, **Kroupa B**, Dieckmann K, Pötter R 2005 Impact of IMRT and leaf width on stereotactic body radiotherapy of liver and lung lesions *Int J Radiat Oncol Biol Phys.* **61**(5) 1572-81

Oral presentations national and international

Kroupa B, Wolff U, Aiginger H "Entwicklung und Erprobung eines Phantoms für dreidimensionale Dosismessungen mit verschiedenen Messverfahren", Annual meeting of the Austrian Physical Society, Graz (A) September 1998

Kroupa B, Georg D, Pötter R "Evaluierung des IMRT-Optimierungsmoduls des Bestrahlungsplanungs-Systems HELAX-TMS", Workshop of the Austrian Society for Medical Physics, Annual meeting of the Austrian Society for Radiation Oncology, Radiobiology and Medical Radiation Physics, Semmering (A) October 2001

Bogner J, Dvorak P, **Kroupa B**, Dieckmann K, Georg D "Extracranial stereotactic radiotherapy of lung and liver cancer – a clinical comparison of two treatment planning systems"; 7th Biennial ESTRO meeting on Physics and Radiation Technology for Clinical Radiotherapy, Geneva (CH) September 2003, *Radiotherapy and Oncology 68 (Suppl. 1) 2003* p. S45

Dvorak P, Bogner J, **Kroupa B**, Georg D "Extracranial stereotactic radiotherapy of lung cancer – a comparative dosimetric study", 7th Biennial ESTRO meeting on Physics and Radiation Technology for Clinical Radiotherapy, Geneva (CH) September 2003, *Radiotherapy and Oncology 68 (Suppl. 1) 2003* p. S36

Georg D, **Kroupa B**, Winkler P, Pötter R "Normalized sensitometric curves for the verification of hybrid IMRT treatment plans with multiple energies", 7th Biennial ESTRO meeting on Physics and Radiation Technology for Clinical Radiotherapy, Geneva (CH) September 2003, *Radiotherapy and Oncology 68 (Suppl. 1) 2003* p. S37-S38

Winkler P, **Kroupa B**, Aiginger H, Pötter R, Georg D "Normierte sensitometrische Kurven zur Verifikation von IMRT-Bestrahlungsplänen mit mehreren Energien", Annual meeting of the Austrian Society for Medical Physics, Linz (A) October 2003

Bogner J, Georg D, Dvorak P, **Kroupa B**, Dieckmann K "Extracranial stereotactic Radiotherapy at the University of Vienna – Ongoing Studies", 1st Austrian, Italian and Slovenian Medical Physics Meeting, Udine (I) November 2003

Stock M, **Kroupa B**, Georg D "Praktische Aspekte der Gammaevaluierung in der IMRT-Verifikation", Annual meeting of the Austrian Society for Medical Physics, Wiener Neustadt (A) June 2004

Georg D, **Kroupa B**, Mock U, Dieckmann K, Pötter R "How straight forward is inverse planning really?", ESTRO23, Amsterdam (NL) October 2004, *Radiotherapy and Oncology 73 (Suppl. 1) 2004* p. S212

Poster presentations national and international

Dvorak P, Spevacek V, Novotny J Jr., Hrbacek J, Bogner J, **Kroupa B**, Georg D "Verification of three-dimensional IMRT dose distribution in the inhomogeneous media using a polymer-gel dosimeter", ESTRO23, Amsterdam (NL) October 2004, *Radiotherapy and Oncology 73 (Suppl. 1) 2004* p. S339

Stock M, **Kroupa B**, Georg D "Practical aspects of the gamma-evaluation in the verification of step-and-shoot IMRT-treatments", ESTRO23, Amsterdam (NL) October 2004, *Radiotherapy and Oncology 73 (Suppl. 1) 2004* p. S112-S113